Use Authorization

In presenting this thesis in partial fulfillment of the requirements for an advanced degree at Idaho State University, I agree that the Library shall make it freely available for inspection. I further state that permission to download and/or print my thesis for scholarly purposes may be granted by the Dean of the Graduate School, Dean of my academic division, or by the University Librarian. It is understood that any copying or publication of this thesis for financial gain shall not be allowed without my written permission.

Signature _____

Date _____

Large-Scale Testing of a Precast Bent for Accelerated Bridge Construction in Seismic Zones

by

Jared Cantrell

A thesis

submitted in partial fulfillment

of the requirements for the degree of

Master of Science in the Department of Civil and Environmental Engineering

Idaho State University

April 2021

COMMITTEE APPROVAL

To the Graduate Faculty:

The members of the committee appointed to examine the thesis of JARED CANTRELL find it satisfactory and recommend that it be accepted.

_____

Major Advisor

Dr. Mustafa Mashal

_____

Committee Member

Dr. Arya Ebrahimpour

_____

Graduate Faculty Representative

Dr. Andrew Chrysler

ACKNOWLEDGMENT

I would like to express my sincerest of gratitude to the students who assisted on the project in so many ways. Mahesh Mahat and Mahesh Acharya for the numerous hours of labor on construction, fabrication, pouring, instrumentation, and testing to complete the research. Furthermore, I would like to thank Corey Marshall, Kathryn Hogarth, Samantha Kerr, Karma Gurung, and Aashish Thapa for their contributions throughout the project. I would like to extend by gratitude to Ali Shokrgozar for his assistance and diligence concerning the analytical modeling and data analysis for the research. The project would have suffered greatly without the contributions of students.

I would like to specifically thank my Major Advisor and Supervisor, Dr. Mustafa Mashal. He has consistently encouraged and provided me opportunities far beyond what I had ever expected since having met him. This research being just one of the incredible opportunities I have been able to participate, learn, and grow from. I am also extremely grateful for Dr. Arya Ebrahimpour, Committee Member, as he is always willing to share his extensive knowledge and experience. He has been incredibly gracious and patient when offering advice and direction when needed most. I would also like to than Dr. Andrew Chrysler for being the Graduate Faculty Representative.

I would like to specifically thank my family. Throughout the project my parents, Todd and Terri Cantrell, have continually pushed me with their love and support, as have my two sisters, Lisa and Sarah. I would also like to thank my Grandmother, Mickey Cantrell, who has constantly supported and encouraged me throughout this project, never letting me faulter.

The project would not have been possible without the financial support of Idaho Transportation Department. Nor without the contributions of Leonard Ruminski, Bridge Designer at Idaho Transportation Department.

TABLE OF CONTENTS

LIST OF FIGURES

LIST OF TABLES

Large-Scale Testing of a Precast Bent for Accelerated Bridge Construction in Seismic Zones

Thesis Abstract—Idaho State University (2021)

Accelerated Bridge Construction (ABC) has gained popularity around the United States in recent decades. ABC offers many advantages over traditional cast-in-place (CIP), such as reduced traffic disruption and rapid erection, among numerous others. Despite these advantages, application of ABC in seismic regions is still a challenge due to difficulties associated with developing equivalent response from precast connections as that of CIP during seismic loading. In this research, a new precast pier system is proposed to emulate the traditional CIP seismic design (i.e. formation of plastic hinges during earthquakes). The precast elements are connected using fully encased concrete-filled steel tubes. Large-scale experimental testing of equivalent precast and CIP bents is carried out to investigate the seismic performance of the proposed pier system and to compare it against the traditional cast-in-place construction. Experimental results exhibit good performance of the precast connection when subjected to quasi-static cyclic loading. The performance of the precast connection during experimental testing of piers has outperformed the CIP benchmark specimen in ductility and strength.

Key Words: Accelerated Bridge Construction; ABC; precast concrete; large-scale testing; seismic; bridges; concrete-filled steel tube; cast-in-place bent; precast bent

CHAPTER 1 INTRODUCTION

1.1. INTRODUCTION

For the last few decades Accelerated Bridge Construction (ABC) has been a rapidly developing process in Civil Engineering. This can be contributed to the advantages it offers over that of traditional Cast-In-Place (CIP) construction. Among the advantages of ABC when building new, replacing, or rehabilitating bridges are reduced traffic disruption, improved on-site safety, increased quality, rapid erection, reduced work site footprint, and reduced onsite construction time. Despite these advantages, CIP construction is prevalently used in areas of seismic activity as the resulting structure is considered to be "monolithic". This type of construction is performed fully on-site in the field with elements of the bridge substructure being constructed in sequential stages. Resulting in bridge substructures that exhibit superior performance when subjected to seismic activity over that of many existing ABC options. In contrast, ABC is an approach which emphasizes and uses innovative methods, materials, and designs to effectively reduce onsite construction duration in a safe and cost-effective manner (U.S. Department of Transportation/Federal Highway Administration 2019). However, ABC traditionally results in a non-monolithic structure with less ductile connections that can fail due to the concentration of forces and deformations at these locations during seismic activity. The concentration of forces and deformations during seismic events exhibit the limited ductility and strength of traditional precast connections in comparison to monolithic structures.

Stemming from ABC's limitations to emulate a monolithic connection is a slow adoption and application toward utilization of the technology in bridge substructures. In contrast, ABC is a widely accepted process for constructing bridge superstructures, through such processes as Prefabricated Bridge Elements and Systems (PBES) and Slide-In Bridge Construction (SIBC),

among others. The process has been slow to prove adequate for the demands found within the bridge substructures. This requires the precast connections to perform equivalent to that of a monolithic structure. As ABC is made advantageous by its dependence on reducing onsite work it is required that such solutions for substructure connections be easily and quickly assembled while limiting the requirements of forming and pouring onsite.

1.2. PROBLEM STATEMENT AND MOTIVATION

Bridge substructures experience high demands of ductility and strength during seismic activity causing a large concentration of forces and deformations at pier connections. This has largely led to the use of CIP construction to produce monolithic connections within the bridge substructure to withstand the demand concentrated on the connections. Existing applications of ABC precast connections for purposes of emulating monolithic connections include rebar couplers, grouted ducts, pocket, and member socket connections. Which are tested and proven methods of successfully emulating CIP connections and meeting the demands within a bridge substructure subjected to seismic activity. The applications, however, are not without disadvantages as alignment issues have been a prevalent issue since the introduction of the technology and continues to cause problems for contractors due to the high precision and tight tolerances required. Such disadvantages can and have led to costly mistakes resulting in scrapping of precast elements requiring a recast or in some cases converting the design of the substructure to a CIP construction mid project.

As these issues have persisted, a need for a simpler more easily constructible solution has been sought by Idaho Transportation Department (ITD) bridge engineers. Through consideration of the high demands experienced by bridge substructure connections and the shortcomings of existing ABC applications for bridge substructure construction in areas of seismicity, a simpler

precast connection has been proposed. This connection needs to be experimentally explored and validated prior to implementation.

1.3. PROPOSED TECHNOLOGY

In this research, a simplified precast connection is investigated for use in precast substructure elements using a telescoping grouted steel pipe connection. The connection consists of a protruding hollow-structural-steel (HSS) pipe from the piers which is inserted into a larger HSS pipe cast in the footing and/or pier cap with a rubber bearing. Figures 1.1 and 1.2a below demonstrate the proposed connection in a pier-to-footing and a pier-to-cap connections, respectively. The pier pipe is fitted with centering fins to align it within the center of the foundation or cap pipe insert. After full erection of the piers and pier caps the voids between the HSS pipe are grouted in place. This requires minimal construction bracing. The simple proposed connection offers simplified construction, increased construction tolerances, improved safety, and provides increased erection speed. The cap as provided in Figure 1.2b demonstrate a hollow cap. The hollow cap is an option which provides for variability of project and construction site conditions. The cap can be constructed as hollow, partially hollow, or solid dependent on the available equipment, precaster abilities, or project limitations. The connection is comprised of non-proprietary elements allowing for improved detailing specifications. Additionally, the bearing placed between the pier and footing/cap allows for small deformation without cracking and crushing of concrete, thus providing slight dampening in a traditionally fully rigid element. The proposed connection is similar to Concrete Filled Steel Tube (CFST) presented by the Washington Department of Transportation Bridge Design (WSDOT) Manual (WSDOT 2019). The connection is intended to develop the full plastic moment capacity of an equivalent cast-in-

place section while outside of the connections the pier remains similar to that of a typical precast reinforced concrete element.

The moment capacity for the proposed pipe connection is dependent upon the pipe size and its material properties. The embedment depth of the pipe into the footing/cap is dependent upon the capacity of the CFST. The connection is dependent upon the bond between the concrete and the pipe to develop the moment capacities required. This approach required that the embedment length be calculated so as to fully engage the pipe strength within the connection. Two methods from existing literature are considered in this research, one from a Wasserman and Walker publication “Integral Abutments for continuous steel bridges” (Wasserman and Walker 1996) and the second from WSDOT Bridge Design Manual.

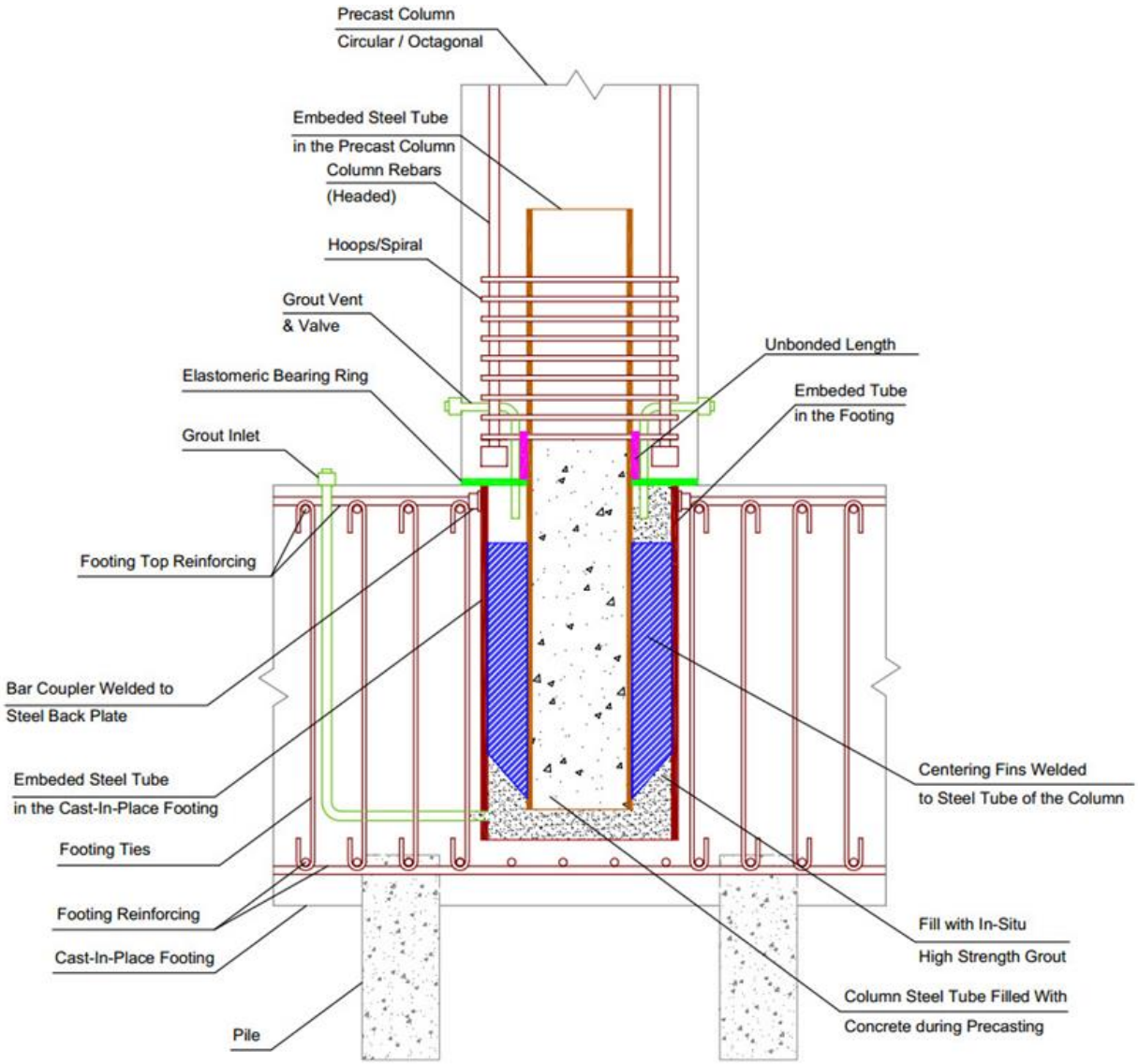

Figure 1-1: Pier-to-Footing Connection

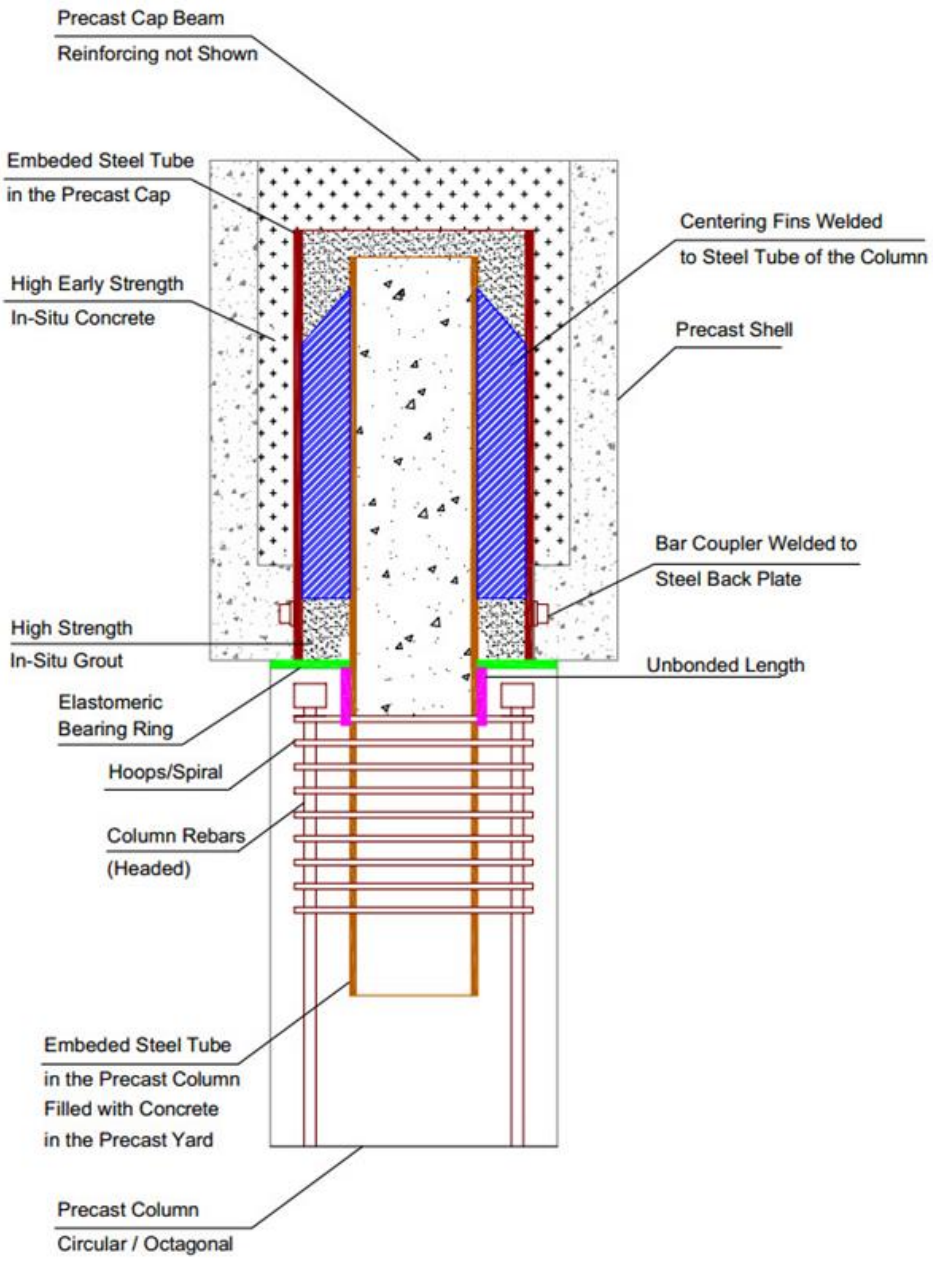

a) Pier-to-cap Connection

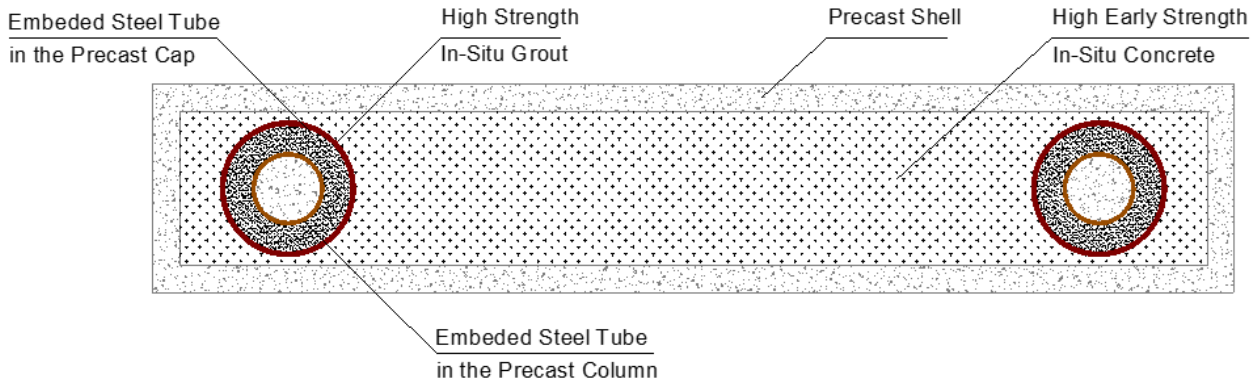

b) Cap detail

Figure 1-2: Pier-to-Cap Connection Details

1.4. OBJECTIVES

This research will focus on large scale testing of two pier bents systems to demonstrate the performance and ability of the proposed precast bridge substructure connection to emulate a monolithic structure. To achieve a successful experimental comparison, a CIP bent and precast bent of similar dimensions will be constructed and tested to compare the performance of the proposed precast connection to that of CIP construction under seismic loading.

Specific objectives of this research project are to:

1. Construct and test a large scale two pier bridge bent using CIP construction under quasi-static cyclic loading.
2. Construct and test a large scale two pier bridge bent using ABC and precast technologies implementing the proposed pier connection to experimentally validate the connections performance.
3. Compare the seismic performance of the proposed pier connection to the CIP constructed bent.

To accomplish objective 1 and 2, the two large scale specimens will first be designed in reference to typical mid- to long-span bridges common to Idaho. Following that the two specimens will be constructed and tested. Objective 3 will be accomplished through comparison of the experimental results and observations made throughout the full process of the first two objectives.

1.5. THESIS OVERVIEW

This research is a culmination of a multi-year project in conjunction with ITD to experimentally validate the proposed precast pier connection for adaptation as an ABC technology. It is divided into six chapters.

1. Introduction: A brief overview of the motivation and background that led to the research being carried out. Also, a short discussion of the research scope and objectives is presented.
2. Literature Review: In this chapter a review of existing ABC and precast technologies relevant to this project is provided.
3. Cast-In-Place Bent System: This chapter covers the development from design, construction, and experimental testing of the benchmark CIP bent.
4. Precast Bent System: This chapter covers the development from design, construction, and experimental testing of the precast bent incorporating the proposed precast connection.
5. Comparison of CIP Bent and Precast Bent Systems: A comprehensive comparison of the precast bent's performance to the CIP bent will be presented using the experimental and observational data collected throughout the research.
6. Conclusions and Recommendations: The final chapter summarizes the experimental results of the two systems and their performance comparison presented in Chapter 5.

Conclusions discussing the proposed precast connection's performance and ability to emulate CIP construction are discussed.

Also included are table of contents, figures, tables, and appendices. The appendices include construction drawings, design calculations, and material data sheets.

CHAPTER 2 LITERATURE REVIEW

2.1. INTRODUCTION

This Chapter provides a brief history of the development and application of ABC within the United States. It then highlights works of research into ABC applied in seismic regions. Various technologies are discussed and evaluated associated with bridge substructures. Many of these technologies were selected as they had similar experimental programs as that of the research performed on the proposed connection presented within this thesis. The research discussed provides examples of various ABC technologies presented and researched for the purposes of establishing ABC in seismic regions.

2.2. HISTORY OF ABC IN THE UNITED STATES

The rapid growth and development of the United States has continually pushed the importance of maintaining the existing infrastructure and pushing development of new infrastructure. As the country has grown at increasingly historic rates the resulting demand on the infrastructure has continually increased the need for maintenance and improvements. This driving demand has increased the need for innovative construction practices that can be applied in all environmental conditions, specifically seismic. Through this a number of programs developed to encourage the adoption of ABC and similar technologies were developed.

The Transportation Research Board (TRB) National Cooperative Highway Research Program (NCHRP) published two reports (NCHRP 1985, NCHRP 2003), first in 1985 and the second in 2003. The goal of the research was to apply the use of prefabricated elements for bridge construction, accelerating construction time and reducing costs. As the two reports covered a total of 18 years, new technologies were introduced and used in the industry. Many of

the motives stemming from using prefabricated elements are echoed through the associated advantages with ABC.

Starting in 2002 several preexisting groups worked to offer workshops encouraging the use of innovative technologies in construction. TRB Task Force on Accelerated Innovation in the Highway Industry (A5T60) formed in 1999 (FHWA, 2005) and AASHTO Technology Implementation Group (TIG) formed in 2000 collaborated with the Federal Highway Administration (FHWA) to offer Accelerated Construction Technology Transfer (ACTT) workshops. This initiative grew to offer more than 25 workshops in different states. TRB and TIG worked to identify and support development and use of ABC technologies in industry.

In 2009 FHWA began "Every Day Counts" (EDC), with goals to implement ready technologies and categorize them within highway infrastructure. This initiative has led to thousands of bridge projects using accelerated construction processes. In 2013, ABC-University Transportation Center (ABC-UTC) was established at the Florida International University. With association and collaboration of Iowa State University and University of Nevada, Reno (Mashal, 2015). ABC-UTC conducts various research in numerous areas of ABC and gathers ABC projects and research to provide ease of access to a larger industry audience to further ease implementation.

2.3. ABC RESEARCH IN SEISMIC ZONES

Mashal and Palermo (2019a) reported on findings in 2019 regarding experimental investigation on a low-damage seismic design for ABC. Low-damage seismic design is intended to reduce the resulting damage from seismic activity and eliminate the formation of a traditional plastic hinge near the interfaces of the pier connections. The design implemented an unbonded post-tensioned strand inside a precast pier. The pier interfaces at each the footing and cap are

fitted with externally mounted dissipaters of various designs. The low-damage seismic connection is shown in Figure 2.1 below. As can be seen from the image a steel jacket is used to further confine the pier end and assist to armor the pier from spalling while rocking. After the quasi-static experimental testing was completed no observable damage was present. The system also exhibited no post seismic displacement, as the unbonded tendon provides a self-centering action as lateral forces drop. As the experiment exhibited a successful innovation for an ABC precast system the design was used in the Wigram-Magdala Link Bridge in Christchurch, New Zealand. Since its completion the bridge has withstood a 7.8 magnitude earthquake and is still in use.

Figure 2-1: Low-Damage Seismic Connection Detail (courtesy of Mashal and Palermo 2019a)

In similar experimental research Mashal and Palermo (2019b) investigated two connection types in a single bent. The bent consisted of grouted ducts for the cap connection and a socket connection for the footing connection. The experiment consisted of two half-scale bent specimens constructed. One to simulate the traditional CIP constructed bent and the second to

demonstrate the effects of the grouted ducts and member socket connections. The connections performed well under the quasi-static loading during the experimental program with the grouted ducts connections at the cap far out performing the socket member connections at the footings. The performance of the grouted ducts is partly constituted to an unbonded length applied to the start bars, allowing for a larger area of the bar to deform during loading. The connection demonstrated less cracking and reduced spalling thus resulting in less strength degradation at the plastic hinges.

In 2015 Tazarv and Saiidi (2015) published their experimental work regarding the use of pocket connections in seismic regions. This research proved that with proper design among the components of the cap and pocket the effects of the pocket are negligible regarding seismic performance. This research further proved the ability of the pocket connection to emulate CIP connections. The research resulted in various iterations of pocket connection (Figure 2.2), that proved suitable for ABC practices.

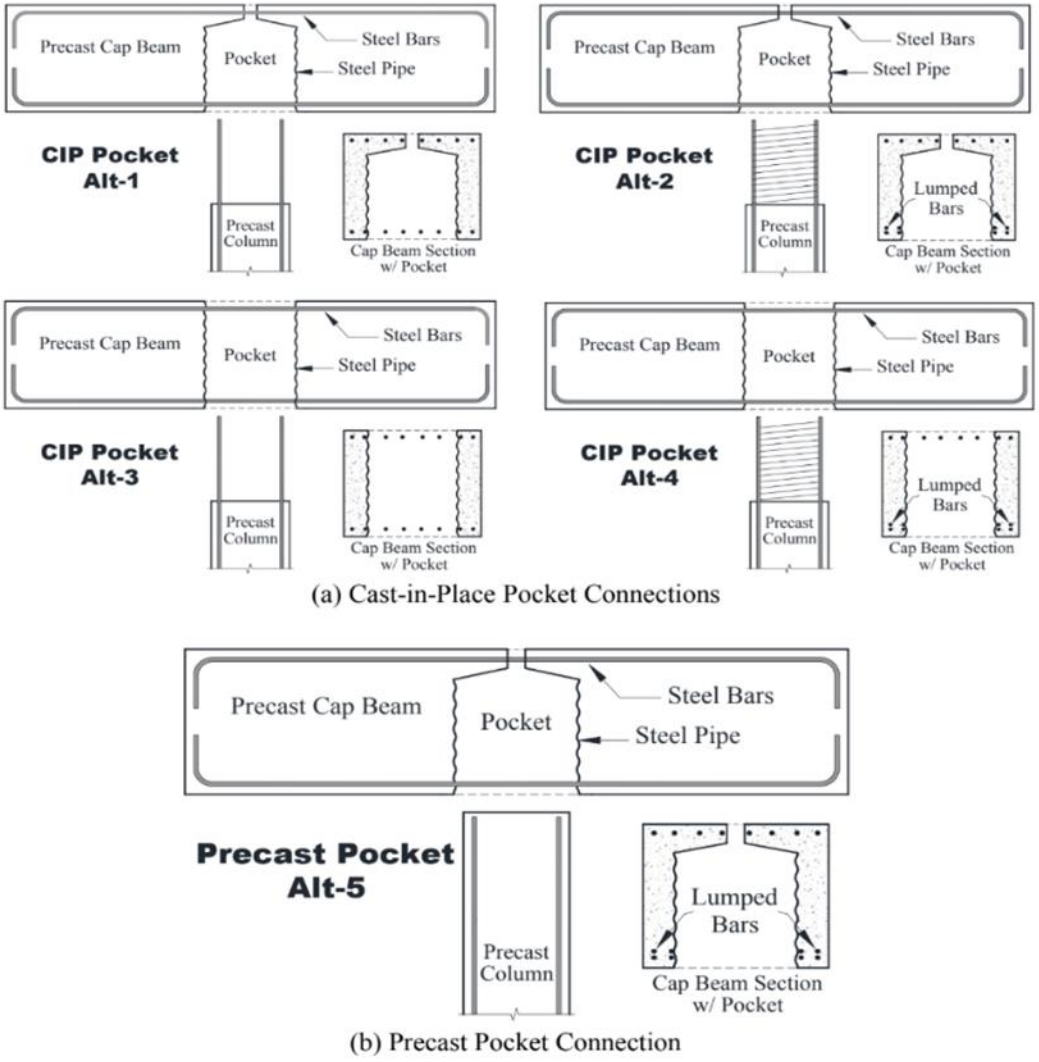

Figure 2-2: Pocket Connection Iterations (courtesy of Tazarv and Saiidi 2015)

Mehrsoroush and Saiidi (2014) investigated telescopic pipe pin connections as a footing application. The pipe pin is comprised of two steel pipes for shear and a single threaded rod for tension. A connection detail is provided in Figure 2.3, showing the many components of the pipe pin connection. The connections where use in a two-pier bent system having socket connections at the pier-to-cap interface. The full specimen detail is provided in Figure 2.4.

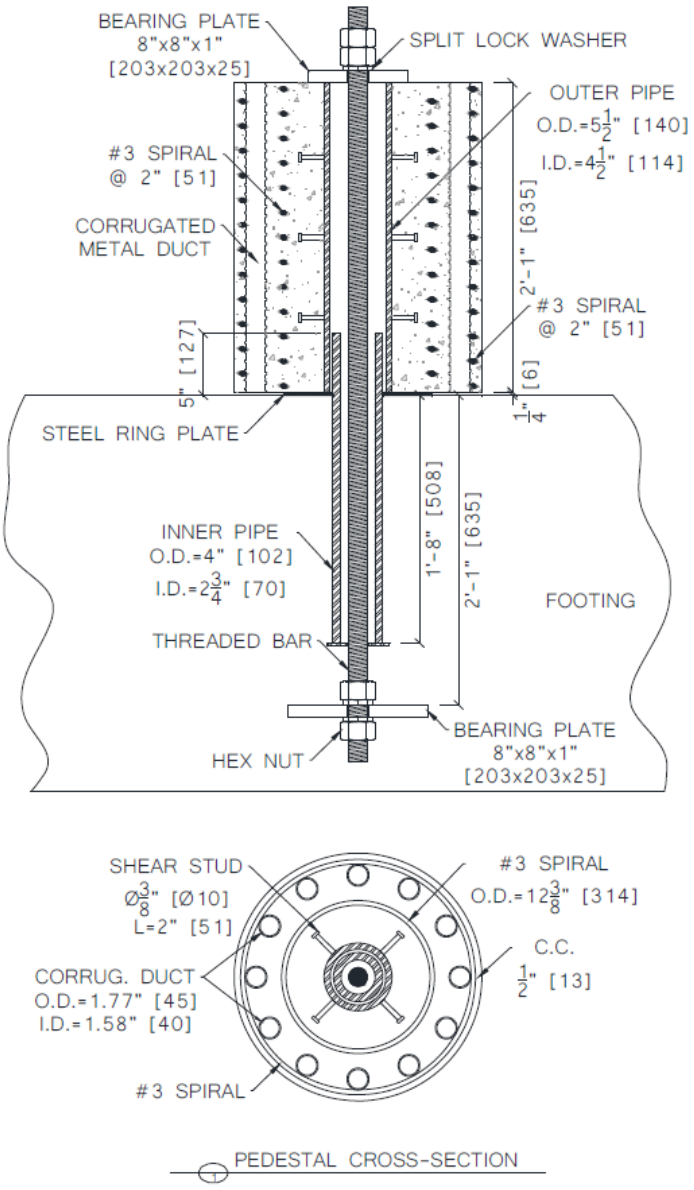

Figure 2-3: Telescopic Pipe Pin Connection Detail (courtesy of Mehrsoroush and Saiidi 2014)

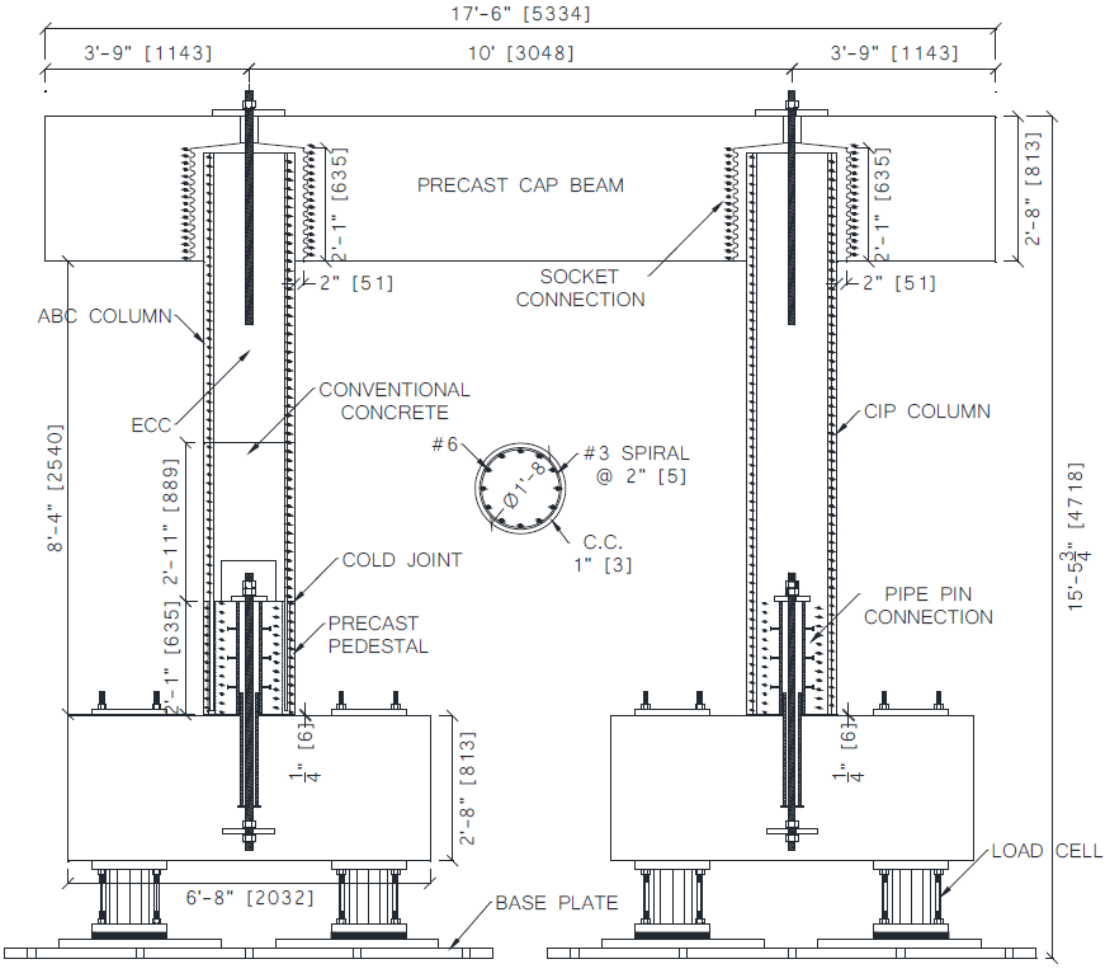

Figure 2-4: Two Pier Bent Specimen (courtesy of Mehrsoroush and Saiidi 2014)

The quasi-static experimental program showed the piers to reach 10% drift. However, the specimen with the pipe pin and socket connections did not achieve similar force levels to the comparative CIP specimen as debonding of bars in the upper half of the pier compromised the bent's overall strength. The connections did demonstrate reduced damage within the plastic hinge region.

Grouted duct connections are another innovative connection that has been established for ABC applications. Often used for pier connections in both the footing and cap, with uses as

element connections as well. The connection has been established as a competent connection for use in both seismic and non-seismic regions. Grouted ducts have become increasingly popular within the bridge construction industry. However, the connections do have associated difficulties. Grouted duct connections require very tight tolerances during fabrication and construction, as they require a high number of rebar to align across multiple bridge elements. Careful attention to detailing is required through the full process involving grouted ducts. Research works include Brenes et al. (2006), , Haraldsson et al. (2011, Restrepo et al. (2011), Ebrahimpour et al. (2016).

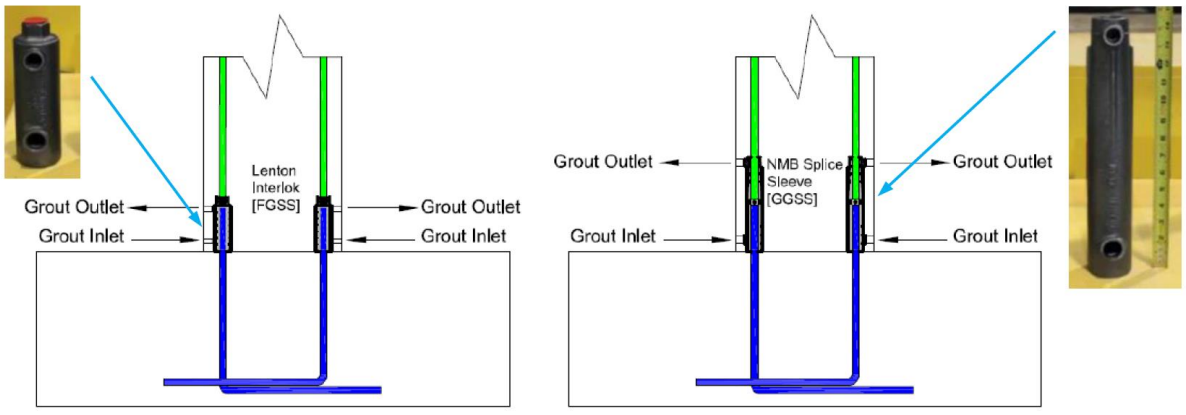

Figure 2-5: Typical Grouted Duct Connections (courtesy of Ebrahimpour et al. 2016)

2.4. CONCLUSIONS

The United States and countries such as New Zealand have made an asserted effort to continue to integrate the construction industry with innovative techniques and processes. This has further encouraged ground breaking research in the areas of innovative bridge construction process incorporate the ABC approach. This research presents various iterations of connections and designs suitable for the adaptation of precast in moderate to high seismic regions. Many innovative process and designs are continually developed and researched with goals of further

applying ABC and similar practices to industry. The research presented here is also aimed to further improve precast connections and simplify the construction process as a whole.

CHAPTER 3 CAST-IN-PLACE BENT SYSTEM

3.1. INTRODUCTION

This chapter presents design, construction, and experimental testing of a CIP bent system with the intention of establishing a performance level in which to compare the precast bent system (Chapter 4) using the proposed pier connection. A review of the construction process is thus presented discussing the challenges faced during a CIP construction project and the work required. The full testing arrangement used for the experimental work is presented and discussed. Followed by the experimental testing carried out on the system and its resulting performance.

3.2. SPECIMEN SIZING

The first steps in developing the specimen is the determination of the overall size of the specimen. As the research aims to test the proposed connection at a large scale, the specimen sizing is determined near the maximum capacity of the testing facility, Idaho State University Structural Laboratory (SLAB). The overall specimen itself is considered to be sized as a scaled version of a typical mid-to-long span bridge constructed in south-east Idaho. South-east Idaho is proposed to be the place of construction; as it is the most seismically active area of the state where the proposed connection is to be used. An example of a typical mid span bridge in south-east Idaho is presented in Figure 3.1. This particular bridge is constructed over the Bear River south of Preston, Idaho about 70 miles south of Pocatello, Idaho.

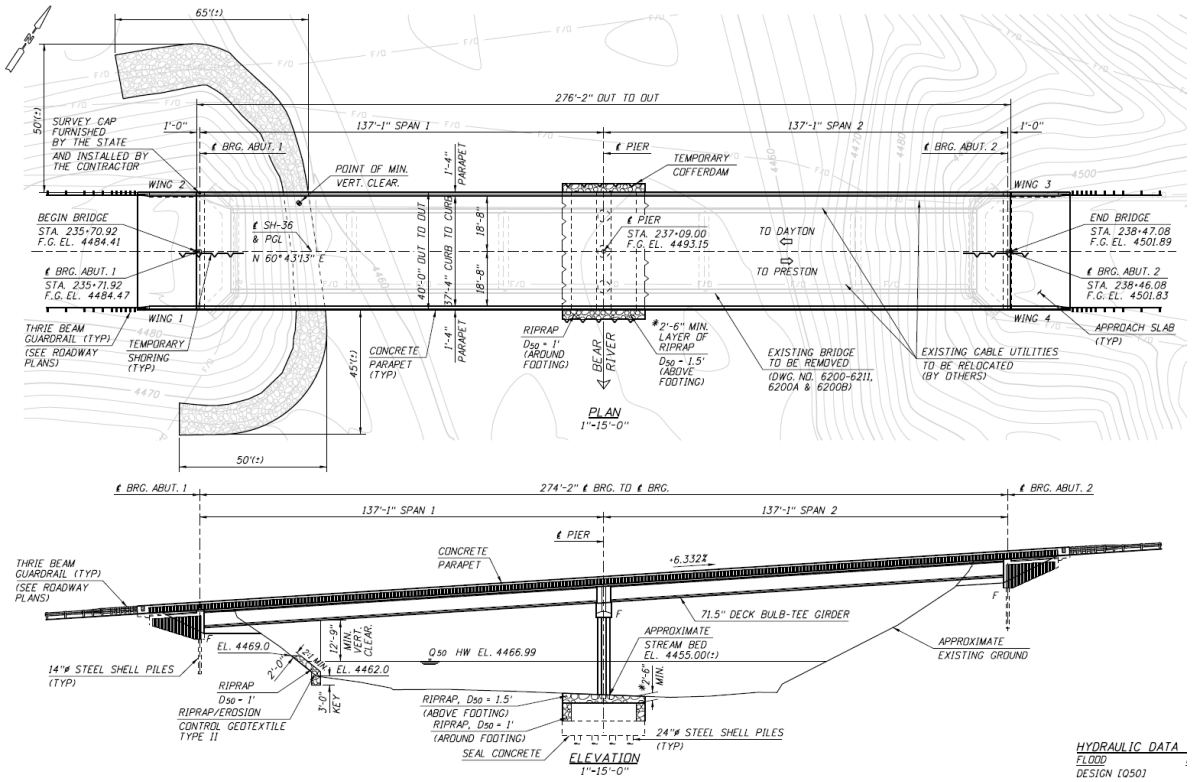

Figure 3-1: Elevation and Top View of SH-36 Bridge over Bear River

The bridge consists of two sperate spans of lengths 137 ft.-1 in. each. Each span is set between the bridge's abutments and a center bent system located approximately in the center of the river. The bent system is comprised of three octagonal piers measuring 4 ft. in width and having an overall height of 29ft.-3in. The pier cap measuring 40 ft. in length, 5 ft. wide, and 4 ft.-6 in. deep and the foundation being 40 ft. in length, 22 ft. wide, and 5 ft.-6 in. deep. A detail of the bent is provided in Figure 3.2. In reference to the general element ratios within a typical bent system, the sizing and capacity limitations within SLAB, and consideration of embedment depths required for the proposed precast connections, discussed in Chapter 4, the size of the bent specimen was determined.

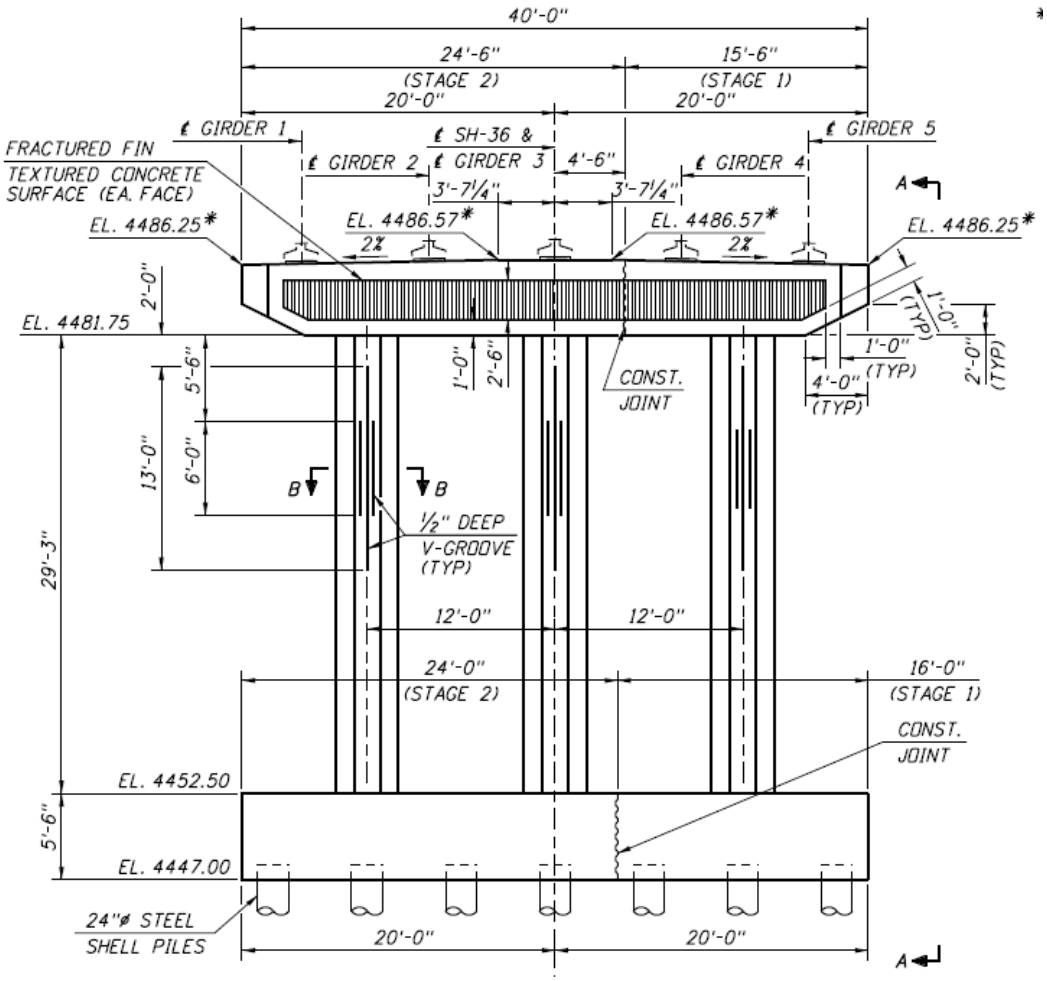

Figure 3-2: Bear River Bent System Elevation View

Through the consideration of the capabilities within SLAB, maximum dimensions were established for a height of the specimen and associated setup to not exceed 13 ft. and the specimen's overall length not to exceed 15 ft. After factoring in the items required for loading and monitoring the specimen during testing, the specimen height was determined to be 11 ft. in total height and have a pier cap length of 15 ft. For determining the depth of the pier cap and footing segments consideration of the embedment required by the HSS pipe in the proposed precast connection had to be considered in order to achieve similar dimensioning between the CIP and precast bent systems. Through this a required depth of 2 ft-6 in. is necessary for both the

footing and pier cap. The footing width and length is determined based on the layout of the SLAB strong floor which has embedded anchors in an 18 in. x 18 in. square pattern throughout the floor. Considering the centrally located pier in each footing and providing adequate anchorage the footings are required to be 4 ft. x 4 ft. square.

For sizing of the piers, past experiments performed in the lab were considered to determine the final width. Previous experiments on single piers acting as cantilevers had been performed with a pier width of 18 in. with steel reinforcing ratios of 2% (ρ=2%). While also attempting to match the capacity of the previous experiments a reduced pier width of 14 in. was determined suitable; as the bent system would produce higher demands during testing than that of previous cantilever piers tested. From the pier width and consideration of cap reinforcing and cover concrete a 2 ft. width for the cap is necessary. Through consideration of the lab limitations, past experiments, typical bent ratios, and requirements for the both the CIP and precast specimen the resulting specimen depicted in Figure 3.3 is determined.

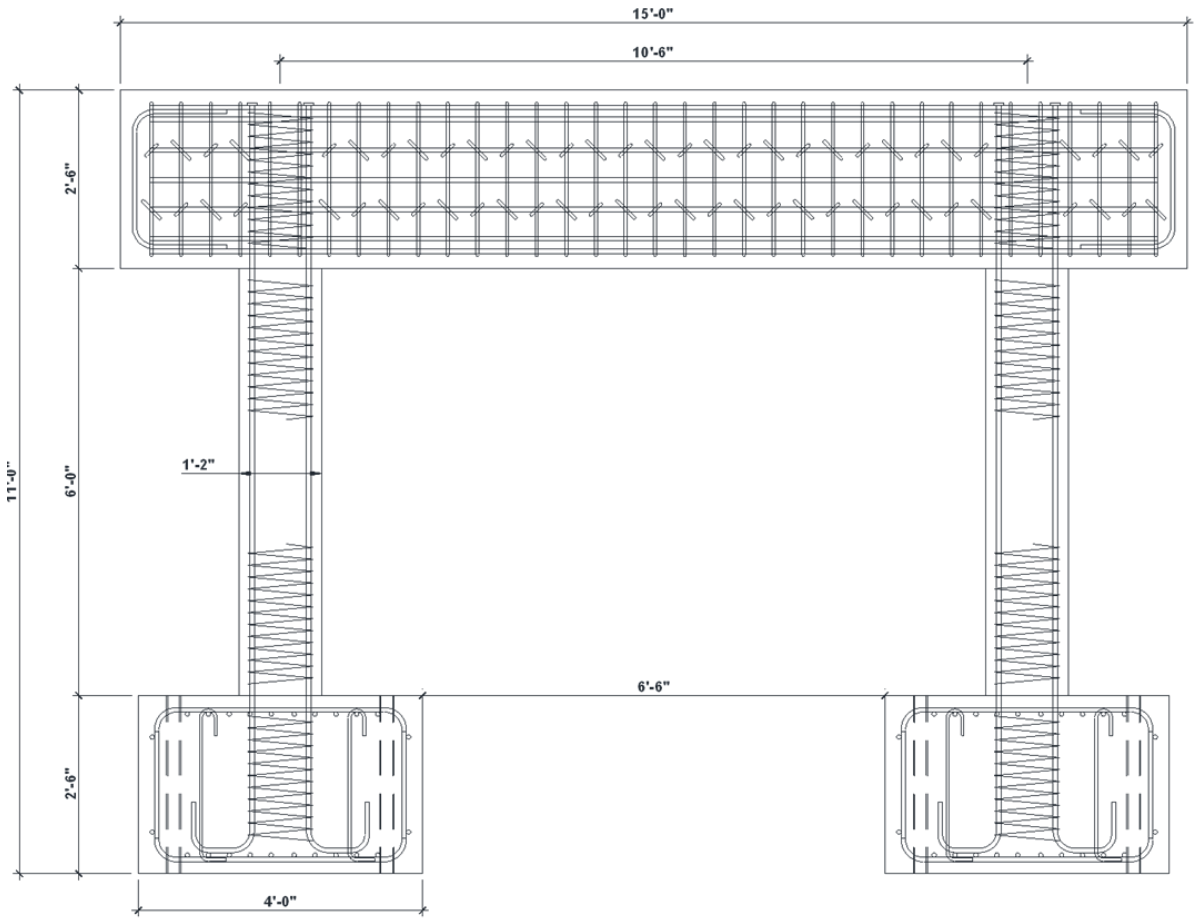

Figure 3-3: CIP Bent Specimen

3.3. CAST-IN-PLACE BENT DESIGN

After establishing the overall specimen dimensioning to accommodate the limitations and experimental goals, the design of the system is performed. For properly designing the bent the 8th Edition of AASHTO LRFD Bridge Design Specification (AASHTO 2017) is considered. Through the design process the reinforcing steel is determined for accomplishing the targeted strength of system. An analysis of the lab capabilities and past experiments deemed a safe target strength of 60-70-kip force applied during testing as an achievable target force applied to the bent system.

Considering each individual pier as an individual system comprised of two connections, pier-to-footing and pier-to-cap, each contributing to the overall strength of the bent system, an approach which considers each connection to constitute 25% of the overall pushover force required for the system was established. Considering the previously established safe operating force for the lab (60-70-kip) a target force of 15-kip is considered for the design of each pier connection. This 15-kip force is considered as the base shear force for each connection. With a reinforcing ratio of 2% (ρ=2%) determined the longitudinal reinforcing steel is determined to be seven #6 Grade 60 rebar. Grade 60 rebar has a yield strength of 60 ksi and modulus of elasticity of 29,000 ksi. Additionally, in accordance with AASHTO (AASHTO 2017) design a continuous reinforcing spiral is provided throughout the length of the pier. The #3 Gr. 60 reinforcing spiral is broken at both the pier-to-footing and pier-to-cap interface, with the spiral continuing in both the footing and cap for the full length of the longitudinal reinforcing. The #3 spiral is terminated at each end by mechanical splice. The #3 spiral is spaced at a constant pitch of 1.5 in. throughout the full length of the longitudinal reinforcing. The required cover concrete of 1.5 in. is provided between the reinforcing spiral and pier surface.

The resulting connection capacity is thus calculated considering a concrete with compressive strength, f'_c, of 4,000 psi. The pier design moment capacity of approximately 61.7-kip-ft. is calculated. Considering the loading height to the actuator center of 83-3/4 in. from the footing surface, the resulting design base shear is 8.8-kip. With an ultimate base shear of 13.6-kip. Which is 91% of the target base shear per connection as discussed above. Note threaded terminators are used in the cap to develop the required embedment strength where reinforcing congestion makes it difficult to utilize hooks or bends for producing

development length. A pier cross-section is provided in Figure 3.4 below, with a pier detail in Figure 3.5.

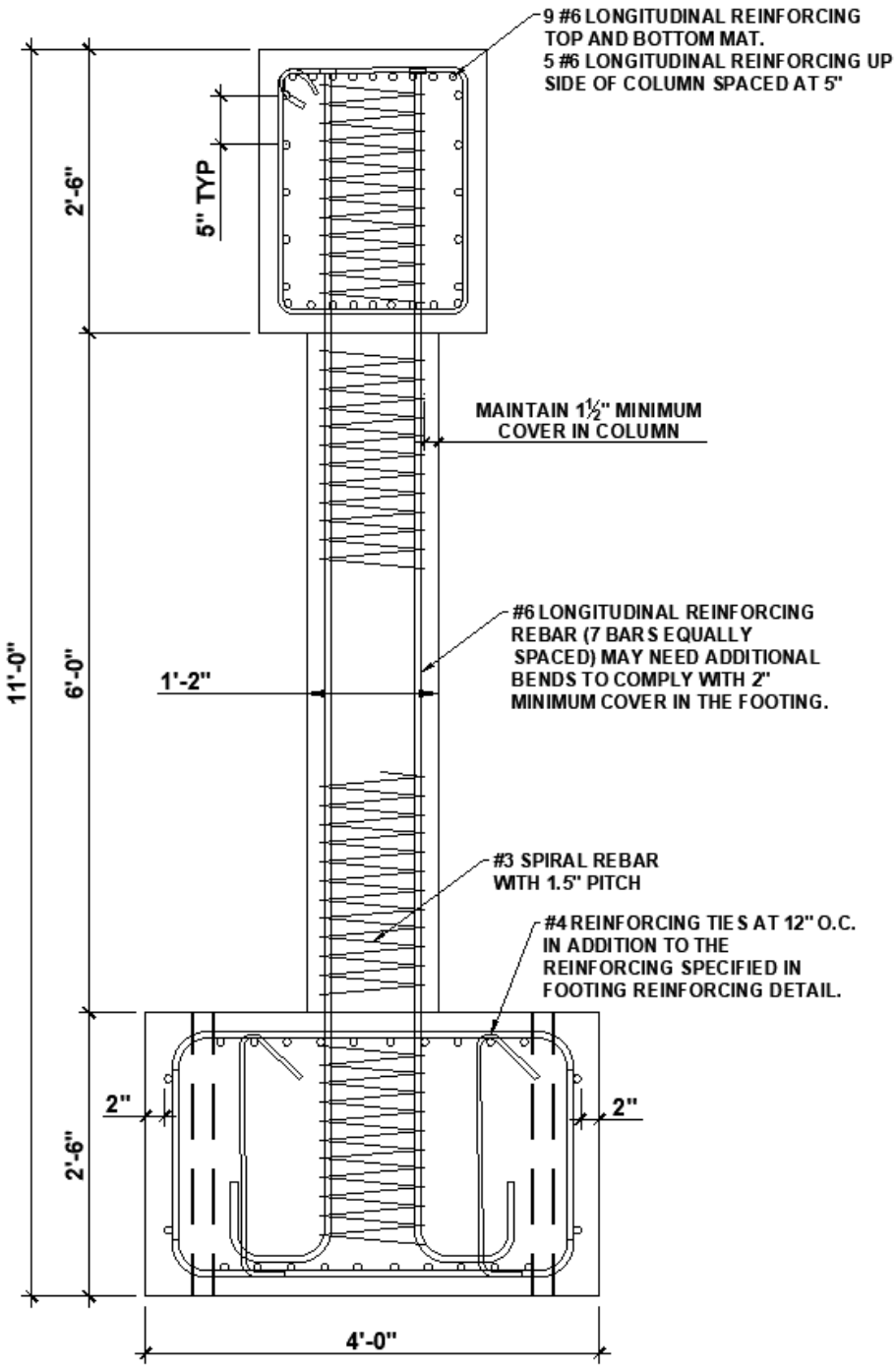

Figure 3-4: CIP Pier Cross-Section

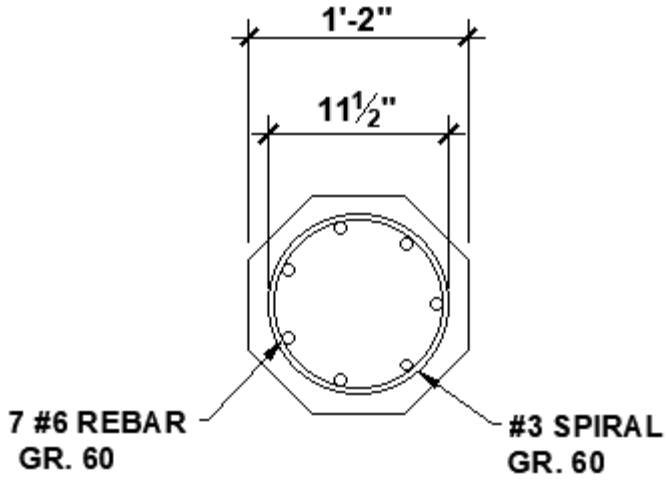

Figure 3-5: CIP Pier Detail

For the cap design, a computer modeling program, SAP-2000, is used to determine the required moment and shear demands experienced by the cap. The full bent is developed from the footing surface up. As the experiment is being carried out as an investigation of the pier connections a conservative approach toward designing the pier cap is taken in order to ensure the failure is forced to the four pier connections. The resulting moment and shear demand within the cap are 340-kip-ft. and 111-kip, respectively. As a conservative approach is taken to ensure failure is forced to the piers the design moment and shear is taken to be 500-kip-ft. and 150-kip, respectively. The design process using concrete of compressive strength 4,000 psi, of the beam yields a required 11 #6 Gr. 60 rebar be provided top and bottom with #4 Gr. 60 stirrups provided 4 in. center-to-center spacing. Additionally, as per ITD general practice two alternating #4 Gr. 60 cross-ties are provided for each stirrup. Figures 3.6 and 3.7 provide the final CIP cap beam drawings.

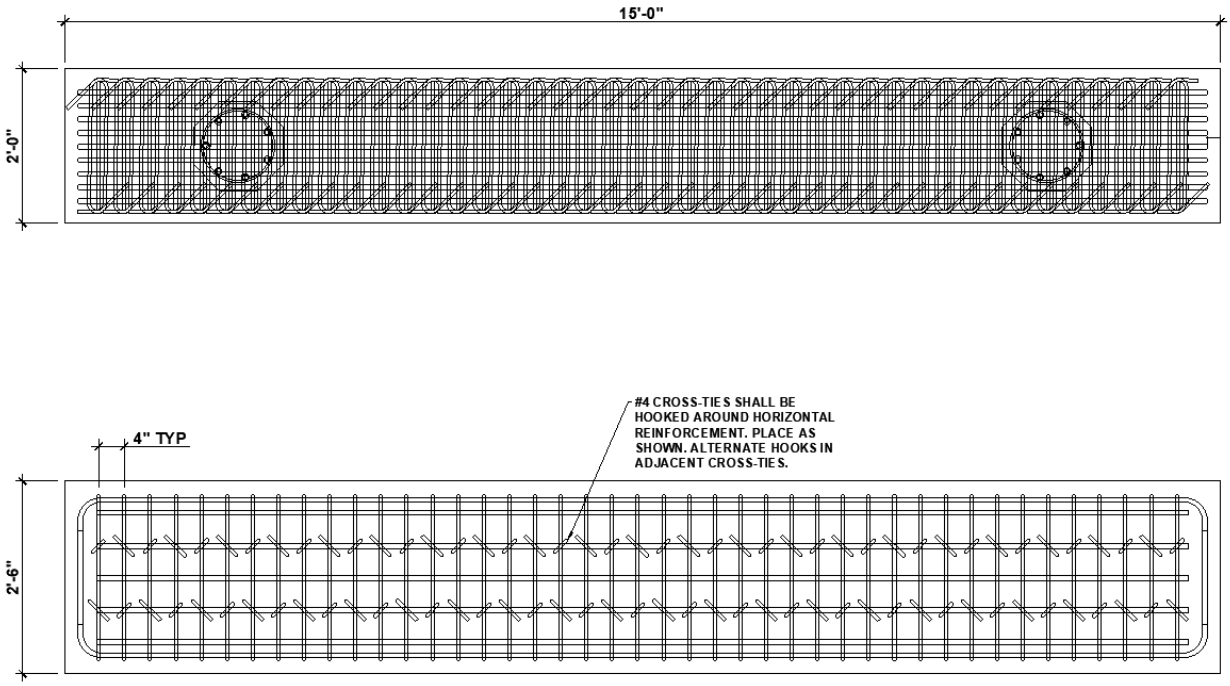

Figure 3-6: CIP Cap Beam

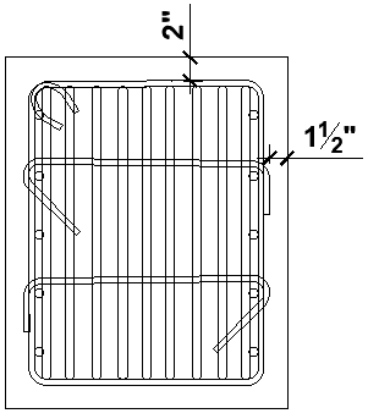

Figure 3-7: CIP Cap Beam Cross-Section

The footings are similarly designed in a conservative fashion to ensure failure is forced into the pier. As the footing dimensions are largely controlled by the lab and proposed precast connection requirements, the reinforcing is determined as 10 #6 Gr. 60 rebar provided top and

bottom in each direction. Using Response-2000 the footing is calculated to have an ultimate moment capacity of 532-kip-ft. Providing a significant factor of safety over the moment demand created by the pier connection. Figure 3.8 provides a top view of the footing and rebar layout for the bent system.

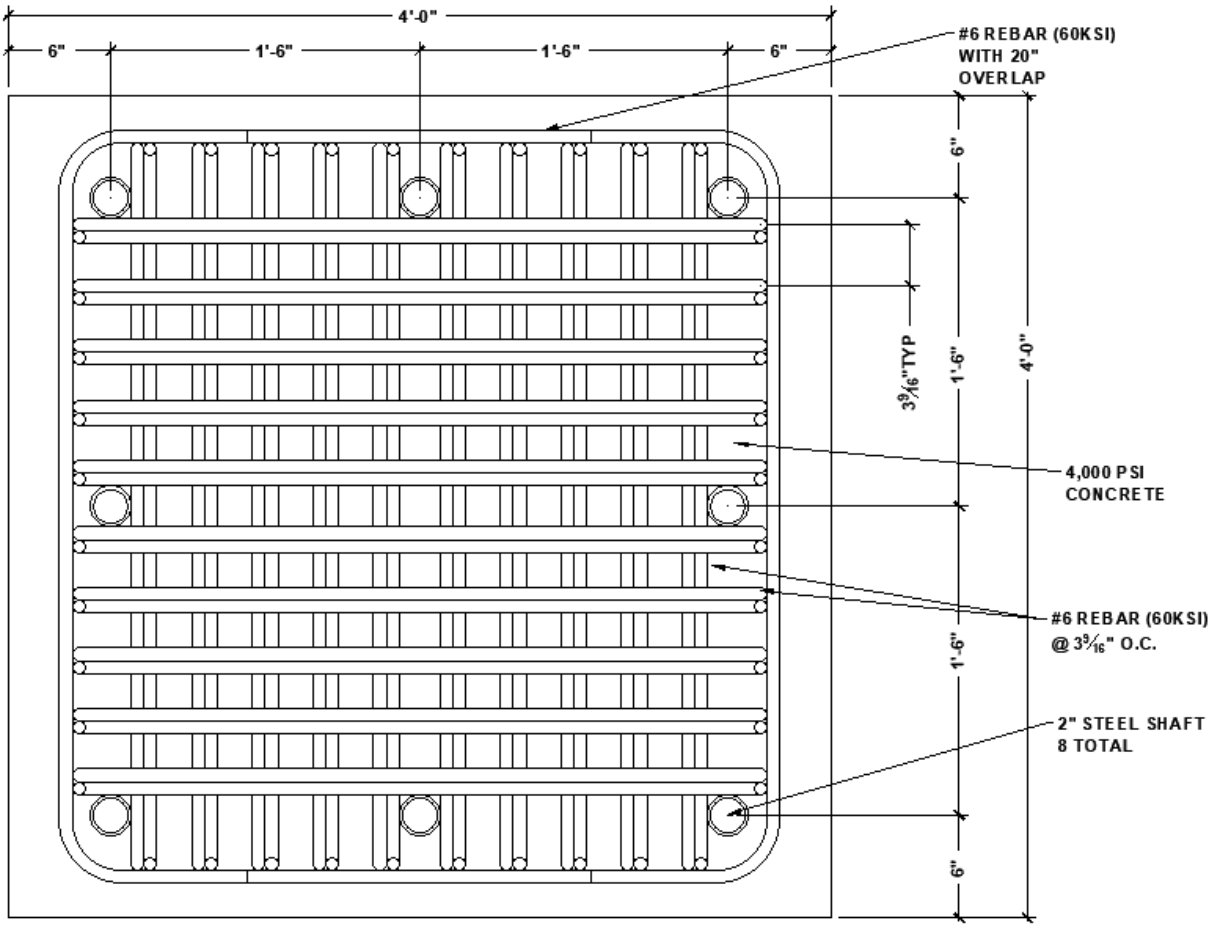

Figure 3-8: CIP Footing

3.4. CONSTRUCTION

After determining the final dimensioning and design details the CIP construction began. Typical CIP construction is performed completely onsite with multiple in-place concrete pours taking place. For construction of a bent substructure there are three main pours,

footing, piers, and cap. Forming and rebar fabrication are performed simultaneously throughout the construction. Wood form work is determined as a suitable material as it can serve for both the bents constructed and is considerably more cost effective and less labor intensive than producing steel forms for two specimens.

The footing, longitudinal, and spiral reinforcing in the pier is prepared as a singular cage for each individual pier (Figure 3.9). The pier cage is prepared and then lifted into the lower rebar mat of the footing (Figure 3.9a/3.9b) with the upper mat finished last (Figure 3.9c). After the footing and pier are completed the sleeves are placed for the floor anchors (Figure 3.9d). Finally, the concrete is placed, courtesy of Pocatello Ready Mix, finishing the footings up to the pier-to-footing interface (Figure 3.9e) The interface where the pier is to be poured is left rough to assist in bonding. The total concrete order for pouring of the footings was 3.25 cubic yards.

a) Pier Cage

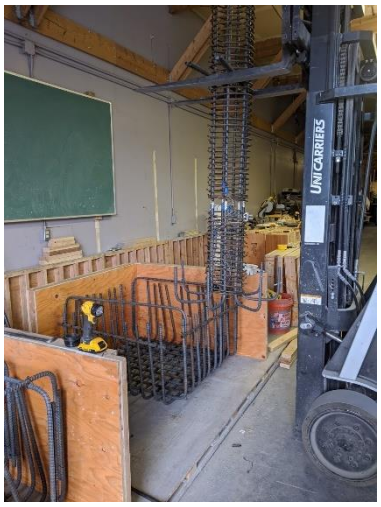

b) Placing of Pier Cage

c) Tying of Top Mat

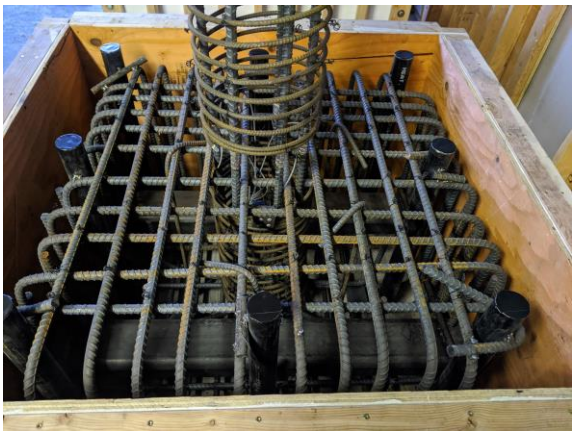

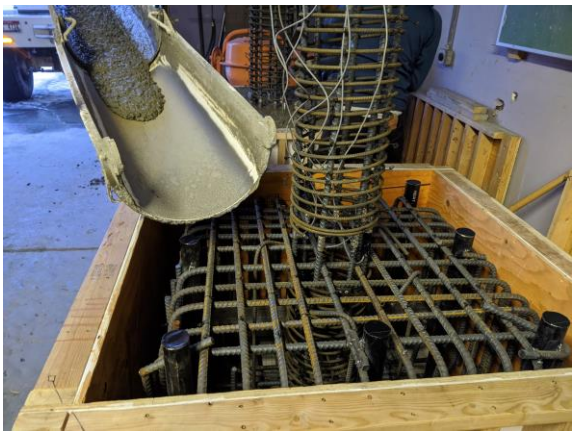

d) Anchor Sleeves **e) Footing Pour**

Figure 3-9: CIP Footing Construction

After footings have adequately cured the form work is removed and are relocated to the SLAB where they are anchored in place (Figure 3.10). The pier spiral is checked for proper placement and secured. For the pouring of the piers in order to follow proper concrete placing procedures the pier form work is built in two 3 ft. segmental sections, which can be assembled during pouring. This ensures the concrete is not dropped at too great a distance resulting in segregation and ensuring proper vibrating is accomplished throughout the full pier. The full 6 ft. of the two piers are poured so as not to have a cold-joint present in the length of the pier. At 7 days the pier formwork is removed allowing for the cap pour preparation to begin (Figure 3.11). The pour for the two piers was a total of 1 cubic yard.

Figure 3-10: CIP Footing Placement

Figure 3-11: Completed CIP Piers

As the cap has to be poured in the lab at a height of 8 ft-6 in. false-work for supporting the concrete during initial curing is necessary. Making use of existing items in the lab proved the

most efficient manner in which to construct false-work. Figure 3.12 provides a view of an assortment of reaction frames and sections serving to provide the necessary false-work for completing the cap pour. The cap reinforcing cage is started on the ground (Figure 3.13a) and lifted into place over top the longitudinal pier reinforcing (Figure 3.13b). Then the final stirrups, cross-ties, form-work, and false-work is placed for pouring (Figure 3.13c).

Figure 3-12: Cap False-Work

a) Cap Cage **b) Cap Cage Placement**

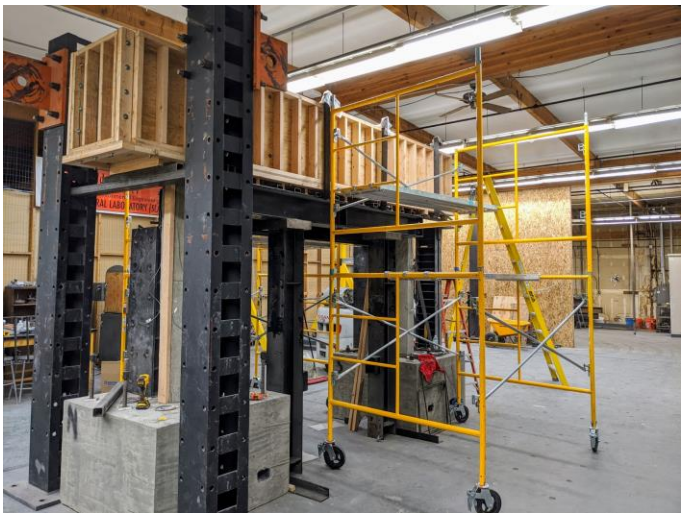

c) Cap Complete False-work, Cage, and Form-work

Figure 3-13: CIP Cap Construction

The full cap, measured to be a total of 75 cubic feet of concrete and estimated to weigh 11,000 lbs., is completed in a single pour to eliminate cold joints (Figure 3.14). The completion of the cap marked the final pour required for the construction of the CIIP bent system. The total CIP bent is constructed of approximately seven cubic yards and estimated to weigh in the range of 26,500 lbs. to 28,000 lbs. After the cap had adequately cured the false-work and form-work is removed, the specimen is painted, and prepared for instrumentation (Figure 3.15).

Figure 3-14: Completed Cap Pour

Figure 3-15: CIP Bent Prepared for Instrumentation

3.5. TESTING ARRANGEMENT

After the CIP bent construction is completed the testing arrangement is erected. For the purposes of testing the connection, a uniaxial load is applied in the transverse or perpendicular direction of the bridge deck. The purpose for loading in this direction is due to a full bridge structure being weak in the transverse direction. This is based upon the assumption that a full bridge, including the superstructure, has significantly higher resistance to loading parallel to the superstructure as the bridge abutments provide adequately stable resists to such loading. An additional vertical load is applied to the system during the entire testing procedure serving as a gravity simulant.

The lateral load is applied cyclically in accordance with the American Concrete Institute (ACI) (ACI Committee 374 2013) via a hydraulic servo-valve actuator. The actuator is a 2.5 gallon-per-minute (gpm) servo-valve actuator with a total achievable stroke of 24 in. A 225-kip tension/compression loadcell is mounted in-line with the horizontal actuator in order to monitor the actuator force through the experiment. The actuator is mounted horizontally to the lab's reaction frames. The reaction frames are comprised of two identical piers fabricated of steel channel, C12x30, laced together with 0.25 in. flat plate. Additional channel and wide flange angle bracing are provided to support the piers. In total the reaction frame is anchored to the floor via twenty-four 1 in. diameter high strength threaded rods (Figure 3.17). The head of the actuator is attached to the cap beam using four 1 in. diameter 120 ksi all thread. During casting of the cap, embedded anchors were fabricated into the cap end. The embedded anchors were provided additional anchoring support in the cap via high strength threaded rod connected to an anchoring plate embedded 12 in. into the cap beam (Figure 3.16). The specimen itself is secured

rigidly to the SLAB strong floor using nine 1 in. rods. The foundations are assumed to be rigidly fixed disallowing soil-structure interaction effects during the testing.

Figure 3-16: Actuator Cap Anchors

The final aspect of the testing arrangement is the application of the gravity load applied vertically at the center of the cap beam. The vertical force of the gravity load corresponds to 4.5% of the axial compressive capacity of the piers. Typically, the target gravity load is 5% of the axial compressive capacity of the specimen, but due to equipment limitations and the limited 3000 psi hydraulic pump the highest achievable axial ratio is 4.5%. For the two 14 in. piers of 4 ksi concrete, the gravity load is determined as approximately 60-kips. The equation for determining the gravity force is given as:

$$\boldsymbol{Gravity\ Force = 0.045\left(A_g f'_c\right)} \qquad \textbf{(3-1)}$$

Where A_g is the gross cross-sectional area of the two piers and f'_c is the compressive strength of the concrete, provides the determination for the gravity force.

The gravity force is applied using a 100-ton 4 in. hollow jack, gravity cylinder. The jack is place on the bent cap, a 225-kip tension/compression loadcell is stacked on top of the jack, and a reaction beam is placed across the top of the loadcell. Two high strength all thread bars are used to bolt the reaction beam to the floor to provide the resisting downward force to the cap, referred to as “gravity bars”. The full test setup is provided in Figure 3.17 below.

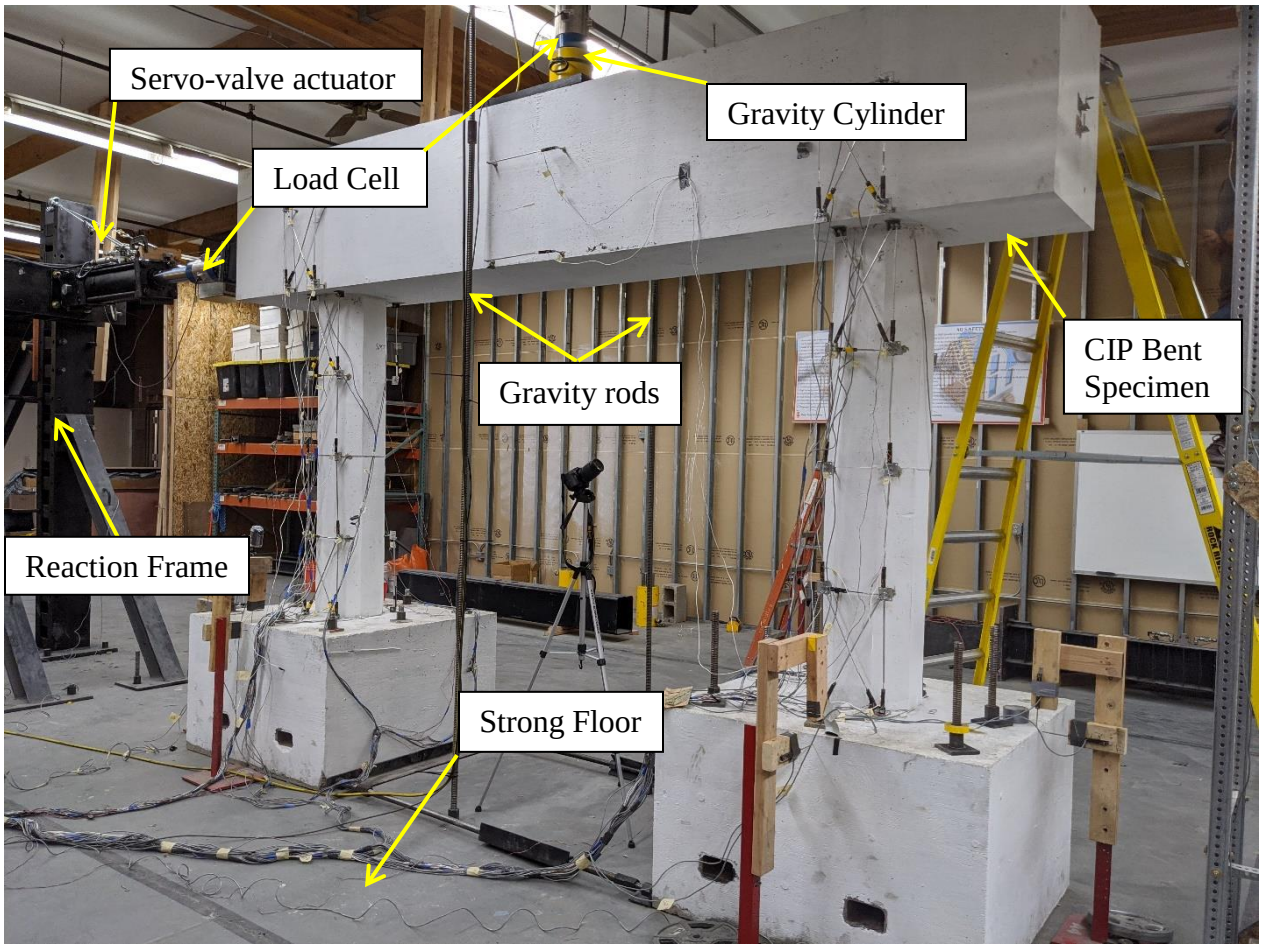

Figure 3-17: CIP Bent Testing Arrangement

3.6. INSTRUMENTATION

Throughout the experiment specific measurements of the system are monitored in order to document the specimen’s response and characterize its overall performance. Various instruments

are used during the experiment including loadcells, linear potentiometers, string potentiometers, and strain gages. The instruments are programmed using a Campbell Scientific data acquisition system. The system is uniquely programmed for all the various instruments, and set to take five readings per second throughout the entire experiment. A total of 95 instruments are used during the experiment. Figure 3.18 provides a visual of the instrumentation layout on the CIP specimen. Note all instrumentation specifically associated with either the north or south pier are indicated as “XX-N” and “XX-S”, respectively.

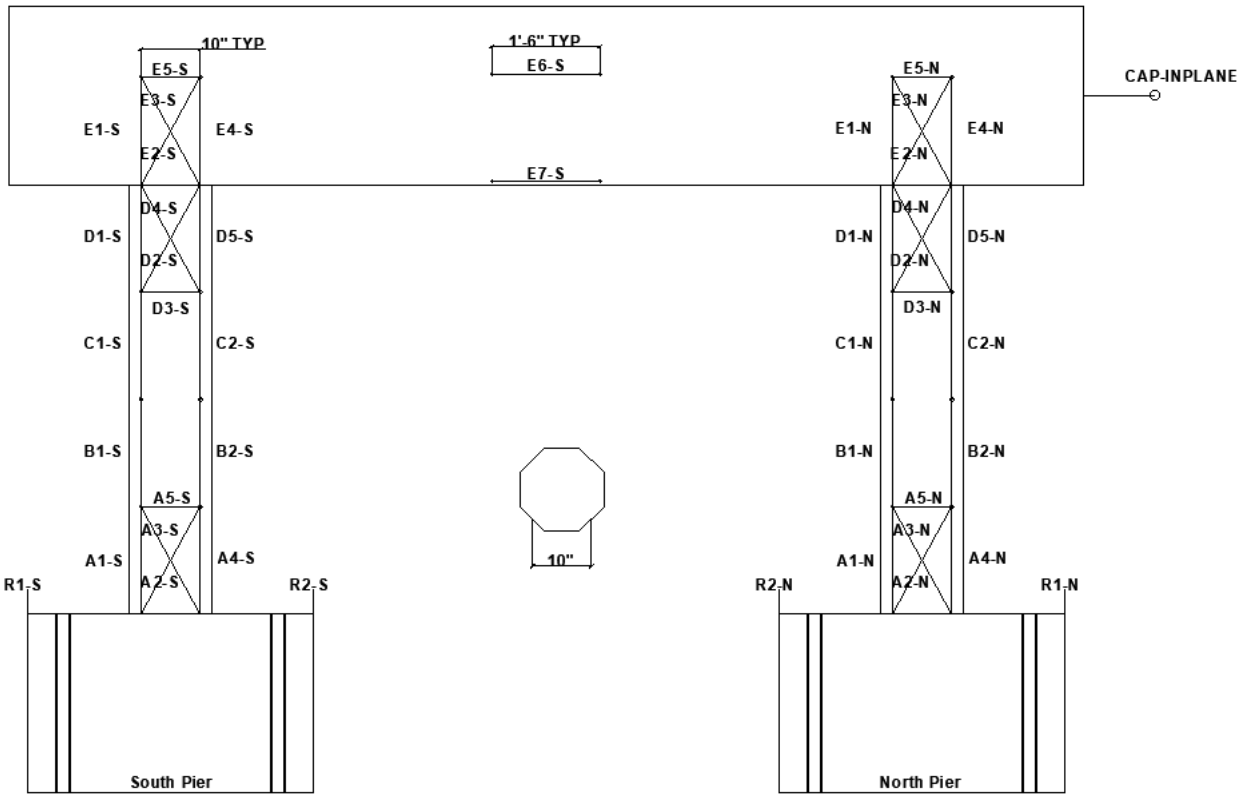

a) Front Elevation

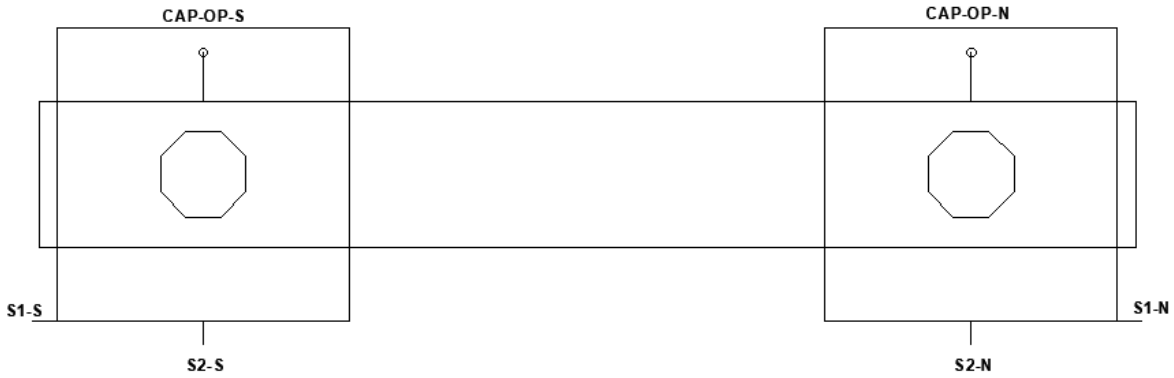

b) Top View

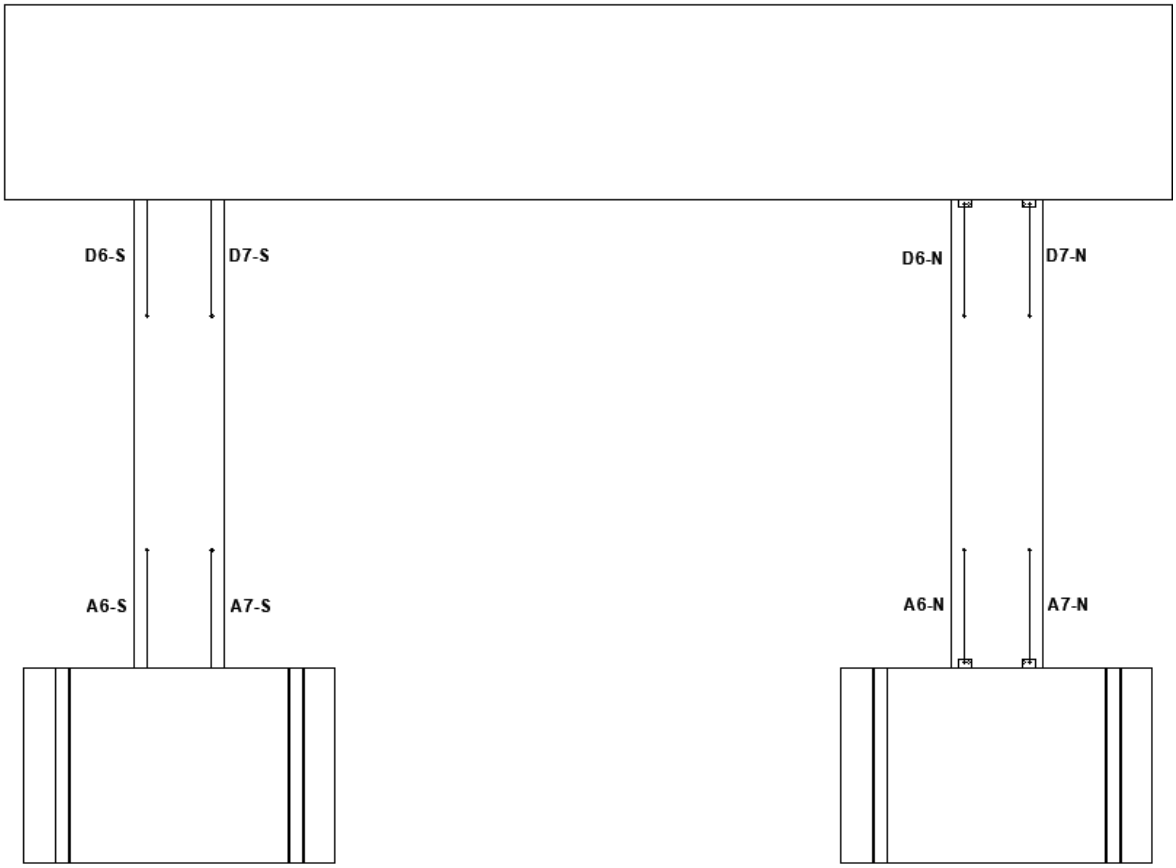

c) Rear Elevation

Figure 3-18: CIP Instrumentation Layout

Specific instruments are mounted as such to measure the global movement of the specimen. These instruments are mounted independently of the specimen and test arrangement in order to provide a true displacement of the specimen. The instruments mounted independently include CAP-INPLANE, CAP-OP-S, CAP-OP-N, R1-N, R2-N, R1-S, R2-S, S1-N, S2-N, S1-S, and S2-S. The instrument labeled CAP-INPLANE is a string-potentiometer, used to measure the true displacement of the cap. It is mounted directly at the center of the actuator on the opposite end of the cap beam. As it is assumed the cap does not experience any noticeable compression during testing, this measurement is used as the true displacement of the specimen. CAP-OP-S and CAP-OP-N are string potentiometers used to monitor the out-of-plane motion of the cap. These measurements are predominately monitored to ensure the cap does not move excessively to one side or the other during testing. Monitoring of this measurement reaffirms the stability of the specimen throughout the experiment and helps to monitor the risk of out-of-plane collapse. Linear spring potentiometers are used for measurements R1-N, R2-N, R1-S, R2-S, S1-N, S2-N, S1-S, and S2-S. The "R" refers to "rocking" as these instruments are mounted vertically, or parallel to the piers, to monitor any lifting of the footing edges, both in- and out-of-plane. Similarly, "S" refers to "sliding" as these potentiometers are used to monitor sliding of the footing in both the direction of loading and the transverse direction. Additionally, a string potentiometer is attached to the actuator to confirm the true stroke of the actuator itself. As this is a non-independently mounted instrument it is simply used to confirm the motion of the actuator head.

Instruments occupying groups "A" through "E" are comprised of both linear spring potentiometers and linear potentiometers with aluminum extensions. The group "A" potentiometers monitor the plastic hinge zones located at the base of each pier. Group "D" and

“E” potentiometers monitor the plastic hinge zones located at the top of each pier. Groups “B” and “C” are used to monitor any curvature experienced by the pier falling outside of the plastic hinge zones.

Additionally, two 225-kip tension/compression loadcells are used to monitor the lateral load and vertical gravity load induced on the specimen. Finally, strain of the rebar is monitored using strain gages. Strain gages are attached to the longitudinal reinforcing bars just above the pier-to-footing interface and just below the pier-to-cap interface prior to pouring concrete.

3.7. LOADING PROTOCOL

As mentioned earlier the loading protocol for the specimen is determined in accordance with the ACI (ACI Committee 371 2013). The peak amplitude values of the quasi-static cyclic loading protocol is determined based on the yield displacement of the bent itself. Figure 3.19 shows the loading protocol given as a graph of cycle number verse drift ratio.

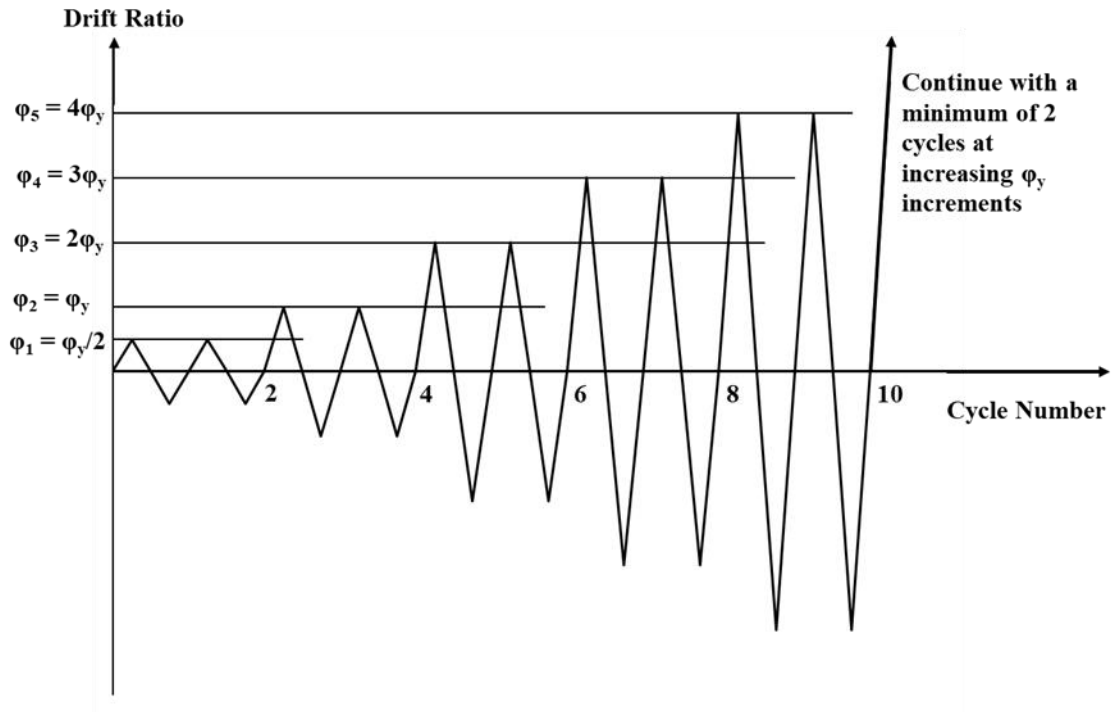

Figure 3-19: ACI Loading Protocol

Determination of the yield displacement is derived using equations provided by the Priestley et al. (2007). Given the following two equations yield displacement, Δ, is calculated:

$$\Delta_y = \Delta_{y1} + \Delta_{y2} \quad \textbf{(3-2)}$$

$$\Delta_{y1} = \varphi_y \frac{(L_1 + L_{sp})^2}{3} \quad \textbf{(3-3)}$$

$$\Delta_{y2} = \varphi_y \frac{\left(L_2 + L_{sp}\right)^2}{3} \quad (3\text{-}4)$$

Where:

Δ_{y1}, Δ_{y2}= Yield drift for each short pier, in.

φ_y = curvature of first bar yield point, in.$^{-1}$

L_1 = Pier height, in.

L_{sp} = Strain Penetration Length, in.

Provided, pier height, is 36 in., and the following two equations for determining $\varphi_{y\ and}$ L_{sp} for a conventional CIP constructed pier.

$$\boldsymbol{\varphi_y = 2.25\frac{1.1f_y}{Ed}} \quad (3\text{-}\mathbf{5})$$

$$\boldsymbol{L_{sp} = 0.15(1.1f_y)d_b} \quad (3\text{-}\mathbf{6})$$

Where:

f_y = Yield strength of steel, 60 ksi.

E = Modulus of elasticity of steel, 29,000 ksi.

d = Diameter of pier, in.

d_b = Diameter of reinforcing longitudinal bar, in.

Considering the above equations as applied to the CIP specimen with a pier diameter of 14 in. (for design) and comprised of #6 longitudinal reinforcing a resulting yield drift total of 0.46 in. is determined. 0.35 in. is used for the programming of the actuator controller to ensure two cycles are performed prior to reaching yield for instrumentation and test set up tests.

From the determination of the yield displacement the final loading protocol used is determined and graphed, as shown in Figure 3.20. During the testing a loading rate of 1 mm/sec is used. As the yield displacement is multiplied for each set of additional cycles, time is taken to observe the

response of the specimen during each two-cycle set. The cycles are continually increasing in displacement magnitude until the bent demonstrates a 20% degradation in strength, or is determined to be unsafe for continued loading due to possible collapse.

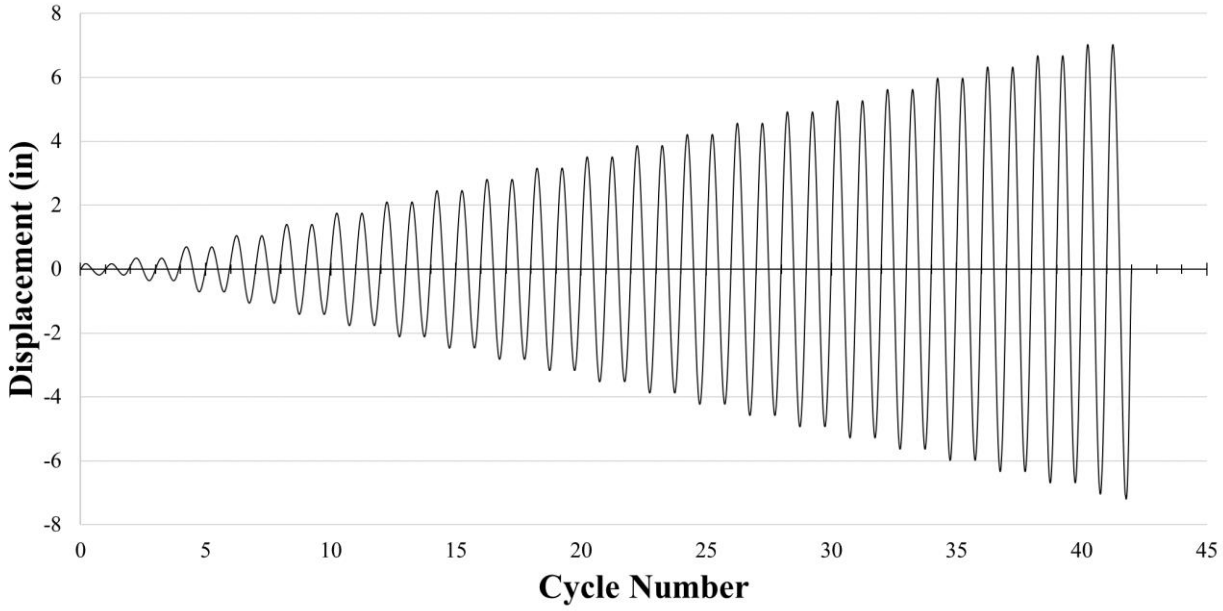

Figure 3-20: CIP Bent Loading Protocol

3.8. MATERIAL PROPERTIES

Following the completion of testing, the concrete samples prepared during each stage of pouring had to be tested to confirm the concrete properties on test day. Three concrete samples from the footing, pier, and cap pours were tested to verify the respective compressive strength of the concrete. Also, two split cylinder samples were tested. The 28-day compressive strength of concrete, f'_c, is targeted to be 4000 psi. Table 3.2 and 3.3 provides a summary of the test day compressive strength and split tension results, respectively.

Table 3-1: CIP Bent Test Day Compressive Strength

Sample	1	2	3	Average (psi)
Footing	6974	7186	7121	7094
Piers	2994	3211	3535	3247
Cap	3084	3276	3266	3209

Table 3-2: CIP Bent Test Day Split Tension

Sample	1	2	Average (psi)
Footing	533	603	568
Piers	352	427	390
Cap	443	374	409

3.9. EXPERIMENTAL TESTING

Starting the experiment at the first cycle of ± 0.18 in., cracks formed at the interface of the pier-to-footing and pier-to-cap (Figure 3.21a). Hairline cracking began in only the face of the pier away from the actuator, noted as the "North" pier for instrumentation purposes, during the second cycle. The interface cracks widened during this cycle as well. During the third cycle hairline cracking developed at all connections, with the furthest forming up to 19 in. from the interface (Figure 3.21b). During the fourth cycle cracks measuring 0.4 mm began to open within 12 in. of the interfaces (Figure 3.21c). Additionally, hairline cracking was extended up to 26 in. from the interfaces. The interface cracks continued to increase in width as well. During the fifth cycle spalling began developing at the pier top connections with cracks developing continuing throughout the pier. The cracks in the pier face were opening as wide as 1 mm while in tension. The sixth, seventh, and eighth cycles saw continued crack development up to 2.5 mm and additional slight spalling at the connection faces (Figure 3.21d). The ninth cycle is the first which concrete spalling developed at the base pier connections (Figure 3.21e). The ninth cycle is also

where the largest measured force, approximately 66-kip, takes place. From this point forward, the specimen strength begins to degrade.

The tenth, eleventh, and twelfth cycles saw cracking continue to develop and spalling develop to exposure of the spiral reinforcing at the top of the pier near the actuator (Figure 3.21f). It is during the fourteenth cycle which exposure of the longitudinal reinforcing occurred at the top of the pier near the actuator (Figure 3.21g). The fifteenth and final cycle results in the fracture of longitudinal reinforcing at the top connection of the pier nearest the actuator resulting in a significant drop in lateral force (Figure 3.21h). Having the fifteenth cycle finishing with a max lateral force of 53-kip (80% of greatest lateral force experienced) the test was completed.

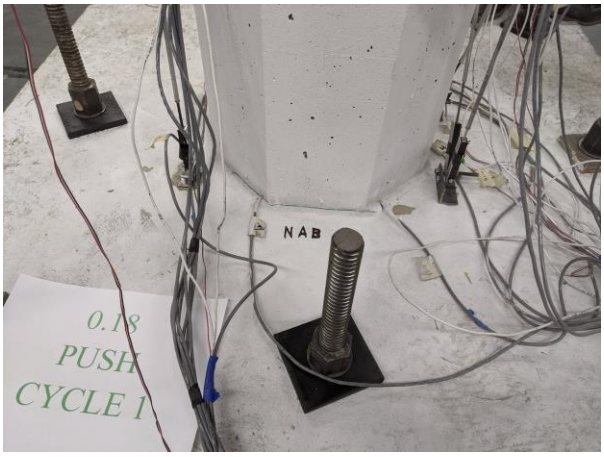

a) Cycle 1: Interface cracking

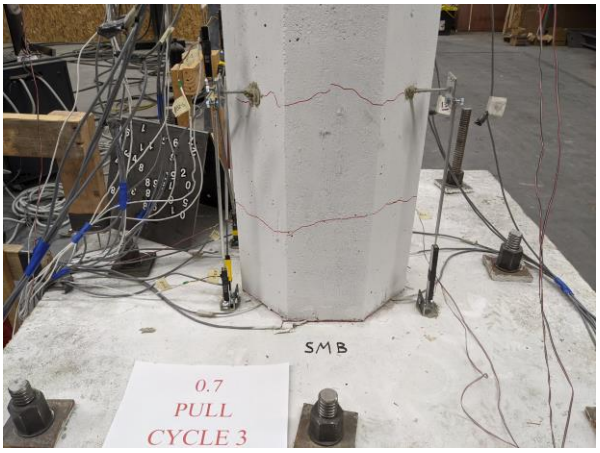

b) Cycle 3: Hairline crack development

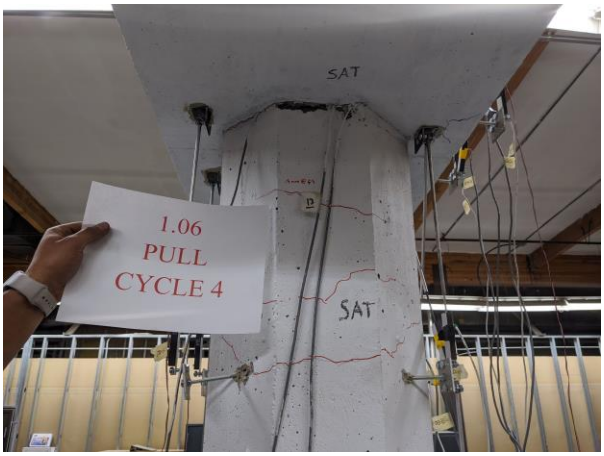

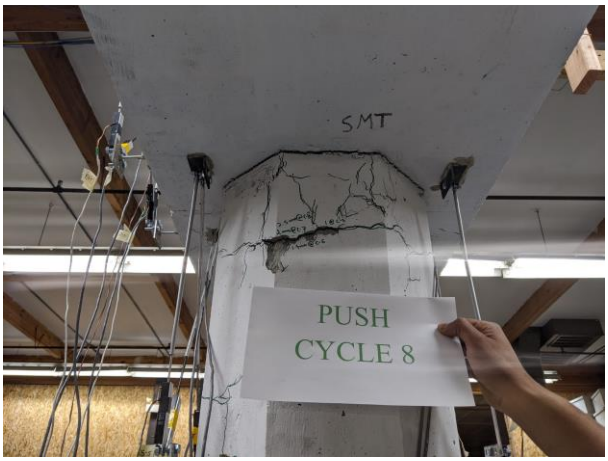

c) Cycle 4: 0.4 mm Crack Development

d) Cycle 8: Spalling and 2.5 mm cracking

e) Cycle 9: Base Connection Spalling

f) Cycle 13: Spiral Exposure


g) Cycle 14: Longitudinal Exposure **h) Cycle 15: Longitudinal Rebar Fracture**

Figure 3-21: CIP Bent Testing

An item of note during the test is the flex experienced by the reaction frame. This constituted to a lower achieved specimen displacement than what was targeted at each cycle. This is due to the inability of the reaction frame to be completely rigid against the lateral force of the actuator. Table 3.1 provides a recap of the target values programmed for the actuator and the actual displacements experienced by the specimen, as measured by the independent string potentiometer labeled CAP-INPLANE. The ultimate drift achieved by the bent prior to 20% strength degradation was 4.94%. This is comparable to the targeted displacement programmed for the thirteenth cycle.

Table 3-3: CIP Bent Loading Protocol Summary

	Programmed Values		Actual Displacements	
Cycle	Displacement (in.)	Drift (%)	Displacement (in.)	Drift (%)
1	0.18	0.21	0.09	0.11
2	0.35	0.42	0.15	0.18
3	0.7	0.84	0.35	0.42
4	1.06	1.27	0.56	0.67
5	1.41	1.68	0.86	1.03
6	1.76	2.10	1.08	1.29
7	2.11	2.52	1.4	1.67
8	2.46	2.94	1.73	2.07
9	2.81	3.36	2.06	2.46
10	3.17	3.79	2.4	2.87
11	3.52	4.20	2.75	3.28
12	3.87	4.62	3.1	3.70
13	4.22	5.04	3.44	4.11
14	4.57	5.46	3.78	4.51
15	4.92	5.87	4.14	4.94

Following the completion of testing the data captured during the CIP bent test is analyzed and presented to be compared to the precast bent in Chapter 5. The maximums achieved during the testing of displacement and lateral load were 4.14 in. and 66-kip, respectively. The lateral load correlates to total moment capacity of 460-kip-ft. If assumed the four connections shared the lateral load equally, this equates to base shear at each connection of 16.5-kip. Figure 3.22 and 3.23 provide Force vs. Displacement and Force vs. Drift hysteresis of the full CIP bent testing. As can be seen the specimen reached its design base shear of 35.2-kip. The hysteresis suggests the bent yielded at 0.42 in. displacement (Figure 3.22). Suggesting to be the first yield of the longitudinal rebar. Similarly, from the Force-Drift hysteresis it is seen the bent yielded at a drift ratio of 0.5% (Figure 3.23).

As can be noted from the figures, the positive vertical axis shows the specimen in push. As the test begin by first pulling the specimen, and continued to begin all cycles in pull, it can be observed the bent had higher strength in pulling than push can be attributed to two factors. The bent underwent softening during the first pull of the cycle thus exhibiting higher strengths in all cycles. Additionally, the reaction frame exhibited slightly higher stiffness during the pulling stage as opposed to experiencing higher displacement during the pushing stage.

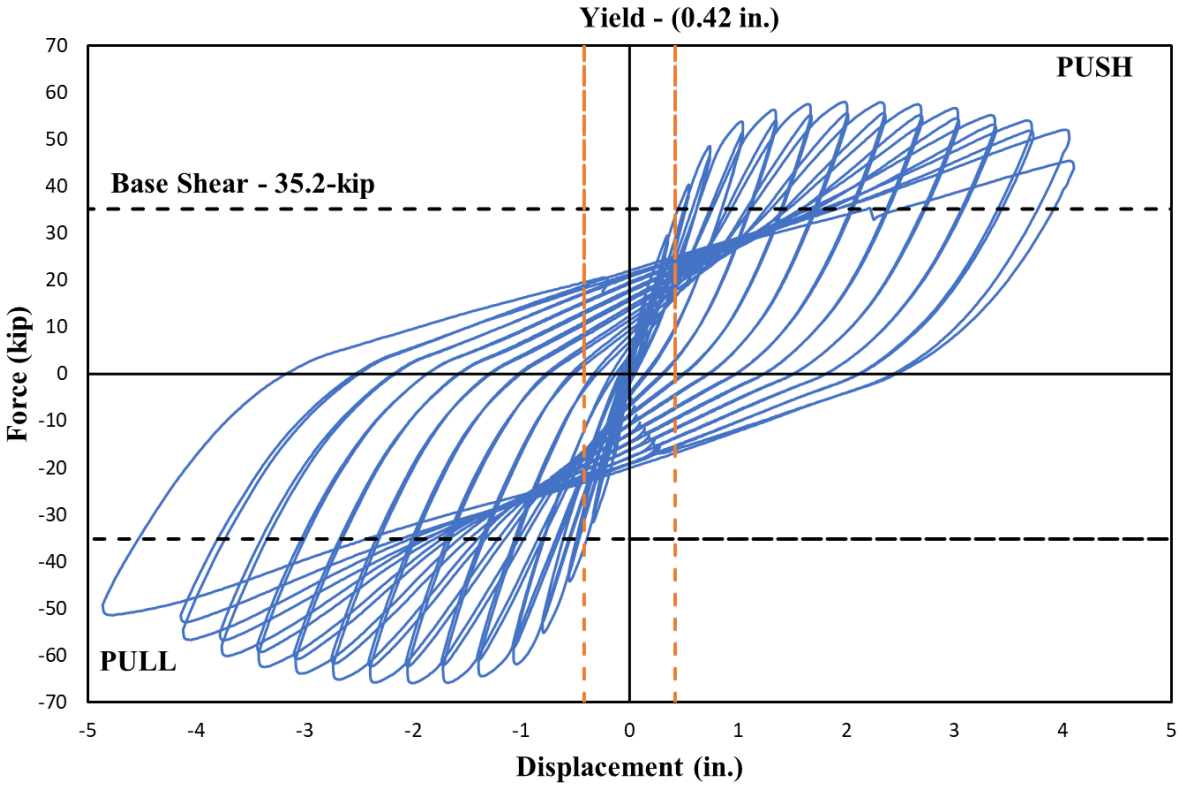

Figure 3-22: CIP Bent Force-Displacement Hysteresis

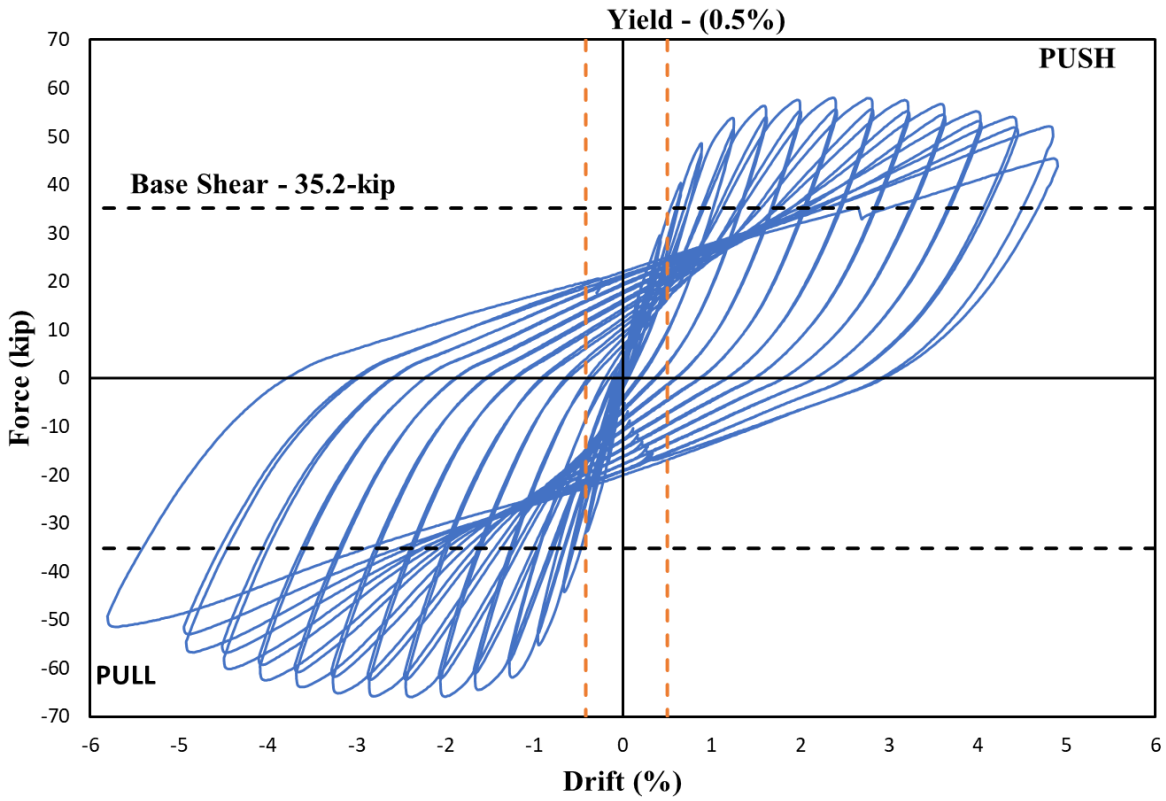

Figure 3-23: CIP Bent Force-Drift Hysteresis

Figure 3.24 provides the resulting Force-Drift backbone curve. The backbone curve is comprised of the peak loads achieved at each cycle. Observation of the curve provides further evidence of the bent performance and its yield progression.

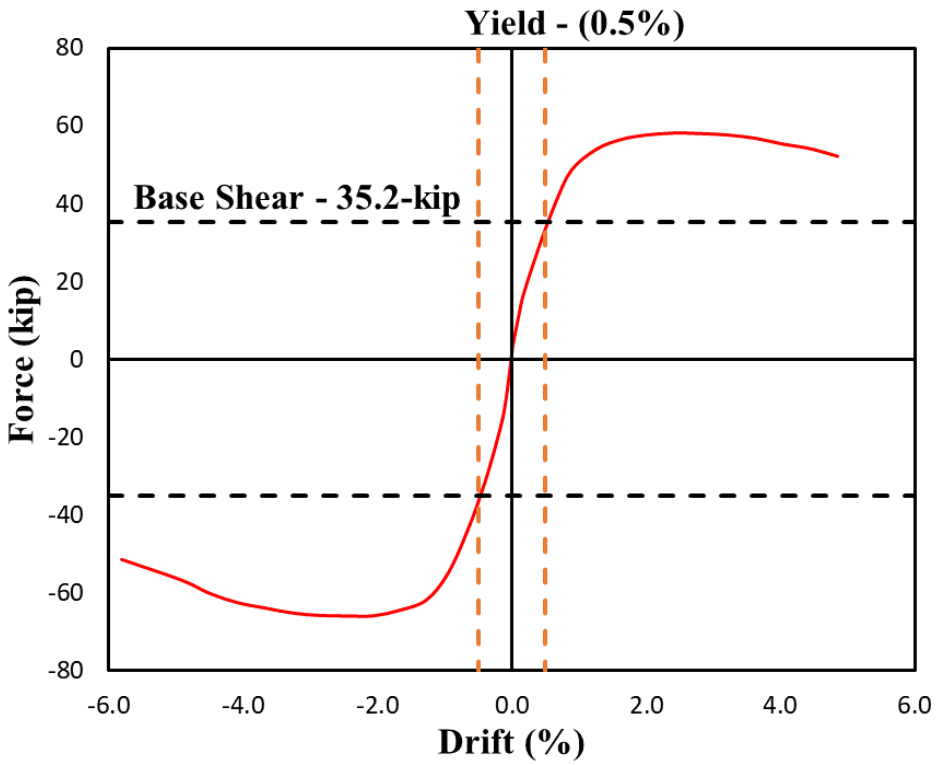

Figure 3-24: CIP Bent Fore-Drift Backbone Curve

Further analysis of the potentiometers, specifically located in the plastic hinge regions (groups A, B, C, and D), provides a close breakdown of each connection's reaction through moment-curvature. The progression of the yield that is captured by the instrumentation at each plastic hinge can be observed in Figure 3.25, providing the moment-curvature of each. Observation of the top of the south pier (Figure 3.25a) shows a narrower hysteresis produced as opposed to the other connection. This correlates to the level of damage and spalling observed at each connection, with this particular connection being the one to sustain the most and ultimately fail the longitudinal reinforcing as noted in the previous section. Further observation of the plots shows a consistent increase in the strength degradation at each cycle once the bent reached its capacity. Through comparing the two south pier plots to the north plots it can be seen the south

pier experienced a higher level of drift correlating to the increased damage observed on the pier during testing. Therefore, the observations made during testing have a good correlation with the experimental results collected via the instrumentation.

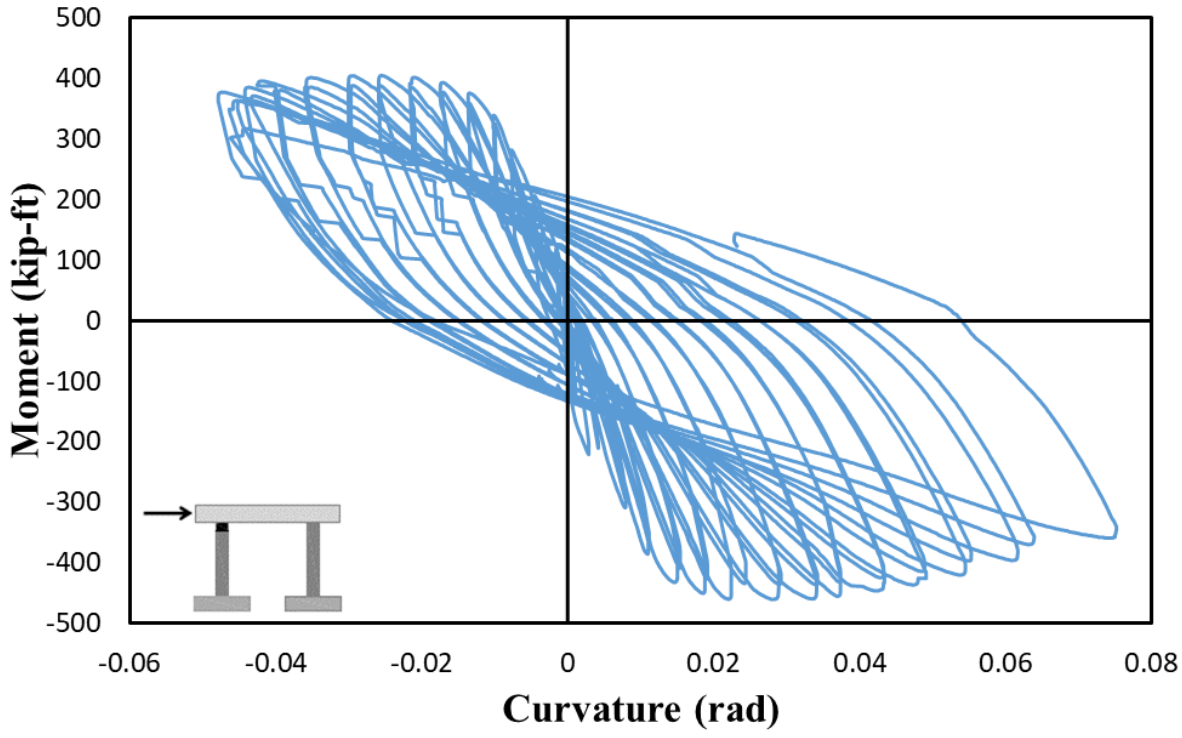

a) South Pier: Top (D1-S – D4-S)

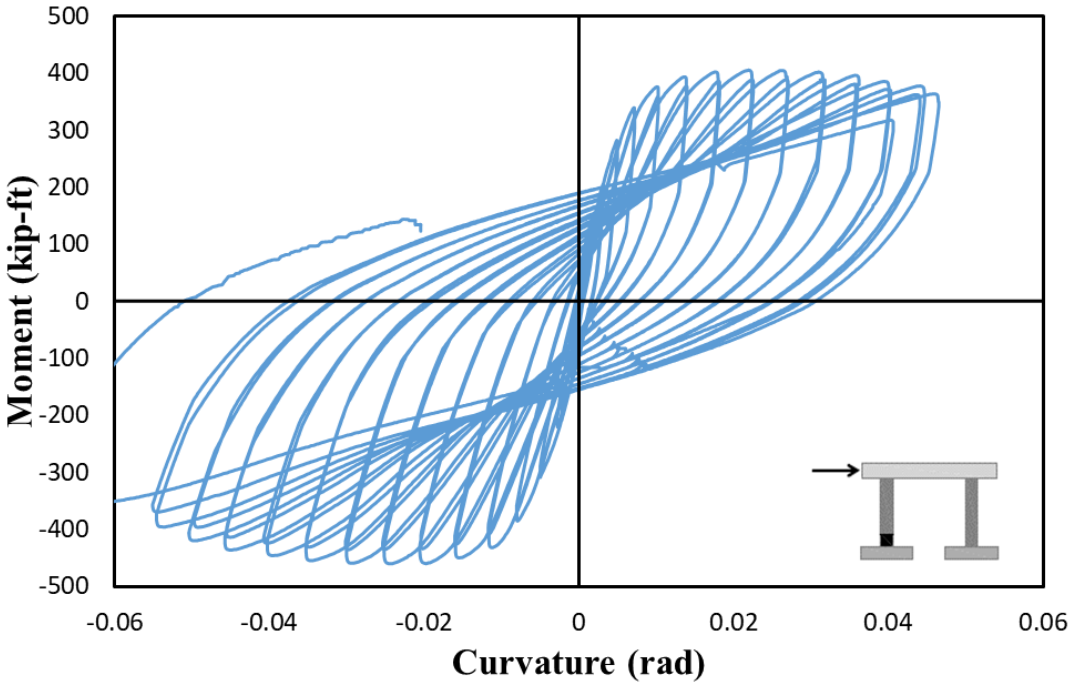

b) South Pier: Bottom (A1-S – A4-S)

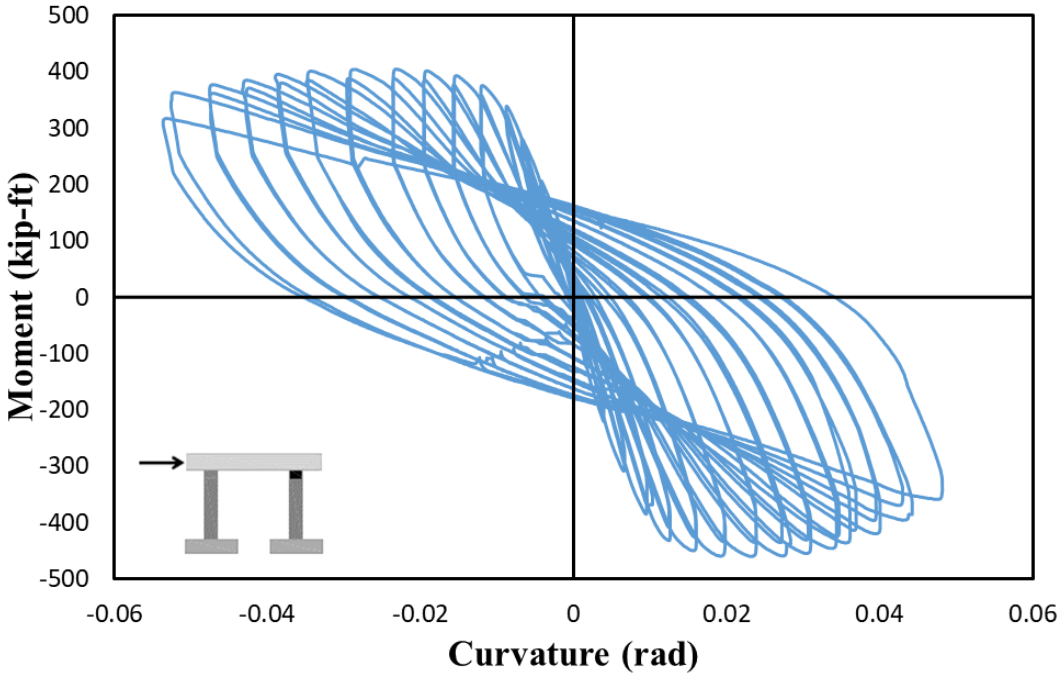

c) North Pier: Top (D1-N – D4-N)

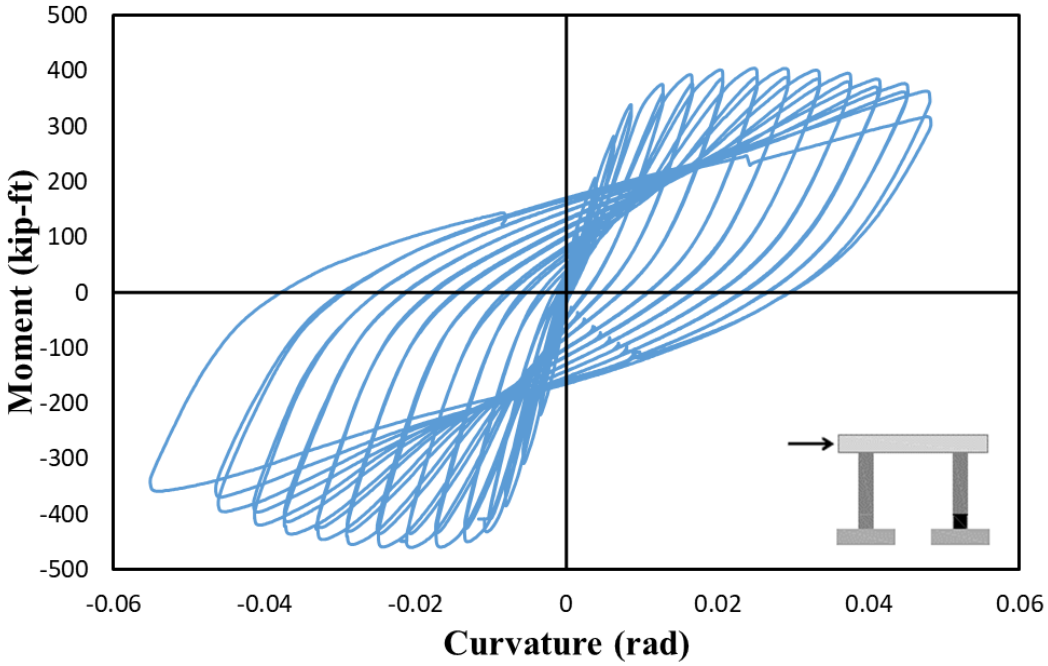

d) North Pier: Bottom (A1-N – A4-N)

Figure 3-25: CIP Bent Moment-Curvature Hysteresis

The energy dissipated per each cycle for the bent is presented in Figure 3.26. The dissipated energy was calculated using numerical integration of the hysteresis loop at each cycle considering the area enclosed within the loop. To accomplish this a MATLAB program is utilized to break the hysteresis down to individual loops and calculate the enclosed areas, which are then summed together resulting in a "Cumulative Dissipated Energy". For the CIP bent specimen the resulting cumulative dissipated energy is expressed in kilojoules (kJ). The resulting is 342 kJ.

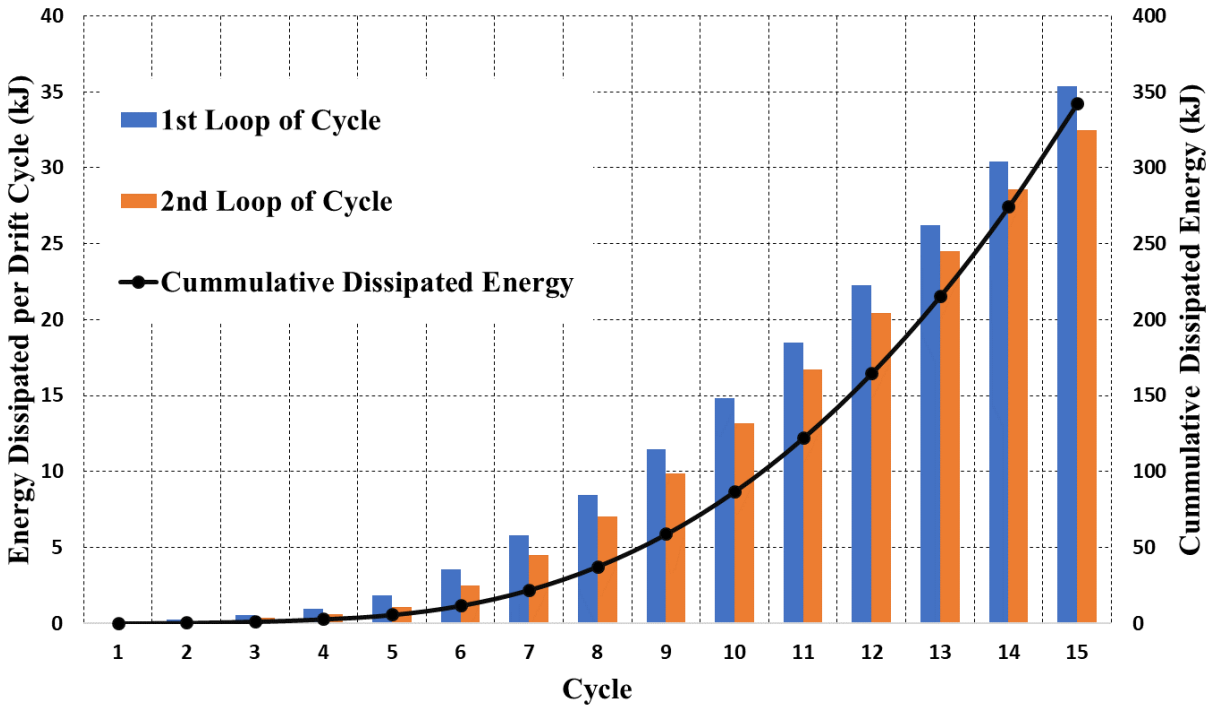

Figure 3-26: CIP Bent Dissipated Energy per Cycle and Cumulative

Experimental results are used to determine the experimental yield curvature and yield moment by Caltrans Idealized Model (Caltrans 2013). A bilinear approximation similar to the example provided in Figure 3.27. The moment capacity can be obtained by balancing the area between the idealized M-ϕ and actual. The global yield curvature and yield moment is determined to be 0.702 in. and 380-kip-ft.

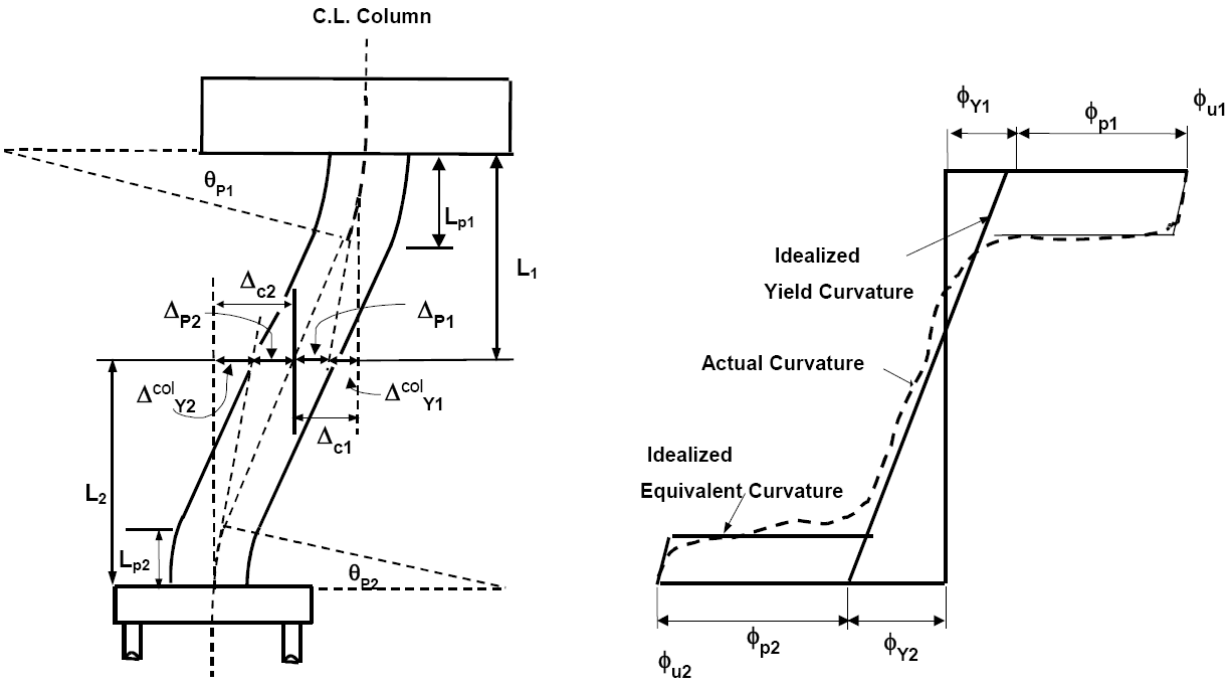

a) Displacement capacity of a pier in a bent with fixed-fixed supports

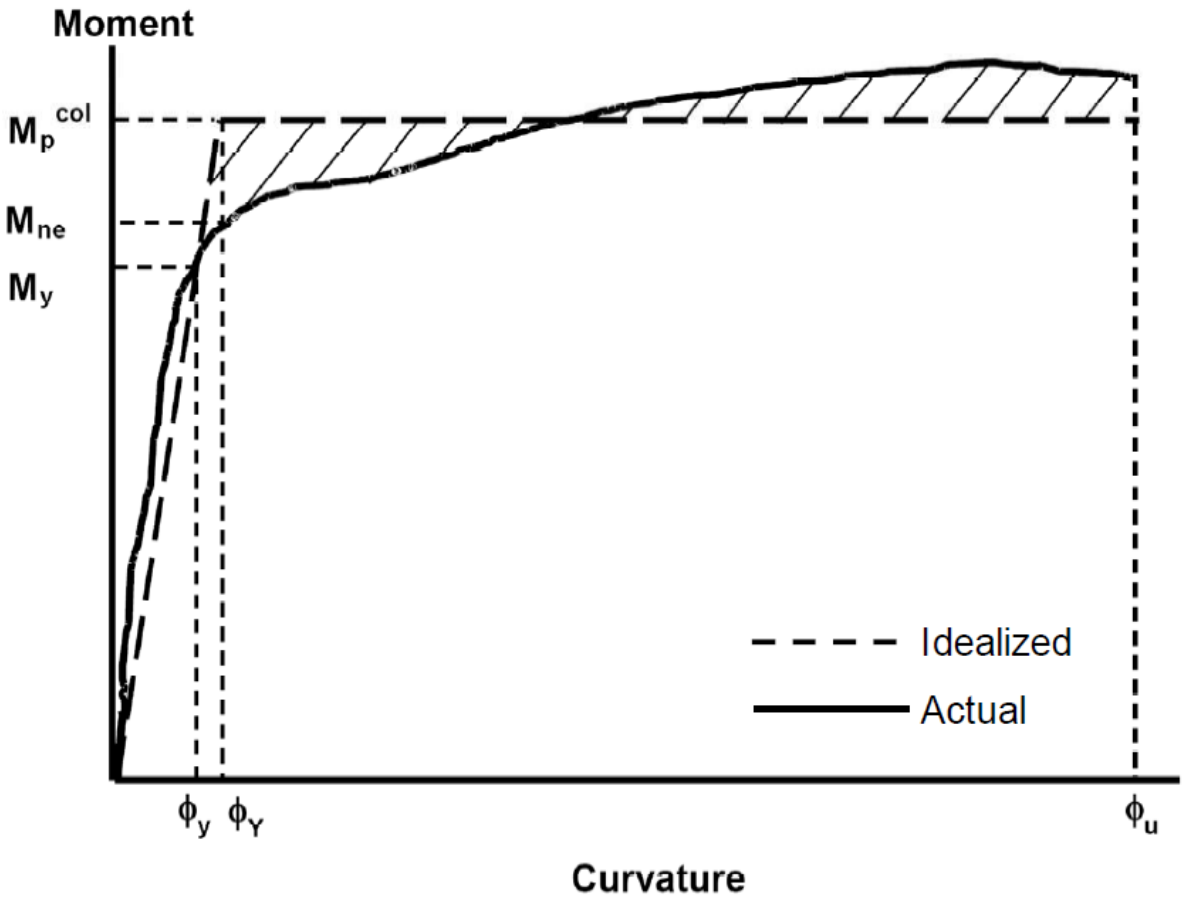

b) Moment-curvature curve

Figure 3-27: Caltrans Idealized Mondel for M-ϕ Analyais (courtesy of Caltrans 2013)

Where, from Figure 3.27:

ϕ_y = Curvature at the first bar yield point (in-1)

ϕ_Y = Curvature at the global yield point (in-1)

ϕ_u = Ultimate curvature at the failure point (in-1)

M_y = Moment capacity at the first bar yield point (kip-ft.)

M_P = Plastic moment capacity (kip-ft.)

For this experiment the backbone curve is analyzed using displacement in place of curvature providing the following results. The backbone curve average of the push and pull direction is considered. The global yield moment capacity produced from the experimental results is used to obtain the base shear yield of 56.2-kip corresponding to a yield displacement of 0.596 in. The ultimate base shear provided from the backbone curve gives a total base shear of 61.9-kip at a displacement of 2.2 in. The bilinear approximation is shown in Figure 3.28, below.

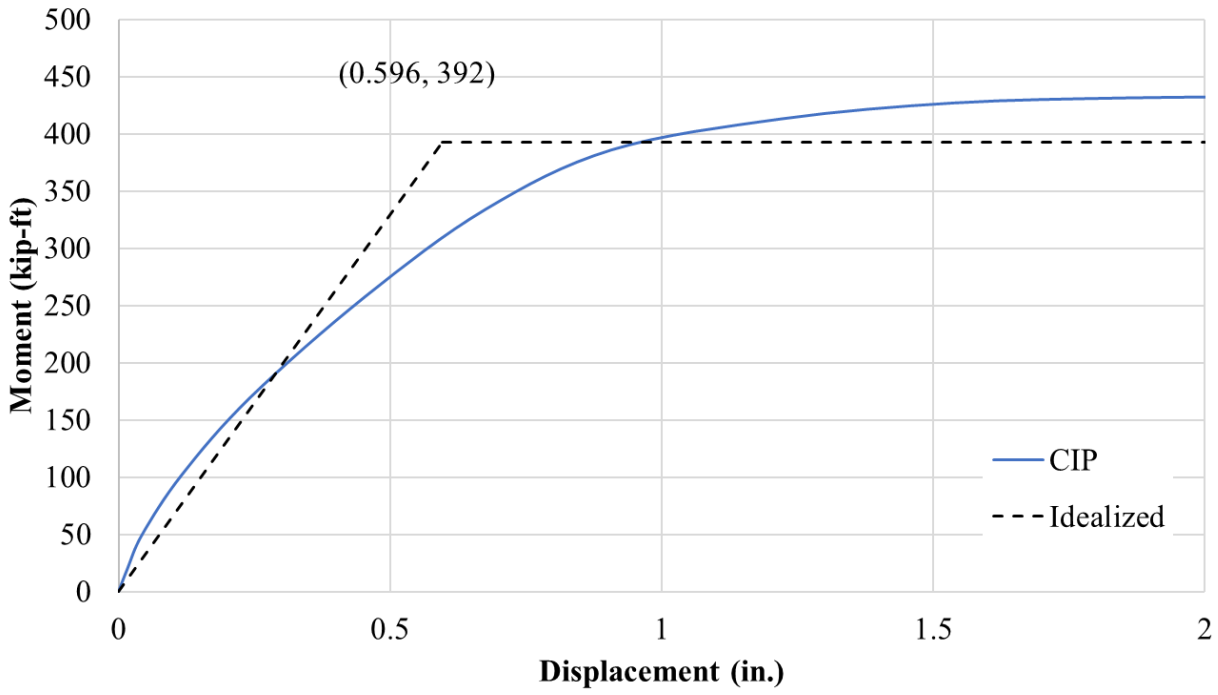

Figure 3-28: Bilinear Approximation for CIP Bent

Further analysis of the experimental results allows for the determination of the overstrength factor (Ω_0), an important seismic parameter. The overstrength factor is determined as the ultimate base shear capacity at ultimate ($V_{ultimate}$) divided by the base shear at initial yield (V_{yield}). The equation is given below. The resulting overstrength factor of 1.76 is obtained.

$$\boldsymbol{\Omega_0 = \frac{V_{ultimate}}{V_{yield}}} \quad \textbf{(3-7)}$$

Displacement ductility is calculated in a similar fashion as seen int the equation below. And provides further seismic parameters on the performance of the CIP bent.

$$\mu = \frac{\delta}{\delta_y} \quad \textbf{(3-8)}$$

Where:

μ = Displacement ductility

δ = Displacement at the ultimate base shear point on the backbone plot (in.) for the displacement ductility at the ultimate base shear capacity

δ = Deflection at $0.8V_{ultimate}$ in the backbone plot (in.) for the ultimate displacement ductility

δ_y = Deflection at yield (in.)

Resulting in a displacement ductility of 3.69 for ultimate base shear and 7.48 at failure point.

The residual drift of the CIP bent is presented in Figure 3.29, providing the permanent deformation of the pier after the completion of each cycle. At the point of failure, the CIP bent was maintaining 61.5% (3.04% drift ratio) of the drift applied, 4.94%.

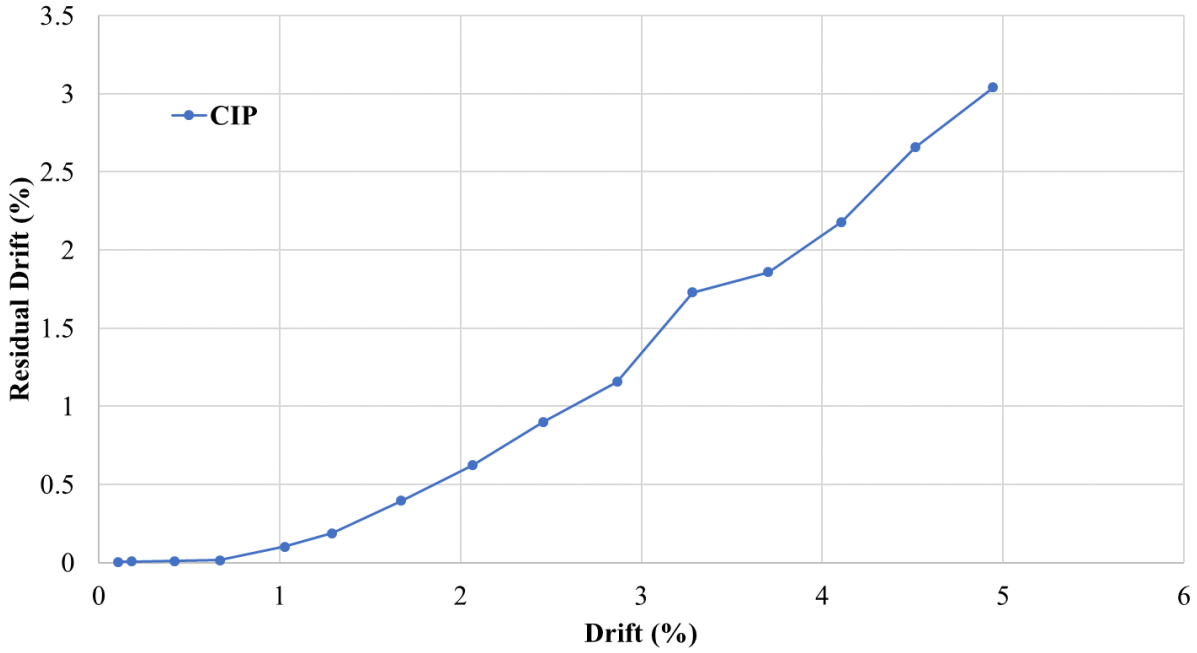

Figure 3-29: Residual Drift of CIP Bent

3.10. CONCLUSIONS

As the CIP bent specimen is tested to serve as a benchmark comparison for the proposed connection to be tested in the precast bent in Chapter 4, the finding from the CIP bent and the response of the system under testing will be compared to that of the precast bent in Chapter 5. The CIP bent is fully constructed to simulate the traditional construction and design of a typical mid to long-span Idaho bridge. For this reason, the design followed closely with AASHTO LRFD Bridge Design Specifications (AASHTO 2017). Similarly, the full specimen is poured in a similar staged fashion as that seen on a typical CIP construction project using traditional materials and methods. The experimental loading program determined from ACI "Guide for Testing Reinforced Concrete Structural Elements under Slowly Applied Simulated Seismic Loads" resulted in a ductile specimen response. The CIP bent having achieved the design base shear, 35.2-kip, correlating with yield drift ratio of 0.5% (0.42 in.) at first yield. With an

approximated global yield point of 0.7% (0.596 in.). The system achieved a maximum base shear and total displacement of 66-kip and 4.14 in., respectively. The bent responded similarly in all four pier connections, as similar plastic hinges developed at each connection. Ultimately, as the experiment progressed the pier nearest the lateral loading actuator began to experience an accelerated degradation of cover concrete thus loading the longitudinal reinforcing resulting in failure of the top connection. The failure of the longitudinal reinforcing resulted in a significant strength loss bringing the strength degradation to more than the targeted 20%. With a shear failure eminent in the top connection the experiment was terminated to ensure a proper level of safety was maintained. Through data analysis the Force-Displacement and Force-Drift plots show the specimen had higher strength in pull as opposed to push. This being due to the fact the pull cycle is performed first resulting in a softening effect observable in the push of the cycles, noted as decreased capacity. This difference in strength is also due to the reaction frame being stiffer in pull than push. Additionally, the total energy dissipated during the experiment by the CIP bent resulted in a total of 342 kJ. The CIP bent resulted in an overstrength factor of 1.76 and displacement ductility values of 3.69 and 7.48 for ultimate base shear and failure point, respectively. Overall, the CIP bent performed relatively as expected and provided the base data targeted for comparison of the precast bent to be test.

CHAPTER 4 PRECAST BENT SYSTEM

4.1. INTRODUCTION

This chapter presents design, construction, and experimental testing of a precast bent system using a proposed pier connection by ITD. The chapter presents an overview of the design, sizing, detailing, testing, and analysis of the precast bent specimen. A review of the construction process is presented discussing the challenges faced during the precast construction and the implementation of the proposed connection and its accompanying aspects. As the proposed connection is similar to that of CFSTs a similar approach, which closely follows the 2019 WSDOT Bridge Design Manual (WSDOT 2019), is used for design. As a comparison to the CIP bent is to be made aspects such as overall specimen dimensions, testing arrangement, loading protocol, and instrumentation are repeated as they were carried out for the benchmark CIP bent.

4.2. PROPOSED CONNECTION

The proposed connections are to be tested as a precast ABC technology used in bridge substructure pier connections. The technology makes use of HSS pipe, suggested to be similar pipe as used in structural piles, with a pipe embedded in both the pier and footing/cap. The pier pipe is typically protruding half its length from the pier end (Figure 4.1). The footing/cap has a fully embedded pipe insert of larger diameter design to accommodate for the pier pipe to telescope into the footing/cap. Figure 4.2 provides a typical footing detail suited for the proposed connection. The full connection assembly provided in Figure 4.3 shows a typical footing connection. As opposed to traditional CIP pier it can be seen there is no longitudinal reinforcing to bridge the interface of the two elements as the HSS pipe is the only item passing through the pier-to-footing interface. The HSS provides the flexural capacity, shear capacity, and

confinement for the connection. Figure 4.4 similarly provides the proposed connection detail for the pier-to-cap connection.

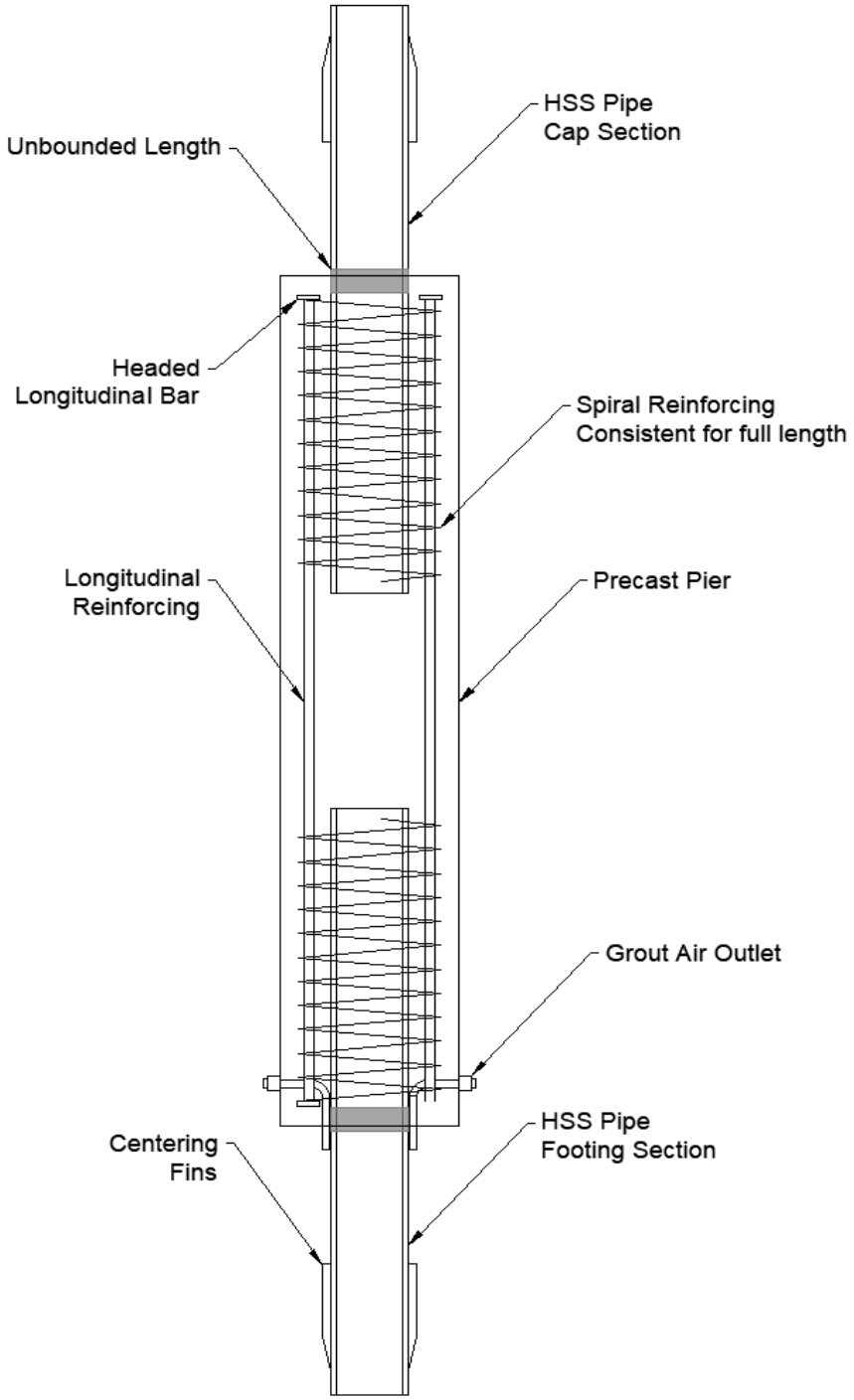

Figure 4-1: Proposed Connection: Precast Pier Detail

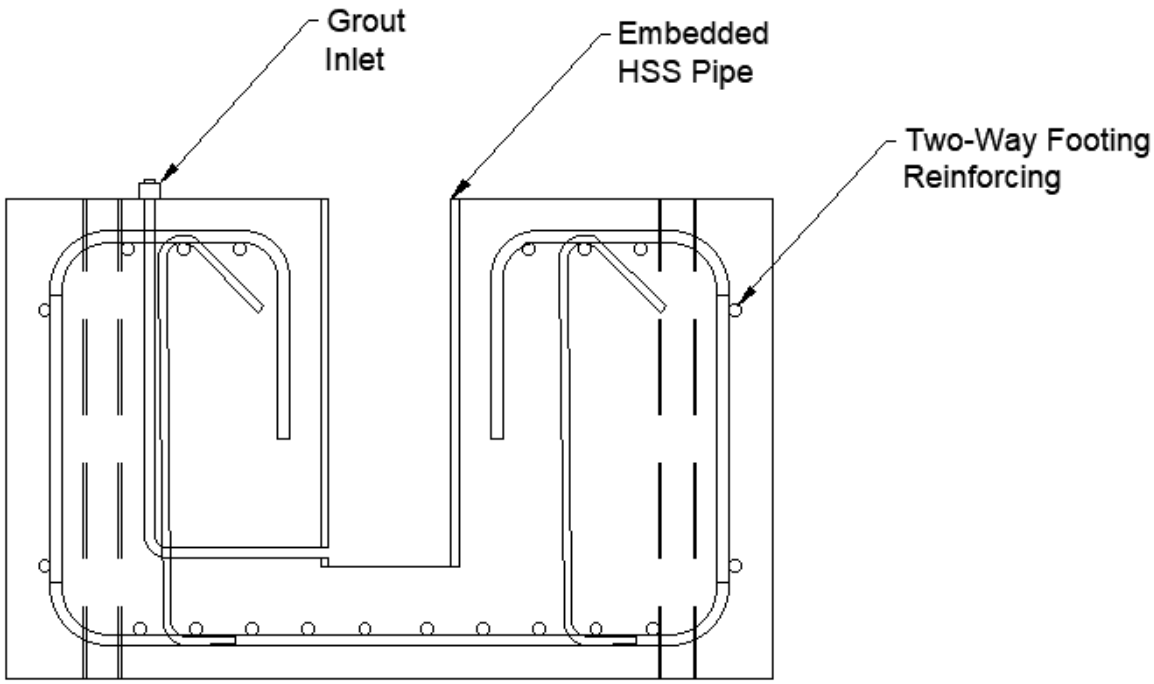

Figure 4-2: Proposed Connection: Precast Footing Detail

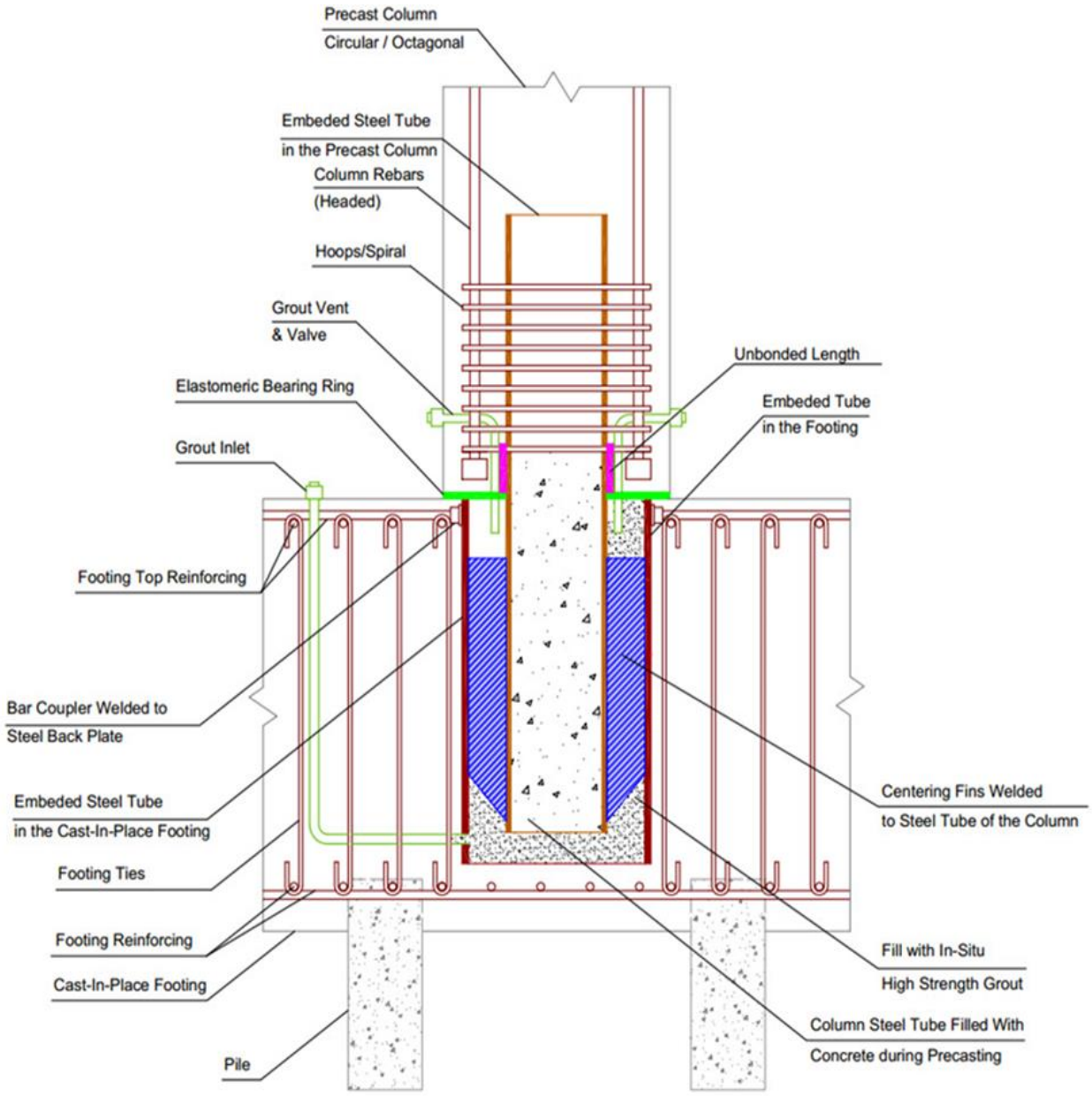

Figure 4-3: Proposed Connection: Pier-to-Footing Connection

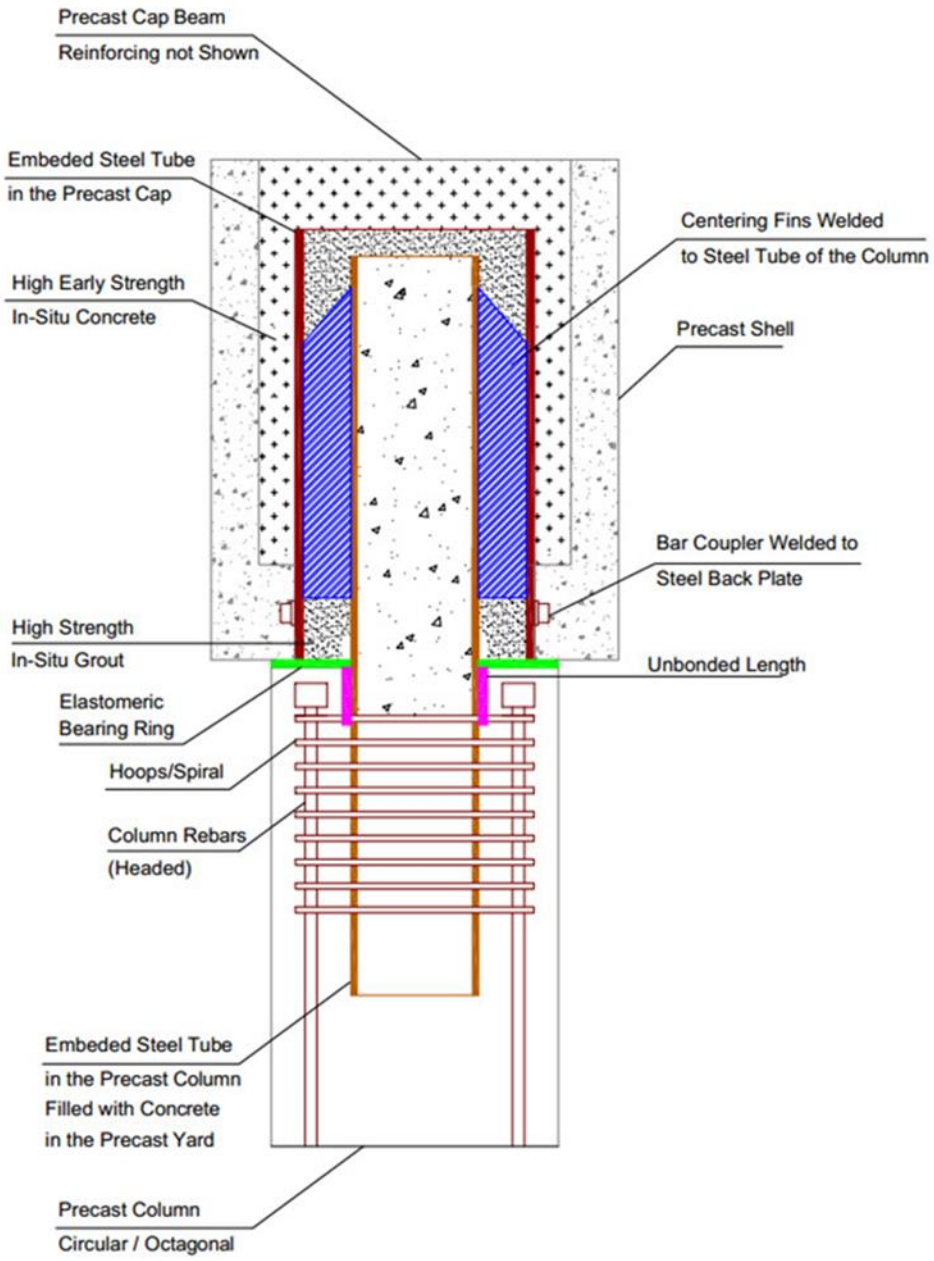

Figure 4-4: Proposed Connection: Pier-to-Cap Connection

As this connection provides similar total steel area at the interface of the connection in a more condensed arrangement than that of typical CIP connections, consideration for a greater yielding of steel must be accounted for. As the pipe is precast into the center of the pier this requires for a smaller diameter as opposed to that of traditional longitudinal reinforcing, which is

provided outside of the HSS pipe for confinement of the pier concrete only. For this an unbonded length of the pipe is provided in order to establish a greater yield area of the steel to be activated during higher seismic loading. This unbonded length is identified in the above figures (4.1, 4.3, and 4.4) on the pier HSS and is positioned just above and below the interface of the footing and cap, respectively.

Additionally, an elastomeric pad is provided at each interface. The requirement for the elastomeric pad is due to the grouted state of the precast connection after completion. As the connection is finished with a grout poured between the two pipes filling the gap to the interface at the pier, a non-rigid material is desired to help eliminate any voids that would be present in a dry concrete-to-concrete interface. The bearing pad helps to seal this connection for the completion of the grout pour and from natural elements (water, road salt, etc.) during the life of the connection. The bearing pad also allows for slight non-destructive movement of the connection during low level loading. Resulting in decreased cracking and spalling during low cycle seismic activity.

As mentioned above the connection is completed using a grout fed into the footing and pushed up through the void until sufficient flow out the air outlets is achieved. For the cap connection the grout can be fed from the top of the cap down into the void until similar sufficient flow is produce out the air valve in the top of the cap. The grout to be used must be non-shrink with a low metallic content to reduce interaction with HSS pipe in regard to corrosion. For all the HSS pipe it is suggested that all surfaces are sand-blasted or similarly prepped prior to concrete or grout application. The gap available above and around the pier pipe inserted into the embedded pipe is dependent upon the grout specifications provided and ensured to allow for full flow of the grout throughout the connection.

Regarding the footing and cap reinforcing interrupted by the embedded HSS sections, sufficient development is to be supplied via rebar bends or terminators to ensure full development of the bar is achieved. The remaining elements of the substructure are designed in accordance with the AASHTO LRFD Bridge Design Specifications (AASHTO 2017) as similar to the CIP bent benchmark specimen as possible.

4.3. PRECAST BENT SYSTEM DESIGN

The steps taken to design the proposed connection for the purposes of this experiment are considered to be similar to CFSTs, as the concrete filled HSS pipe is the ductile element at the interface of the connection. The remainder of the pier is designed to remain elastic throughout loading and is designed as a traditional pier. A consideration made for the proposed connection is the assumption the unconfined cover concrete cast around the HSS pipe does not constitute to the flexural capacity of the connection. The footing and cap design are designed as traditional members with no constitution of strength from the reinforcing interrupted by the embedded HSS pipe.

As mentioned following WSDOT (2019) the pier HSS pipe is first sized. As the design is reliant on a variety of resistance factors, a factor of one is selected as the bent is to be tested to an extreme limit state. Sizing of the HSS pipe is began by ensuring it is not subjected to local buckling prior to developing the pipe strength. WSDOT (2019) offers the use of the below equation for determination of members under loading resulting in activation of beyond the elastic region, plastic:

$$\frac{D}{t} \leq 0.15\frac{E}{F_y} \quad \textbf{(4-1)}$$

Where D is the outside pipe diameter with t being the wall thickness. With E being modulus of elasticity and F_y being the yielding strength of the steel. The selected pipe is determined through a combination of strength capacity, rebar spacing, and other requirements. The selected HSS section is determined as an HSS6x0.500. With properties of 42 ksi yield strength and an ultimate strength ($F_{u)}$ of 58 ksi and modulus of 29,000 ksi. The actual design pipe thickness is 0.465 in. For this particular HSS pipe D/t is equivalent to 12.9 and $0.15E/F_y$ is equivalent to 103.6.

After confirmation that the selected HSS meets the buckling criteria, the moment capacity of the pier must be determined. The equation provided is used:

$$\boldsymbol{M_n(y) = \left(c\left(r_i^2 - y^2\right) - \frac{c^3}{3}\right) * 0.95 f'_c + 4ct\frac{r_m^2}{r_i}F_y} \quad \textbf{(4-2)}$$

Where c is equal to one half the cord length of the tube in compression. C is determined by the following:

$$\boldsymbol{c = r_i cos\theta} \quad \textbf{(4-3)}$$

With r_i equaling the radius to the inside of the steel tube. θ is determined using the following equation:

$$\boldsymbol{\theta = sin^{-1}\left(\frac{y}{r_m}\right)} \quad \textbf{(4-4)}$$

With y being the distance from the centroid of the specimen to the neutral axis during a seismic event. And r_m being the radius to the center of the steel tube. As the neutral axis is expected to be equal to the centroid the variable y is taken to equal zero. Once y is determined the variables θ and c are calculated as 0^0 and 2.54 in., respectively. The final resulting moment

capacity of the connection is 56.7-kip-ft. As the testing arrangement is identical to the CIP bent having a loading height off the top of the footing of 83.75 in. to the center of the actuator the resulting base shear is 8.1-kip. With a total design base shear of 32.5-kip when considering all pier connections present in the precast bent system.

A further design element required for the proposed connection is the embedment length of the HSS pipe into the footing or cap and equally in pier itself. For this, two approaches from literature are considered. The two methodologies are proposed by Edward P. Wasserman (Wasserman and Walker 1996) and WSDOT (2019). Wasserman and Walker's approach is based on "Design of Integral Abutments for Jointless Bridges" by Edward P. Wasserman (1996). The following proposed equation was derived from a method used for application to develop the plastic moment capacity of piles used in bridge abutments. The original derivation used 3.78f'c for the concrete bearing capacity, based on research performed by Burdette, Jones, and Fricke. The derivation used below uses a much more conservative value of 0.7f'c, as allowed by AASHTO for concrete bearing pressure (C5.5.4.2, Pages. 5-30). The resulting proposed equation is:

$$\boldsymbol{l_e = 2\left(\frac{M}{(0.7f'_c b)^{\frac{1}{2}}}\right)} \quad \textbf{(4-5)}$$

$$\boldsymbol{M = Z * F_y} \quad \textbf{(4-6)}$$

$$\boldsymbol{b = \frac{d}{2}\sqrt{\pi}} \quad \textbf{(4-7)}$$

Where l_e is the required embedment depth (in.), M is the plastic pipe moment, f'$_c$ is the compressive strength of concrete (psi), d is the outside diameter of the pipe (in.), Z is the gross

plastic section modulus (in.^{3}), and F_y is the yield strength of the pipe (ksi). Note that the equations above are empirical and require the parameters to be in the proper units.

The method used by the WSDOT was developed experimentally at the University of Washington by Dawn E. Lehman and Charles W. Roeder in "Rapid Construction of Bridge Piers with Improved Seismic Performance", published January 2012 (Lehman and Roeder, 2012). The method was developed for use with CFSTs for foundation connections and bridge piers. The connection uses a steel pipe with an annular ring, as shown in Figure 4.5, imbedded into a pocket connection either preformed or formed with a corrugated steel pipe and grouted in place.

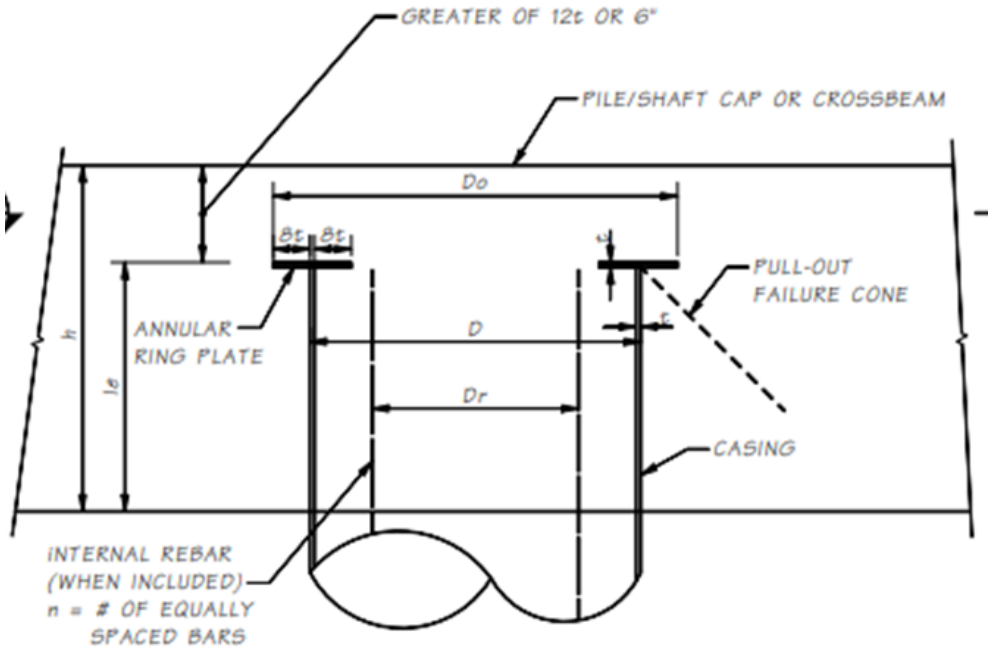

Figure 4-5: WSDOT Pipe Embedment Cross-Section

WSDOT Proposed equation to ensure full plastic behavior of the CFST:

$$l_e \geq \left(\frac{D_0^2}{4} + \frac{5.27DtF_u}{\sqrt{f'_c}} \right)^{\frac{1}{2}} - \frac{D_0}{2} \qquad \textbf{(4-8)}$$

Where l_e is the required embedment length (in.), f'$_c$ the compressive strength of the cap or footing concrete not the grout (ksi), D_0 is the outside diameter of the annular ring (in.), D is the outside diameter of the embedded pipe (in.), t is the wall thickness of the pipe (in.), and F_u is the ultimate strength of the pipe steel (ksi). Again, the equation is empirical. This equation can be reduced for the proposed connection as an annular ring is not used. The resulting simplified equation is:

$$\boldsymbol{le} \geq \left(\frac{\mathbf{5.27}\boldsymbol{DtF_u}}{\sqrt{\boldsymbol{f'_c}}} \right)^{\frac{\mathbf{1}}{\mathbf{2}}} \quad \textbf{(4-9)}$$

For the purpose of conservative construction for the experimental investigation of the proposed connection both methodologies are considered with the greater resulting value used for construction. The controlling resulting embedment length is determined to be 22 in. This results in an HSS section with an overall length of 49 in., as 22 in. is required in the footing or cap, an additional 2.5 in. is considered for the elastomeric bearing pad and unbonded length. Leaving a remaining 24.5 in. to extend into the pier element ensuring effective bonding of the pier HSS pipe section. For the embedded elements within the cap and footing the HSS pipe section is required to be a total length of 23 in. to accommodate for the full 22 in. embedment required and an additional 1 in. for grout flow. Similar to that of the CIP bent the remainder of the pier is designed as a traditional CIP section. Resulting in 7 #6 Gr. 60 longitudinal reinforcing with a #3 Gr. 60 spiral with a pitch of 1.5 in. running the full length of the pier. However, the longitudinal reinforcing is required to terminate within the pier as opposed to running continuously, as in the CIP piers. For this, threaded terminators are used at either end of the longitudinal reinforcing within the pier. The full pier detail is provided in Figure 4.6 below.

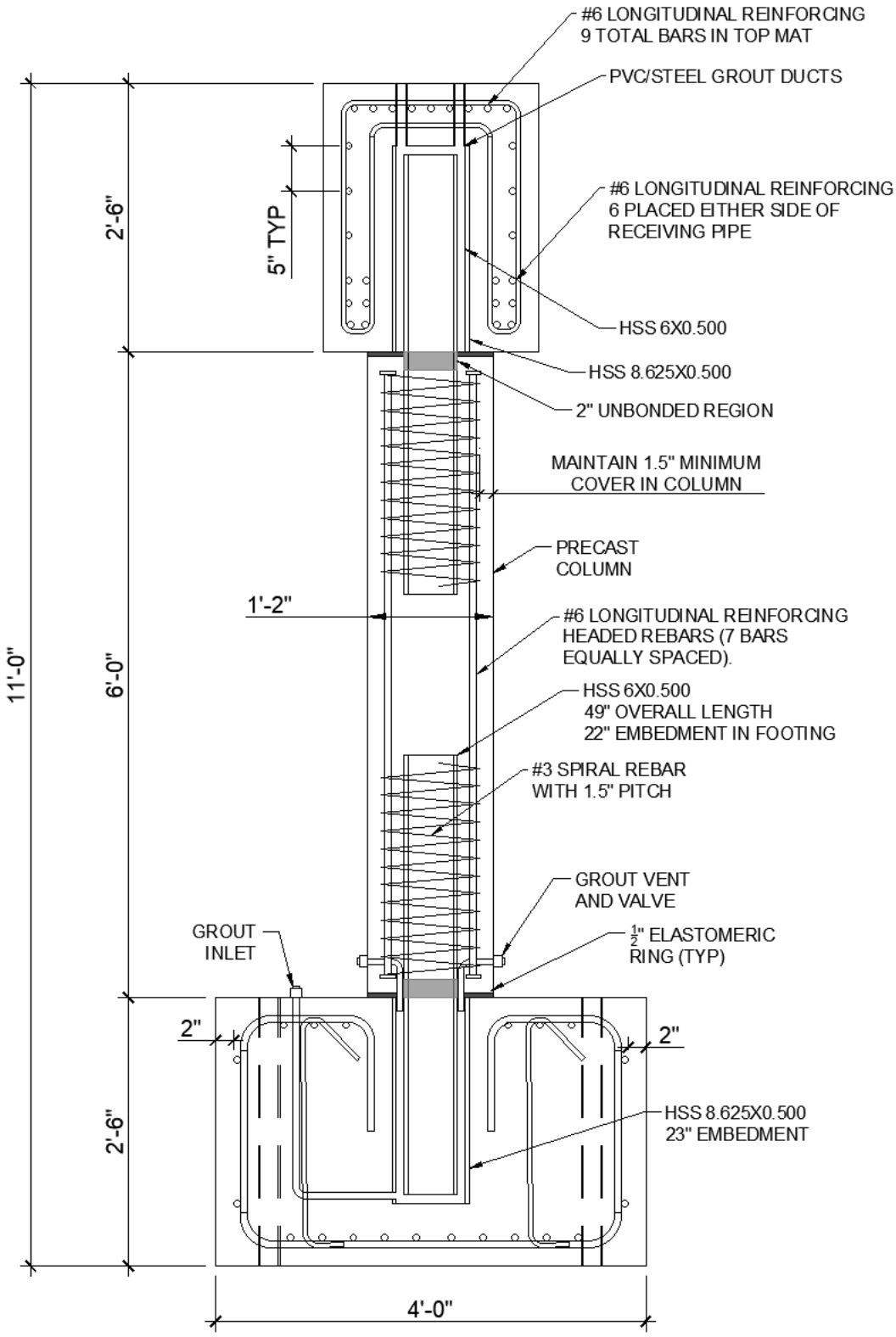

Figure 4-6: Precast Bent Pier Cross-Section

Further examination of Figure 4.6 provides details as to the footing and cap sections. The footing and cap embedded HSS8.625x0.500 are selected, based off the calculated pier pipe and the clearance required for grout flow in the void. This size provides 7/8 in. clearance around the pier pipe when sitting centered in the embedded insert. Beyond the pipe the footing and cap are dimensioned exactly as the CIP bent specimen was. The footing measures 4 ft. x 4 ft. x 2.5 ft. and the cap measures 15 ft. x 2 ft. x 2.5 ft. (L x W x D). With the presence of the embedded pipe adjustments to the top reinforcing and bottom reinforcing of the footing and cap, respectively, had to be made. For the footing this was simply accomplished through adequate 90^0 rebar hooks for any of the interrupted top mat reinforcing with the bars falling outside of the embedded HSS pipe constructed as normal.

The cap design required a unique approach as the experiment aimed to ensure failure occurs in the pier. With the requirement that none of the reinforcing interrupted by the embedded HSS be consider to constitute to the cap's moment capacity the cap is consider to be comprised of two individual concrete beams on either side of the HSS pipe. This results in design of a beam having a cross-section of 7.7 in. x 30 in. to conservatively handle one half of the targeted moment capacity of 500-kip-ft. As can be seen in the cap cross-section in Figure 4.7 the resulting beam is comprised of three layers of two #6 Gr. 60 rebar on either side of the HSS pipe with a resulting moment capacity of 608-kip-ft. Additionally, the top reinforcing is similar to the CIP bent cap with 11 #6 Gr. 60 rebar be provided. The cap is designed with #4 Gr. 60 stirrups provided on 4 in. center-to-center spacing. As in the CIP bent specimen and in compliance with ITD's general practice, two alternating #4 Gr. 60 cross-ties are provided for each stirrup. Also seen in the cap cross section is the grout polyvinyl chloride (PVC) pipe inlet and air vent at the top of the HSS pipe.

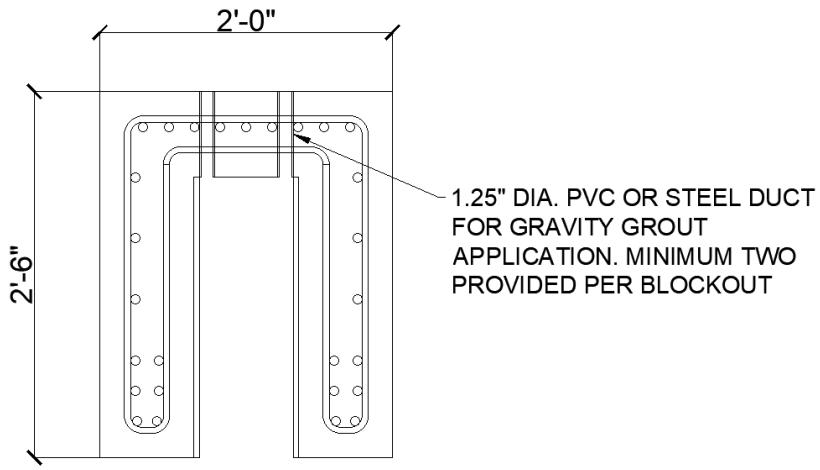

Figure 4-7: Precast Bent Cap Detail

The final resulting precast bent having the same overall dimensions as the CIP bent is provided in Figure 4.8. The figure provides the full detail of bent, showing the implementation of the proposed connection.

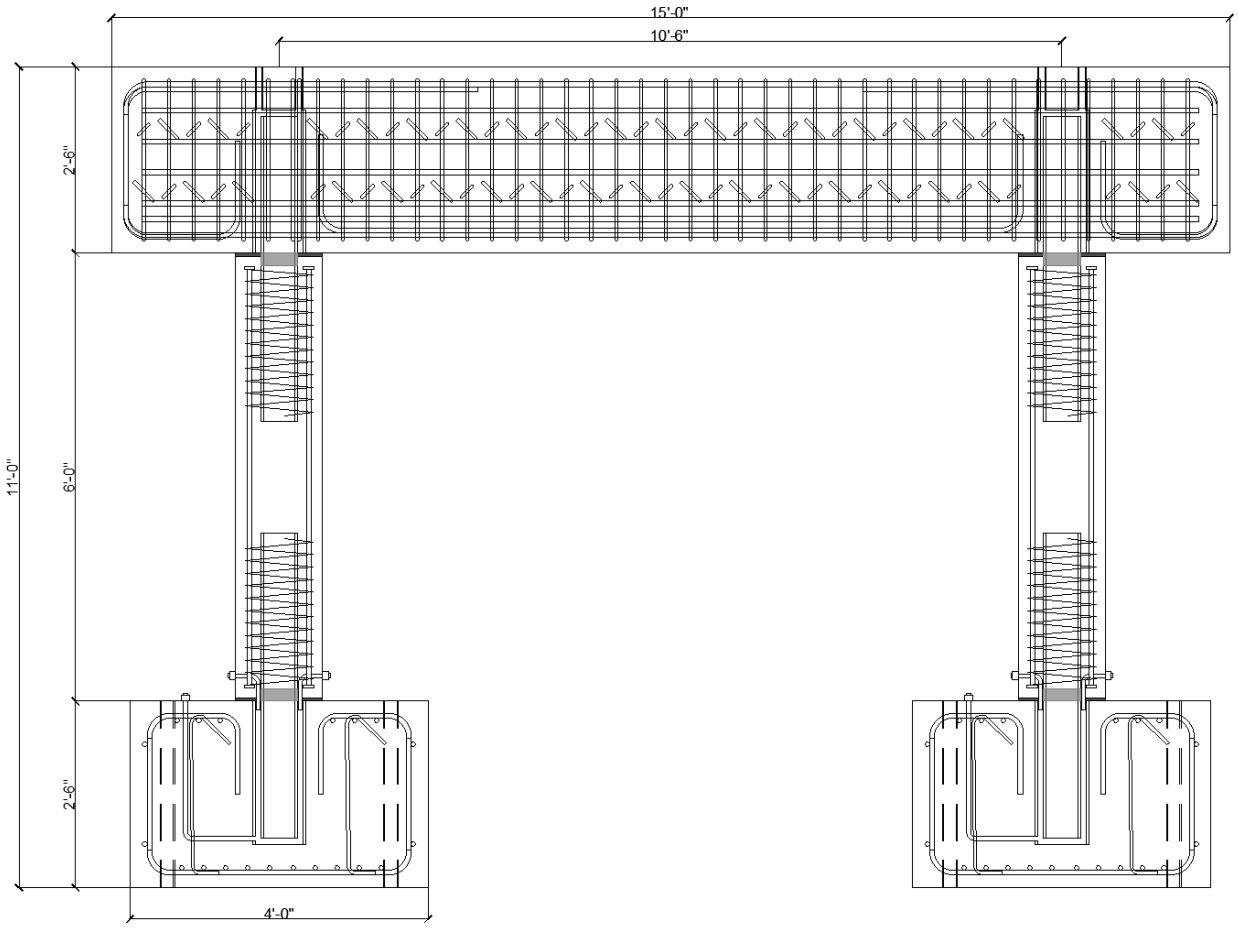

Figure 4-8: Precast Bent Specimen

4.4. CONSTRUCTION

The construction of the precast bent is done completely outside the lab with each element, footing, piers, and cap, poured and moved into the lab for assembly as would be performed on a true ABC bridge project. The cages for each respective element are constructed and placed in the form work reused from the CIP bent. The reuse of the form work for the footing is simply done as the footing forms are not required to be altered or reworked. The HSS pipe is first sand blasted, for improved bond with both the concrete and grout, then fabricated with suitable rebar risers so as to be secured and sit at the proper height for pouring. The grout inlet is also fashioned in place prior to placement. Finally, a wood block is fixed to the bottom pipe end and sealed with

caulk to ensure concrete does not rise into the embedded pipe. The rebar risers, grout inlet and wood block are all shown in Figure 4.9 after fabrication and installation. Figure 4.10 provides the completed footing elements after the full installation of the embedded HSS pipe, grout inlet, rebar cage, and anchoring sleeves.

Figure 4-9: Embedded HSS Pipe Prepared for Install

Figure 4-10: Precast Bent Footing Elements

The pier construction is carried out independently of the footing construction as opposed to the traditional CIP method used for the benchmark specimen. The rebar cage and HSS pipe sections are fabricated and placed in the forms for pouring. The piers for the precast bent are poured horizontally as opposed to vertically for the CIP bent. This greatly reduces the labor involved and increases safety as all work can be completed on the ground as opposed to lifting concrete to the finished pier height. The forms from the CIP bent construction are simply reduced to three sides as the piers are poured on a casting bed outside the lab (Figure 4.11).

Figure 4-11: Precast Bent Pier Prepared for Concrete

Following the completion of the footing and piers the cap construction began. Due to available space on the casting bed the items had to be cast in separate pours. Whereas a true precast operation can likely handle producing the items at one time or as is necessary for the project. The cap is poured similar to that of the CIP bent cap, but is constructed and poured on a casting bed making the full process much simpler and safer. The forms from the CIP bent are again used and are placed after the rebar cage is completed. The HSS pipe embedment's are placed and sealed to the precast bed. The rebar cage is then lowered into place (Figure 4.12) with the forms and grout ducts placed last. Rebar lifting hooks are also installed to assist with

handling and erecting of the cap. The construction of each element is followed by pouring of the concrete, form removal, and relocating of the elements.

Figure 4-12: Cap Rebar Cage Placement

Erection of the precast elements in the lab requires the use of a 5-kip and 12-kip forklift. The 5-kip forklift is capable of handling all precast elements but the cap. It is used as much as possible as it is significantly easier to maneuver and handle in the lab setting as opposed to the 10-kip forklift which is very massive when operated in the lab. The footings are placed and anchored to the floor followed by the erection of the piers. The piers are firstly fitted with alignment fins to ensure proper centering of the piers within the HSS pipe embedment in both the footing and cap. The alignment fins also serve to ensure a minimum gap is maintained on all sides of the pier pipe to ensure grout application is possible. The piers are then lowered into

place (Figure 4.13). After placement the grout air vents located in the base of piers are ensured to not be blocked by the elastomeric pad and allow air flow for grout application.

Figure 4-13: Precast Bent Pier Erection

The cap is then prepared for placement. Due to the height limitation in the lab the 12-kip forklift had to be fitted with an extension frame to place the cap. The extension frame allowed for the cap to reach the necessary height to pass over the top of the pier HSS pipe extending from the pier tops and be lowered down (Figure 4.14). After the placement of the precast cap the connections are grouted using SikaGrout 328. SikaGrout 328 is determined as a suitable material due to its ability to be highly flowable, non-shrink, non-metallic content, and it has an extended working time. As the grout is applied through a gravity feed method the extended working time ensured the full void is filled. After sufficient flow is achieved through the grout vents the specimen is allowed to cure and is prepared for testing.

Figure 4-14: Precast Bent Cap Erection

4.5. TEST ARRANGEMENT, INSTRUMENTATION, AND LOADING PROTOCOL

The test arrangement, instrumentation, and loading protocol for the precast bent is setup and done the same as that of the benchmark CIP bent. The one exception in the instrumentation is the strain gages present on the longitudinal reinforcing in the pier of the CIP bent. As the longitudinal reinforcing in the precast piers does not pass through the interface of the connection, the HSS pipe at each connection is instrumented, with a total of 16 strain gages for the full precast bent. The placement of the strain gages can be seen in Figure 4.15. Refer to the test arrangement, instrumentation, and loading protocol sections in Chapter 3 for the full details.

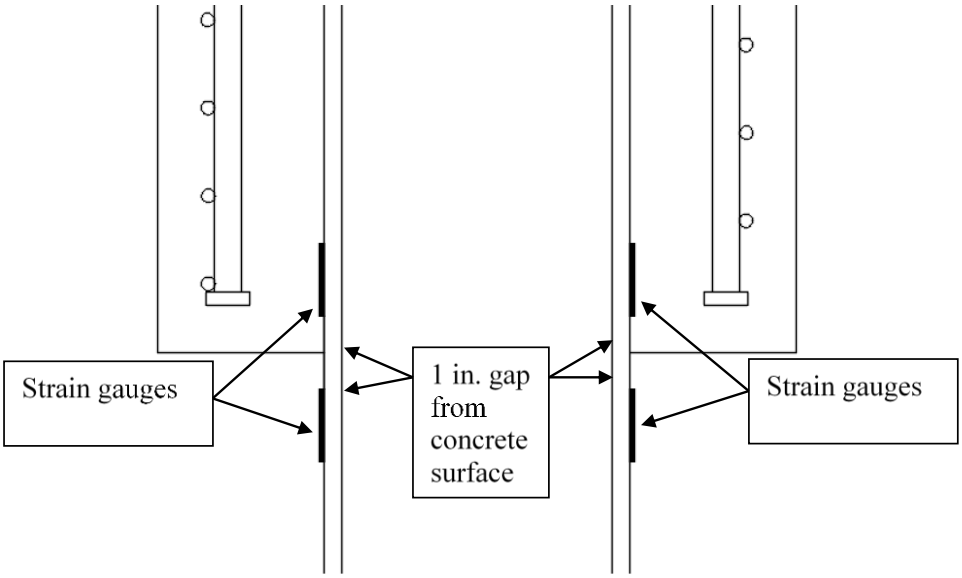

Figure 4-15: Precast Bent Strain Gage Placement

4.6. MATERIAL PROPERTIES

Similar to the CIP bent, after completion of the testing, the concrete samples prepared during each stage of pouring were tested to confirm the concrete properties on test day. Three concrete samples from the footing, pier, and cap pours were tested to verify the respective compressive strength of the concrete. Also, two split cylinder samples were tested. Additionally, the grout properties were tested using three 2 in. cube for compressive strength and two cylinders for the split cylinder tests. The 28-day compressive strength of concrete, f'c, is targeted to be 4000 psi. Table 4.2 and 4.3 provides a summary of the test day compressive strength and split tension results, respectively.

Table 4-1: Precast Bent Test Day Compressive Strength

Sample	1	2	3	Average (psi)
Footing	4464	4352	4347	4388
Piers	5125	5153	4835	5038
Cap	4698	5058	4786	4847
Grout	7560	7070	7385	7338

Table 4-2: Precast Bent Test Day Split Tension

Sample	1	2	Average (psi)
Footing	448	492	470
Piers	562	474	518
Cap	536	403	470
Grout	1041	786	914

4.7. EXPERIMENTAL TESTING

The test again started with a first cycle targeted displacement of +/-0.18 in. achieving a maximum of 0.15 in. no visible cracking developed. The second cycle again developed no visible cracking. A slight gap opening at the elastomeric pad is observable during the second cycle. On the third cycle hairline cracking within 18 in. of the footing and cap interfaces on the pier face developed (Figure 4.16a). The fourth and fifth cycles resulted in additional hairline cracking expanding up and down the full length of the piers and the development of vertical hairline cracks near the ends of the pier (Figure 4.16b). Additionally, slight spalling developed at the top connections resulting in quarter sized concrete pieces. During the sixth cycle top connection spalling developed further and crack development continued with maximum cracking of 0.4 mm (Figure 4.16c). The gap opening at the elastomeric bearing on the tension side was widening to approximately 3/16th in. gap (Figure 4.16d). The seventh, eight, and ninth cycles continued crack development with spalling at the base connections resulting during the ninth

cycle. Overall crack development is significantly less than that of the CIP bent. Cracking frequency is reduced with few large cracks developing after initial hairline crack development resulting in large slab like spalling. It is during the ninth cycle the maximum lateral force of 71.4-kip is achieved. Figure 4.16e demonstrates the significant slab spalling developed during the ninth cycle. The spalling resulted in an approximately 3-kip drop in force and correlated with exposure of spiral reinforcing. The tenth cycle resulted in minimal additional spalling and continued crack development. The eleventh cycle resulted in continued spalling of slabs, with significant increased spalling at the pier top connections (Figure 4.16f). At this point the north pier away from the lateral actuator experienced the majority of spalling. During the twelfth cycle the south pier developed significant spalling at the bottom connection (Figure 4.16g). The fourteenth and fifteenth cycles resulted in continued spalling and cracking development with the gap opening at the elastomeric bearing having increased to approximately ½ in. (Figure 4.16h). To this point both piers had developed spalling at both, the top and bottom, connections resulting in exposed spiral and longitudinal reinforcing. Additional cracking had stopped developing with existing cracking continuing to widen. The HSS pipe had yet to be exposed.

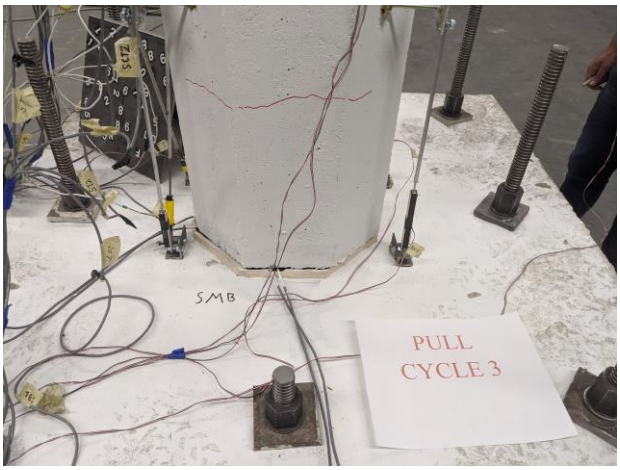

a) Cycle 3: Hairline Cracking

b) Cycle 5: Vertical Hairline Cracking

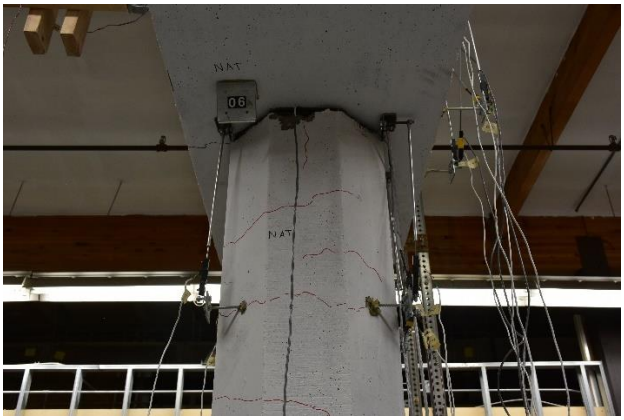

c) Cycle 6: Spalling Development

d) Cycle 6: Gap Opening 3/16 in.

e) Cycle 9: Slab Spalling Bottom

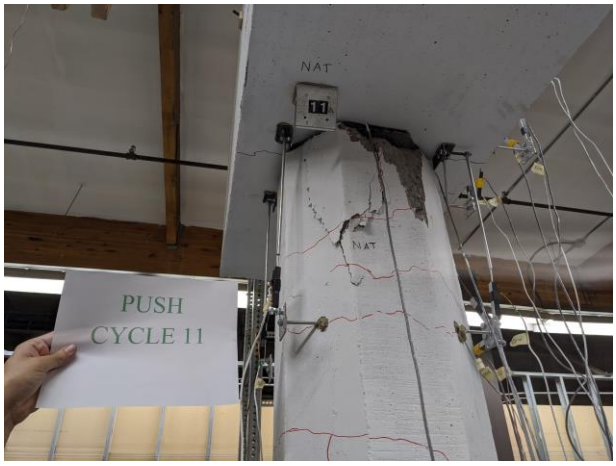

f) Cycle 11: Slab Spalling Top

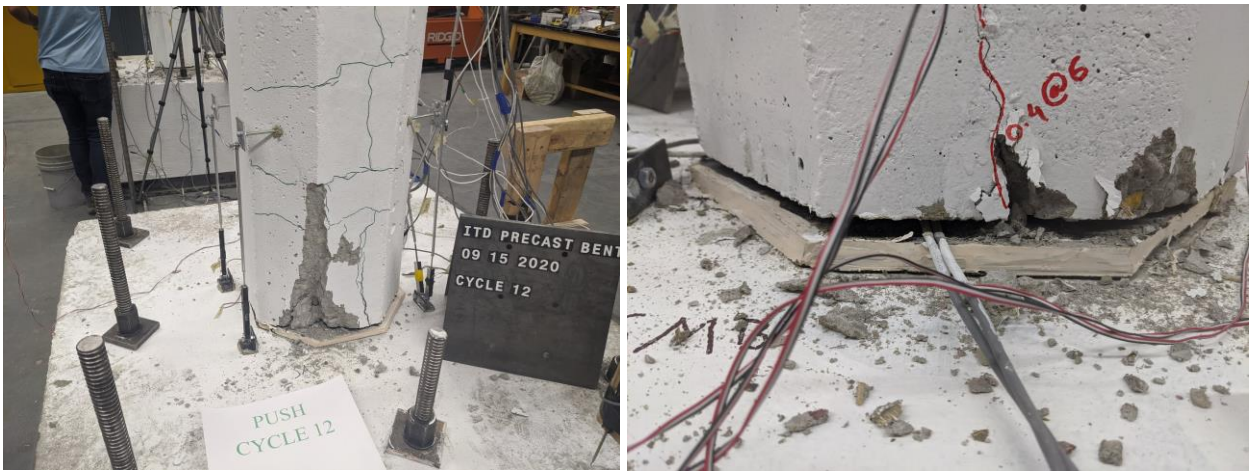

g) Cycle 12: Slab Spalling North **h) Cycle 14: Gap Opening ½ in.**

Figure 4-16: Precast Bent Testing

Spalling continued to develop at all connections from the sixteenth to eighteenth cycles. Exposure of the pipe resulted on the eighteenth cycle (Figure 4.17a). During the nineteenth cycle development of a vertical crack in the pier face perpendicular to the loading actuator developed significantly (Figure 4.17b). The vertical crack continued to develop over the following cycles indicating the spiral reinforcing losing confinement allowing the pier concrete to begin separating from the HSS pipe (Figure 4.17c). During the twenty-fourth cycle the maximum force achieved dropped to 55-kip, achieving the targeted 20% strength degradation. Figure 4.17d provides an image of the north pier bottom connection at failure.

a) Cycle 18: HSS Pipe Exposure

b) Cycle 19: Perpendicular Face Cracking

c) Cycle 24: Confinement Failure

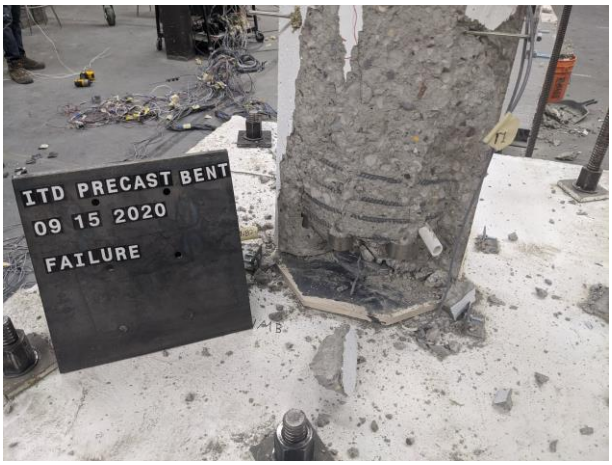

d) Cycle 24: Failure

Figure 4-17: Precast Bent Failure

The HSS pipe had not been exposed enough to evaluate it at the time the test was terminated. Additional concrete is removed manually to better observe the HSS pipe. From observation of the exposed HSS pipe it can be observed that the top connections resulted in a higher level of deformation. Figure 4.18a to 4.18d provide images of the observed deformation. A significant bulge of the HSS section developed below the cap for both top connections. An

additional observation is the separation of the HSS pipe and grout. The separation is the result of the HSS pipe fracturing just inside the interface of the cap. The HSS pipe underwent “necking” while in tension causing it to separate and fracture just inside the interface.

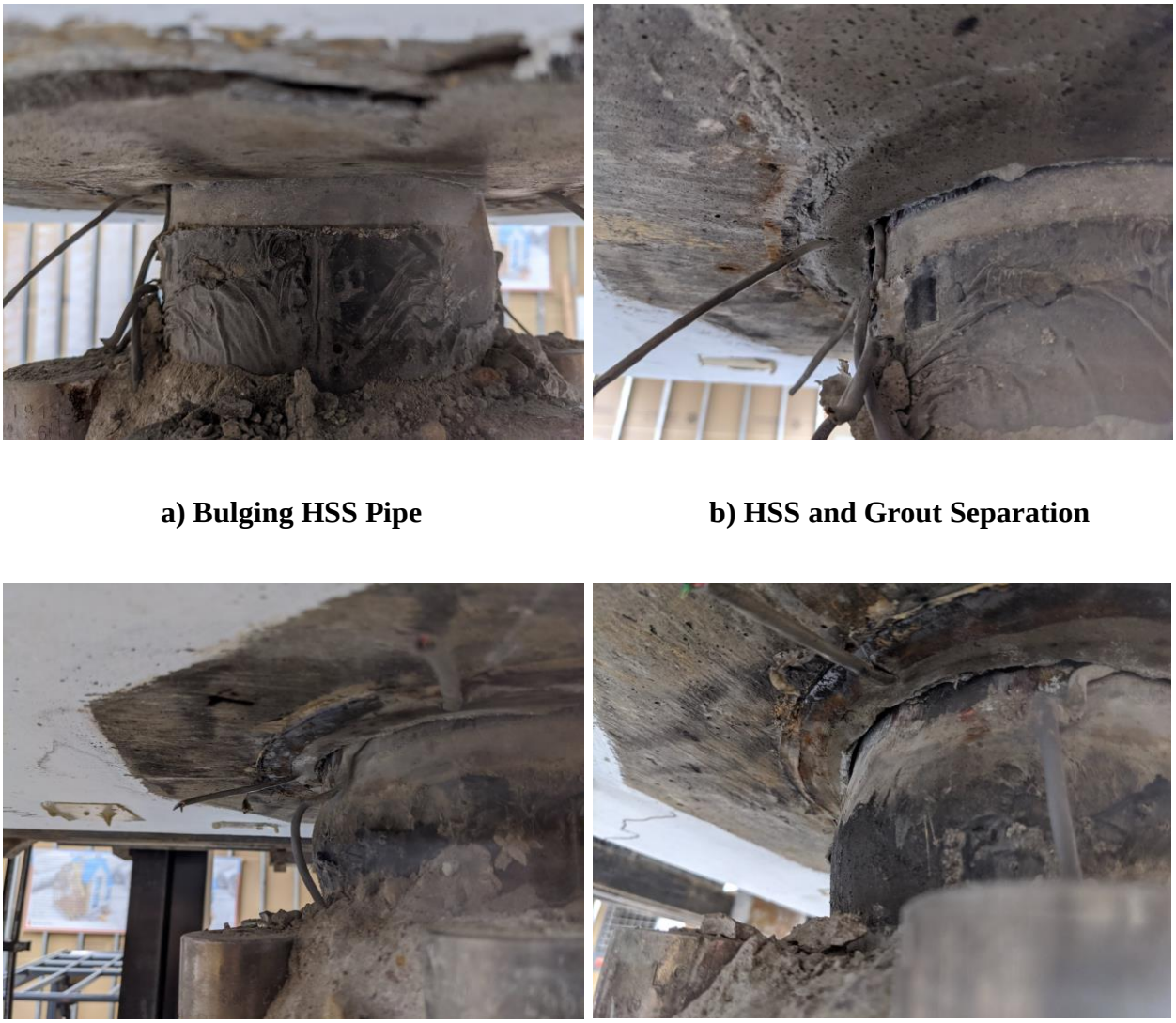

a) Bulging HSS Pipe **b) HSS and Grout Separation**

c) HSS Bulging **d) HSS Bulging and Separation**

Figure 4-18: Precast Bent Top Connection Post Test

The bottom pier connection exhibited far less damage and deformation. Slight bulging was present but minimal in comparison to the top connections. Figure 4.19a provides a view of

the minimal bulging that resulted. The bottom connection did not exhibit any signs of the HSS necking. No separation of the grout and HSS pipe was observed.

e) South Pier

f) North Pier

Figure 4-19: Precast Bent Bottom Connection Post Test

During the testing the bent performed a total of 24 cycles resulting in a maximum actual peak displacement of 7.6 in. A side view of the bent is provided in Figure 4.20 showing the bent at the maximum pushed state during the 24th cycle. The targeted displacement during the 24th cycle is 8.4 in., but similar to the reaction frame flex during the CIP bent test the frame was not acting completely rigid. Table 4.1 provides the targeted displacement and drift ratios and the actual values achieved during the testing of the precast bent.

Figure 4-20: Cycle 24 Peak State

Table 4-3 Precast Bent Loading Protocal Summary

	Programmed Values		Actual Displacements	
Cycle	Displacement (in.)	Drift (%)	Displacement (in.)	Drift (%)
1	0.18	0.21	0.15	0.18
2	0.35	0.42	0.27	0.32
3	0.7	0.84	0.53	0.63
4	1.06	1.27	0.78	0.93
5	1.41	1.68	1	1.19
6	1.76	2.10	1.28	1.53
7	2.11	2.52	1.55	1.85
8	2.46	2.94	1.92	2.29
9	2.81	3.36	2.25	2.69
10	3.17	3.79	2.61	3.12
11	3.52	4.20	3.06	3.65
12	3.87	4.62	3.38	4.04
13	4.22	5.04	3.7	4.42
14	4.57	5.46	4.03	4.81
15	4.92	5.87	4.37	5.22
16	5.27	6.29	5.04	6.02
17	5.62	6.71	5.38	6.42
18	5.97	7.13	5.71	6.82
19	6.32	7.55	6.05	7.22
20	6.67	7.96	6.39	7.63
21	7.02	8.38	6.7	8.00
22	7.37	8.8	7.04	8.41
23	7.72	9.22	7.4	8.84
24	8.07	9.64	7.66	9.15

The data captured during the precast bent test is presented in a similar layout to that in Chapter 3 for the CIP bent specimen. The maximums achieved during the testing of displacement and lateral load were 7.66 in. and 71.4-kip, respectively. The peak lateral load correlates to a total moment capacity of 498-kip-ft. The precast bent demonstrates a stable response through the test progression resulting in significant energy dissipation. The degradation of strength is fairly stable and consistent through the end of the cycles. As assumed for the CIP bent, the four connections shared the lateral load equally, this equates to base shear at each

connection of 17.9-kip. Figure 4.21 and 4.22 provide the resulting precast bent Force vs. Displacement and Force vs. Drift hysteresis. The Force-Displacement hysteresis suggest the precast bent achieved design base shear of 32.5-kip, correlating to a yield displacement of 0.95 in. (Figure 4.21). Similarly, from the Force-Drift hysteresis it is seen the bent yielded at a drift ratio of 1.13% (Figure 4.22). Figure 4.23 provides the Force-Drift backbone curve developed during testing, highlighting the peak force and displacements achieved throughout the test. The curve exhibits a stable consistent degradation of the precast bent strength as the test progressed.

It should be noted for the figures the positive vertical axis shows the specimen in push. As the test began by first pulling the specimen and continued to begin all cycles in pull. It can be observed the bent exhibited higher strength during pulling as opposed to pushing, which can be attributed to two factors. The bent underwent softening during the first pull of the cycle thus exhibiting higher strengths in all cycles. Additionally, the reaction frame exhibited slightly higher stiffness during the pulling stage as opposed to experiencing higher displacement during the pushing stage.

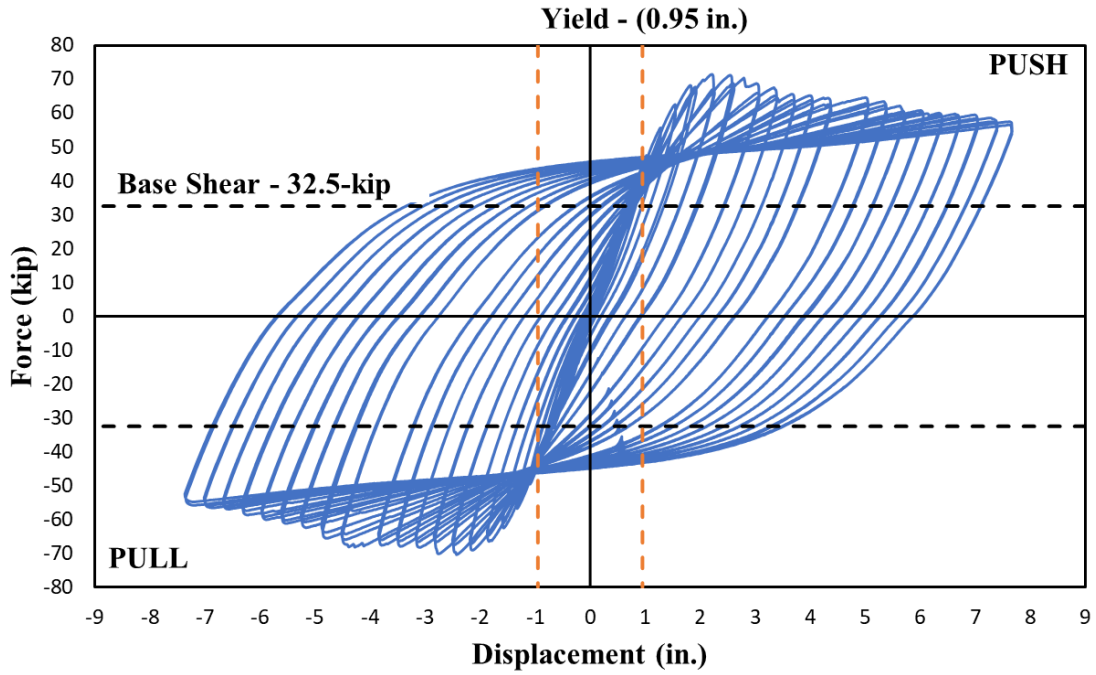

Figure 4-21: Precast Bent Force-Displacement Hysteresis

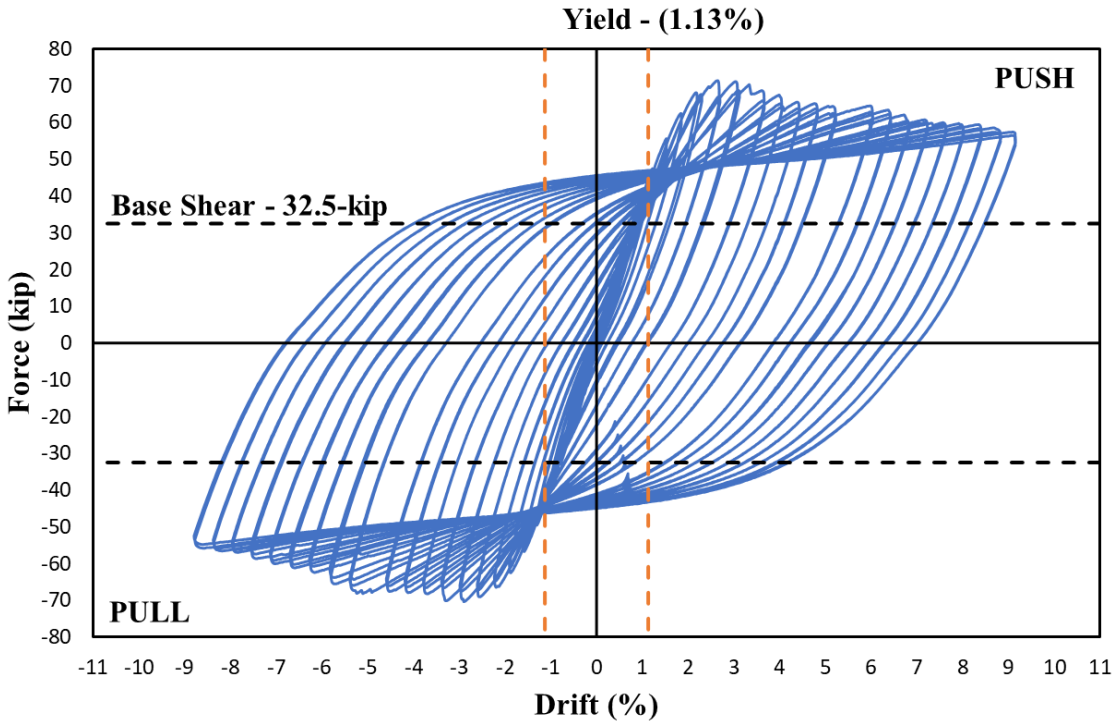

Figure 4-22: Precast Bent Force-Drift Hysteresis

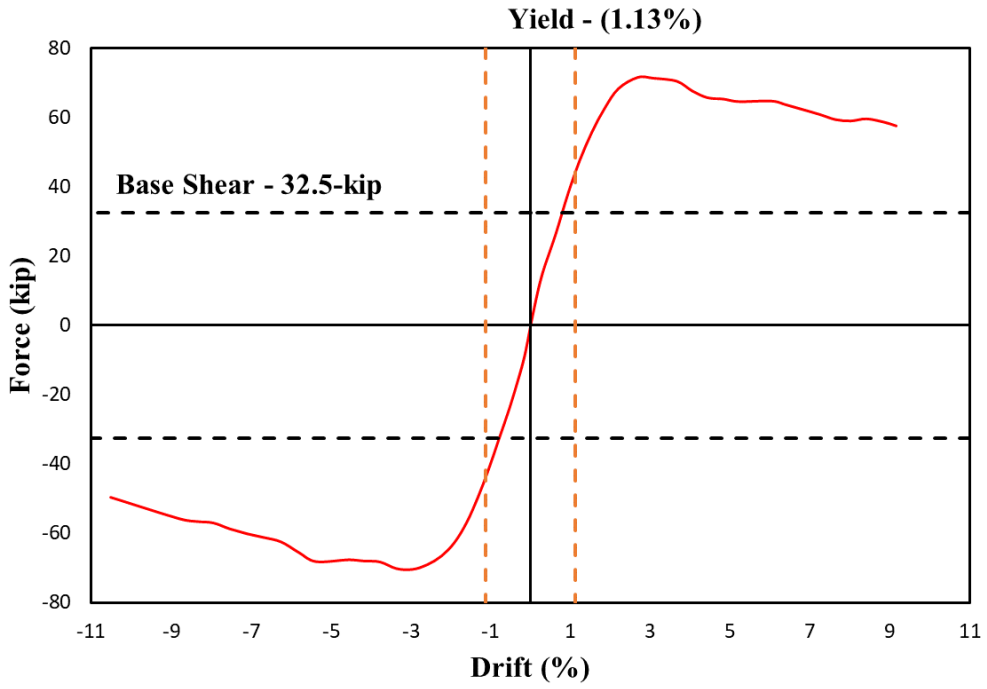

Figure 4-23: Precast Bent Force-Drift Backbone Curve

Analysis of the potentiometers, specifically located in the plastic hinge regions (groups A, B, C, and D), again provide a close breakdown of each connection's reaction through moment-curvature. The progression of the yield, captured by the instrumentation at each plastic hinge, can be observed in Figure 4.23, providing the moment-curvature of each. Observation of four plots shows great stability and consistency across all four connections. Each demonstrated a significant amount of energy dissipation. All four moment-curvature hysteresis can provide easy identification of the 3-kip drop in force which took place during the ninth cycle. This demonstrates good correlation between the observational data and instrumental data collected during the test. Further observation of the plots shows a consistency in the strength degradation once the precast bent reached ultimate lateral capacity.

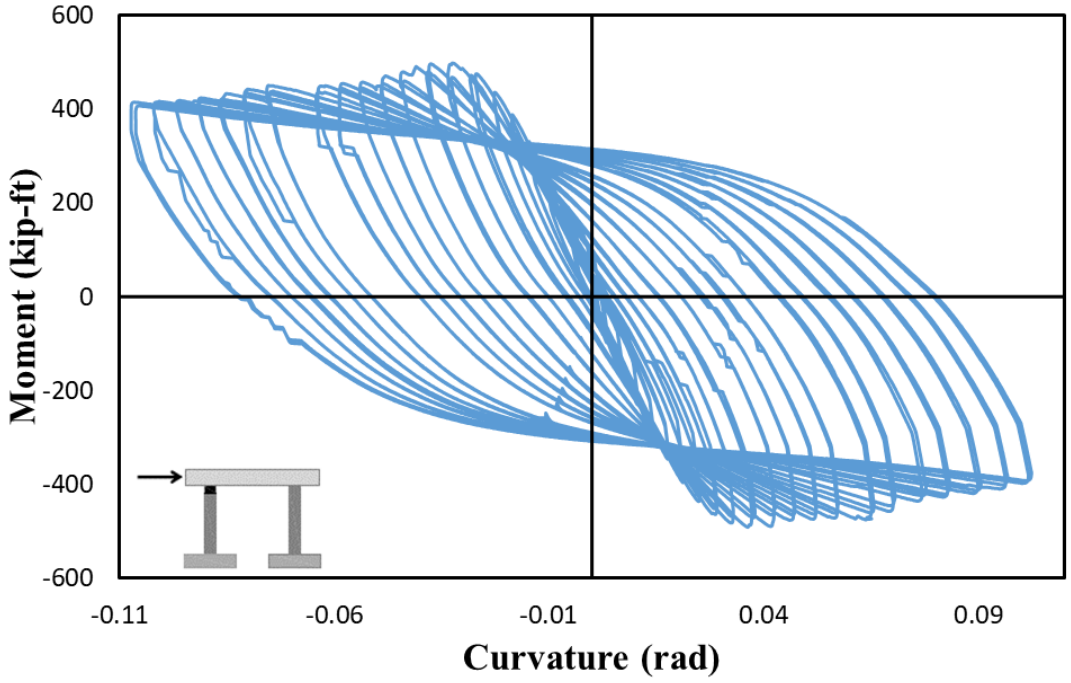

a) South Pier: Top (D1-S – D4-S)

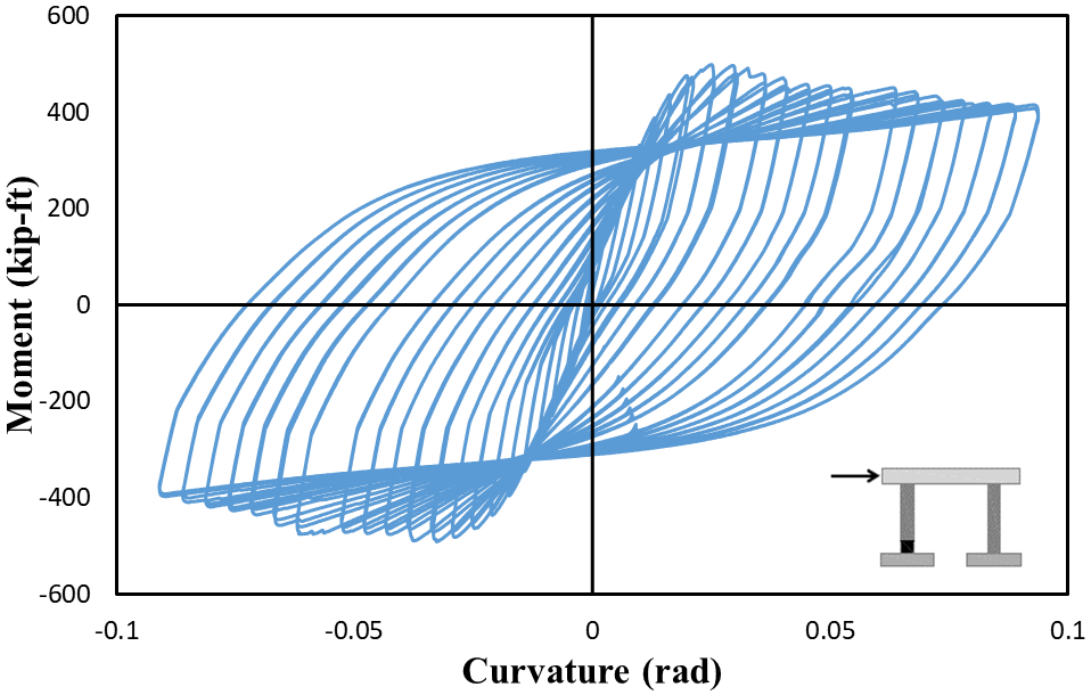

b) South Pier: Bottom (A1-S – A4-S)

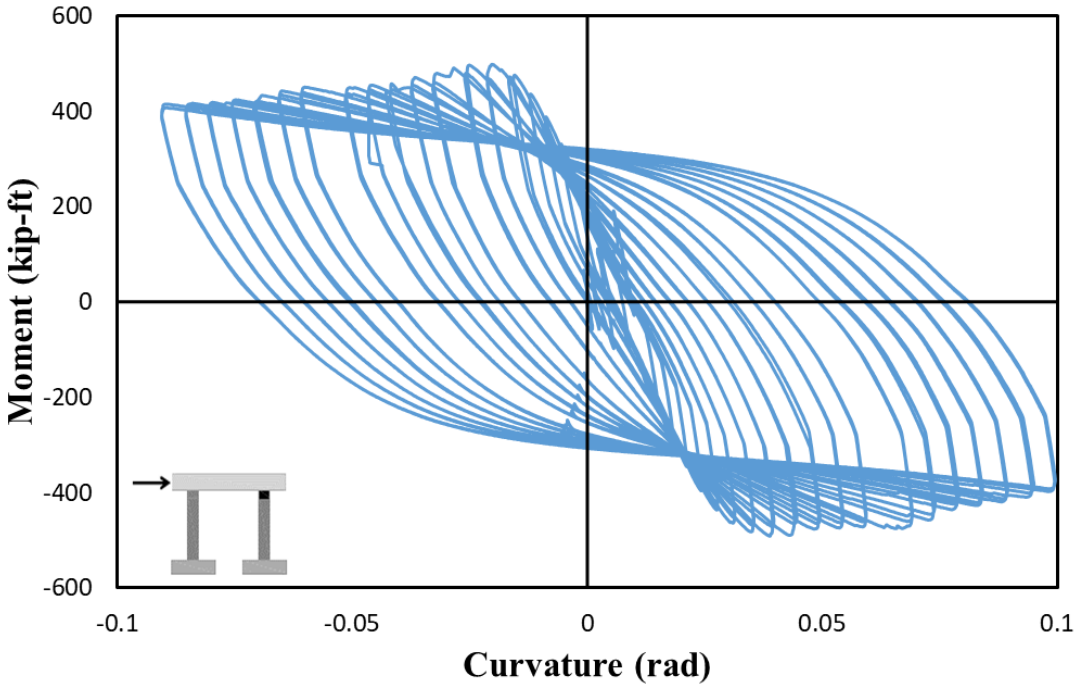

c) North Pier: Top (D1-N – D4-N)

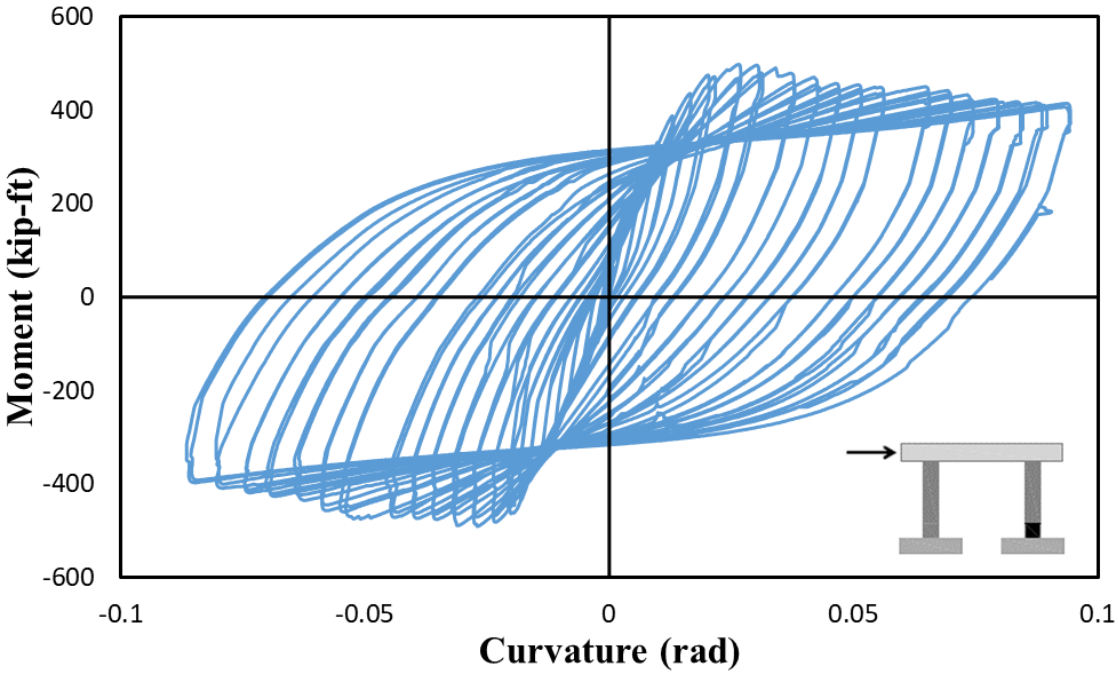

d) North Pier: Bottom (A1-N – A4-N)

Figure 4-24: Precast Bent Moment-Curvature Hysteresis

The final figure provided from the instrument data is the Dissipated Energy (Figure 4.25). Similar to the approach for the CIP bent the energy dissipated at each cycle is determined and the cumulative dissipated energy resulting is 2,125 kJ. This is significantly larger than that of the CIP bent due to the ability of the precast bent to perform 23 full cycles as opposed to the 16 cycles performed by the CIP bent. A comprehensive discussion comparing the two bents is presented in Chapter 5.

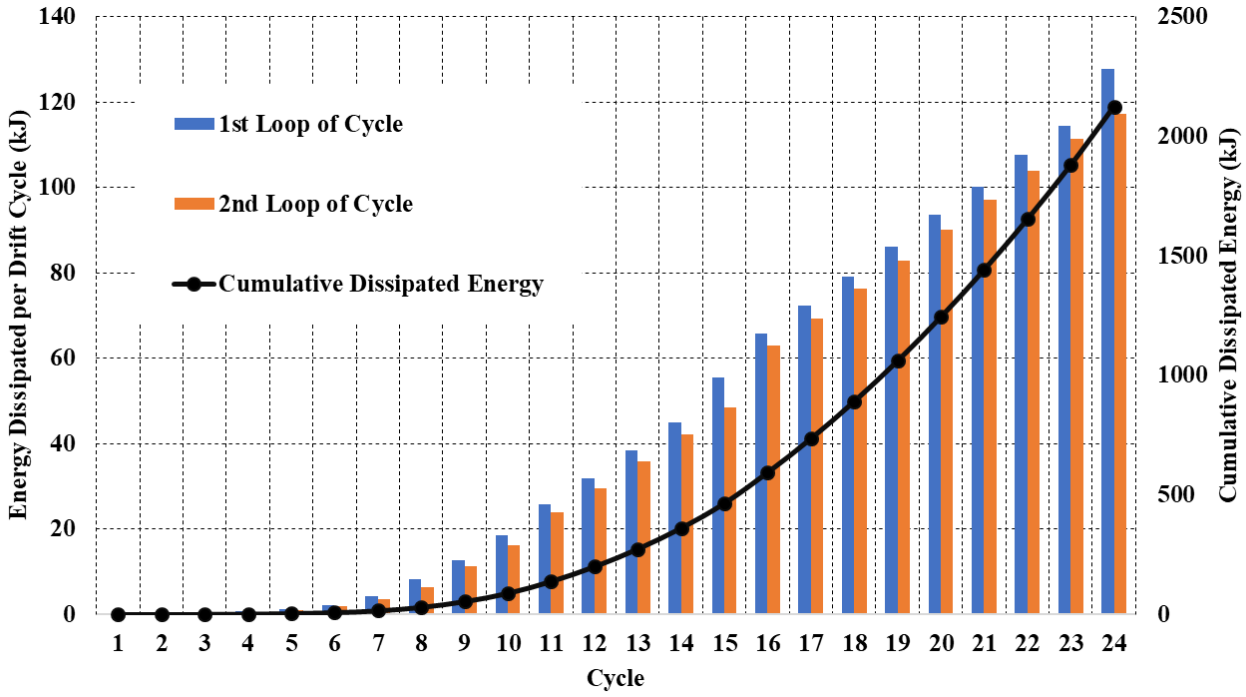

Figure 4-25: Precast Bent Dissipated Energy Per Cycle and Cumulative

Similar to that of the CIP bent backbone curve is analyzed using displacement in place of curvature for a bilinear approximation providing the following results. The global yield moment capacity produced from the experimental results is used to obtain the base shear yield of 62-kip corresponding to a yield displacement of 1.246 in. The ultimate base shear provided from the

backbone curve gives a total base shear of 70.8-kip at a displacement of 2.53 in. The bilinear approximation is shown in Figure 4.26, below. The overstrength factor is calculated in the same fashion as that of the CIP bent and results in a factor of 2.18 for the precast bent. With accompanying displacement ductility's (μ) of 2.03 at ultimate base shear and 6.02 at failure point.

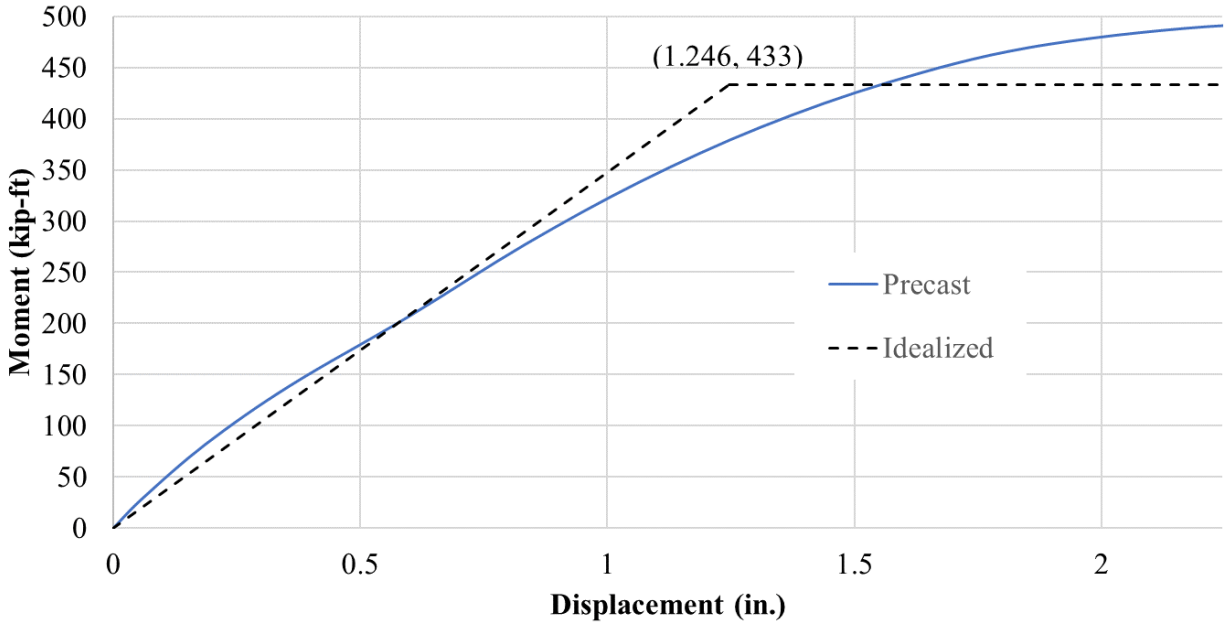

Figure 4-26: Bilinear Approximation for Precast Bent

The residual drift of the precast bent is presented in Figure 4.27, providing the permanent deformation of the pier after the completion of each cycle. At the point of failure or test termination, the precast bent was maintaining 74.8% (6.84% drift ratio) of the drift applied, 9.14%.

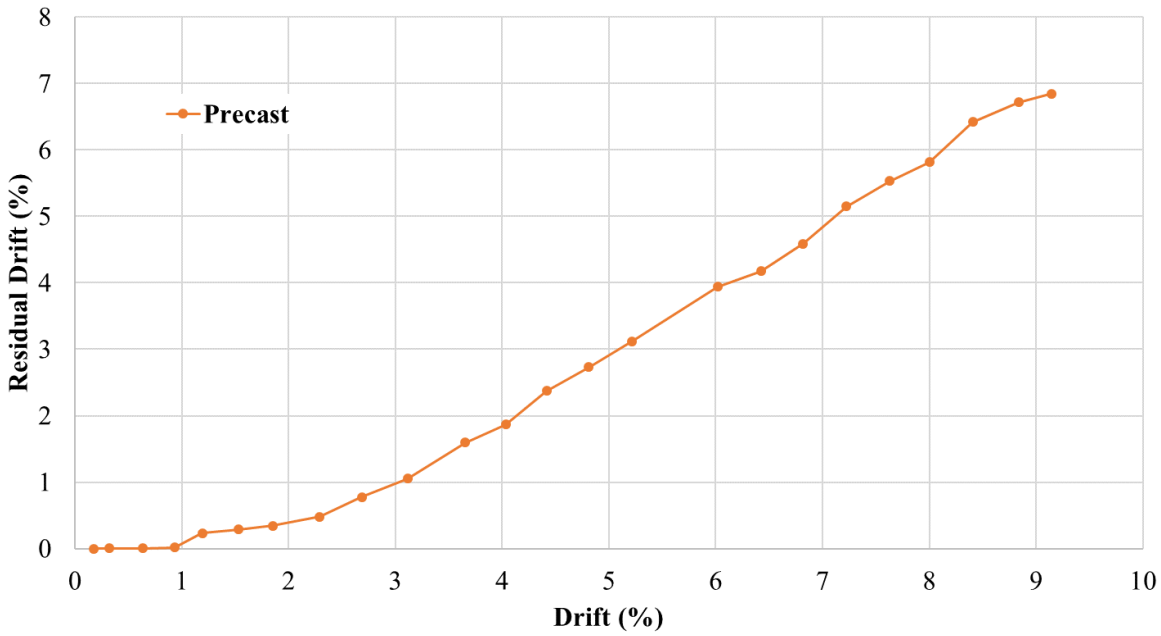

Figure 4-27: Residual Drift of Precast Bent

4.8. CONCLUSION

The precast bent designed, constructed, and tested with the proposed connection is intended to emulate a CIP bent under similar conditions. With the proposed connection allowing for the adaption of ABC in regions of seismicity. Using previously developed design equations for CFSTs from WSDOT Bridge Design Manual and the AASHTO LRFD Bridge Design Specifications, the proposed connection using embedded HSS pipe sections is incorporated into a similarly sized concrete bent as that of previously tested benchmark CIP bent, to be tested in SLAB at ISU. Incorporating specific design details in the proposed connection assisted in the connections ability to emulate a CIP connection. The use of an elastomeric bearing pad at the base and top of the piers allows for the piers to have available flexure at small drifts resulting in significantly reduced cracking and spalling assisting in the ability to develop similar drift capacities as a CIP connection. The embedment of the pipe is determined to ensure full plastic

capacity is developed prior to pullout. As the HSS pipe is accountable for providing the full flexural and shear resistance for the pier, an unbonded length is provided to allow yielding of the section to take place over a larger area of the HSS pipe. The cap and footings of the bent are designed to be capacity protected members. Each had an embedded HSS pipe section providing a socket for which the pier HSS pipe is fitted into using alignment fins for ensuring proper placement and that the gap is maintained for grouting.

The proposed connection proved to provide a safer pour for all elements of the bent as it could be performed completely at ground level. The full precast bent was able to be constructed prior to any grouting with minimal requirement for bracing. The construction did require for additional equipment capable of handling larger elements during assembly. The grouting process was carried out using a highly flowable grout mix that did well to fill the full void between the two HSS pipe sections.

The precast bent performed well during quasi-static cyclic loading as it performed a total of 24 complete testing cycles achieving 20% strength degradation at a drift ratio of 9.15%. Having achieved an ultimate lateral capacity of 71.4-kip, correlating to a moment capacity of 498-kip-ft. Overall, the precast bent demonstrated a stable consistent response through the full progression of testing. Having resulted in reduced cracking than the CIP bent, but with elevated spalling. The precast bent performance far exceeded expectations and will compare favorably to the CIP bent.

CHAPTER 5 COMPARISON OF CIP BENT AND PRECAST BENT SYSTEMS

5.1. INTRODUCTION

This chapter discusses the CIP and precast bent test results as compared to each other. The data analyzed for both bents in the above chapters is compared and discussed as the performance of the two systems is considered. As the specimens were developed, considering a typical mid to long span bridge in Idaho with the intentions of the CIP bent serving as a benchmark for the precast bent with proposed innovative precast connections for adaption of ABC in seismic areas, the two specimens were designed and built to the same dimensions. This resulted in a bent system comprised of two 14 in. octagonal piers having a height of 6 ft. from top of footing to bottom of cap. The loading height for the specimens, taken from the top of footing concrete to center of lateral actuator, was 83.75 in. The two specimens had connection design strengths of 61.7-kip-ft. and 56.7-kip-ft for the CIP and precast bent, respectively. The CIP bent specimen was designed in accordance with the AASHTO LRFD Bridge Design Manual Specifications (AASHTO 2017). The precast bent's connection moment capacity was determined using WSDOT Bridge Design Manual (WSDOT 2019).

5.2. LOADING PROTOCOL AND DRIFT RATIO COMPARISON

The testing of each specimen aimed to be identical in all aspects, however one item of note which differed between the two tests is the stiffness of the reaction frame. As the reaction frame underwent displacement during both tests the resulting loading of the two specimens differed as a result. Table 5.1, provides a side by side comparison of actual displacements induced on the cap beam of the specimens. Note the CIP bent only completed fifteen cycles, where the precast bent withstood 24 cycles prior to 20% strength degradation. Further examination of the table allows for similar points of the bents to be analyzed and compared.

Table 5-1: CIP Bent vs. Precast Loading Displacements/Drifts

	CIP		Precast	
Cycle	Displacement (in.)	Drift (%)	Displacement (in.)	Drift (%)
1	0.09	0.11	0.15	0.18
2	0.15	0.18	0.27	0.32
3	0.35	0.42	0.53	0.63
4	0.56	0.67	0.78	0.93
5	0.86	1.03	1	1.19
6	1.08	1.29	1.28	1.53
7	1.4	1.67	1.55	1.85
8	1.73	2.07	1.92	2.29
9	2.06	2.46	2.25	2.69
10	2.4	2.87	2.61	3.12
11	2.75	3.28	3.06	3.65
12	3.1	3.70	3.38	4.04
13	3.44	4.11	3.7	4.42
14	3.78	4.51	4.03	4.81
15	4.14	4.94	4.37	5.22
16	N/A	N/A	5.04	6.02
17	N/A	N/A	5.38	6.42
18	N/A	N/A	5.71	6.82
19	N/A	N/A	6.05	7.22
20	N/A	N/A	6.39	7.63
21	N/A	N/A	6.7	8.00
22	N/A	N/A	7.04	8.41
23	N/A	N/A	7.4	8.84
24	N/A	N/A	7.66	9.15

From Table 5.1 specific points where the specimens were displaced at nearly identical drift ratios can be identified. For this, the following points will be compared in the following figures, CIP cycle 2 to precast cycle 1, CIP cycle 4 to precast cycle 3, CIP cycle 11 to precast cycle 10, and CIP cycle 15 to precast cycle 14. Additionally, the ninth cycle of each specimen is observed as this is the cycle at which both the CIP and precast bents exhibited maximum lateral capacity.

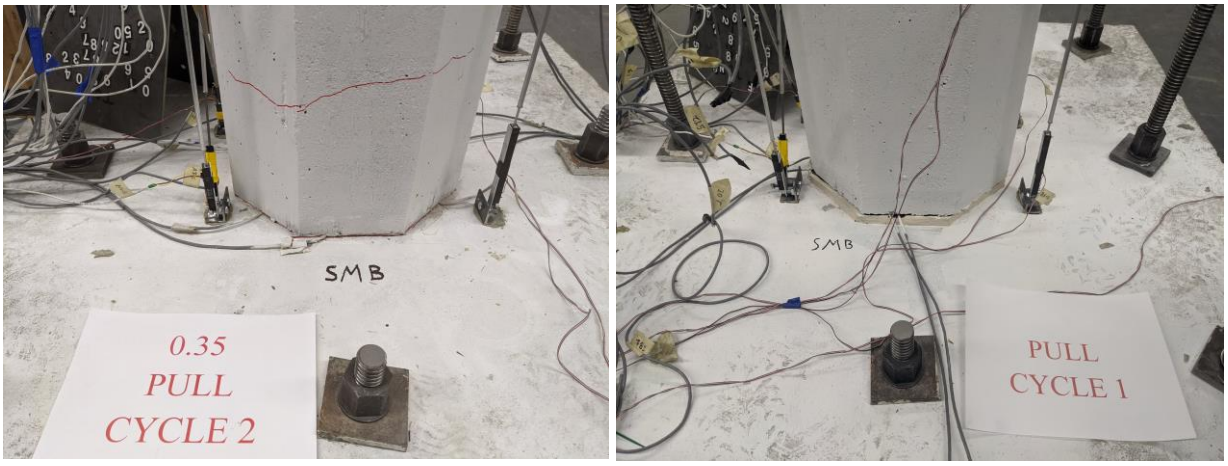

a) CIP Bent: 0.18% Drift **b) Precast Bent: 0.18% Drift**

Figure 5-1: CIP and Precast Bents Cycle 2/1

As can be observed in Figure 5.1, the CIP bent hairline cracks began developing in the plastic hinge zone at drift ratios as low as 0.18%. Whereas the precast bent did not develop hairline cracking until the third cycle, correlating to a drift ratio of 0.32%. The precast bent did have a slight gap opening at a low cycle, present at the elastomeric bearing. The developments of the hairline cracking in the precast pier is presented in Figure 5.2, along with the CIP bent at a similar drift ratio showing cracking development expanding well beyond the plastic hinge zone.

a) CIP Bent: 0.67% Drift **b) Precast Bent: 0.63% Drift**

Figure 5-2: CIP and Precast Bents Cycle 4/3

After this point the two specimens began to significantly differentiate in observable damage. As the CIP bent progressively developed cracks with significant widening of some taking place. The precast bent did not develop a similar level of cracking as the CIP bent did, instead it produced far fewer and less significant cracks. The precast bent resulted in larger slab type spalling earlier than the CIP bent, and was soon the dominate damage taking place as opposed to the CIP bent which underwent far more cracking. Figure 5.3 presents the states of the CIP and precast bent at drift ratios of 3.28% and 3.12%, respectively.

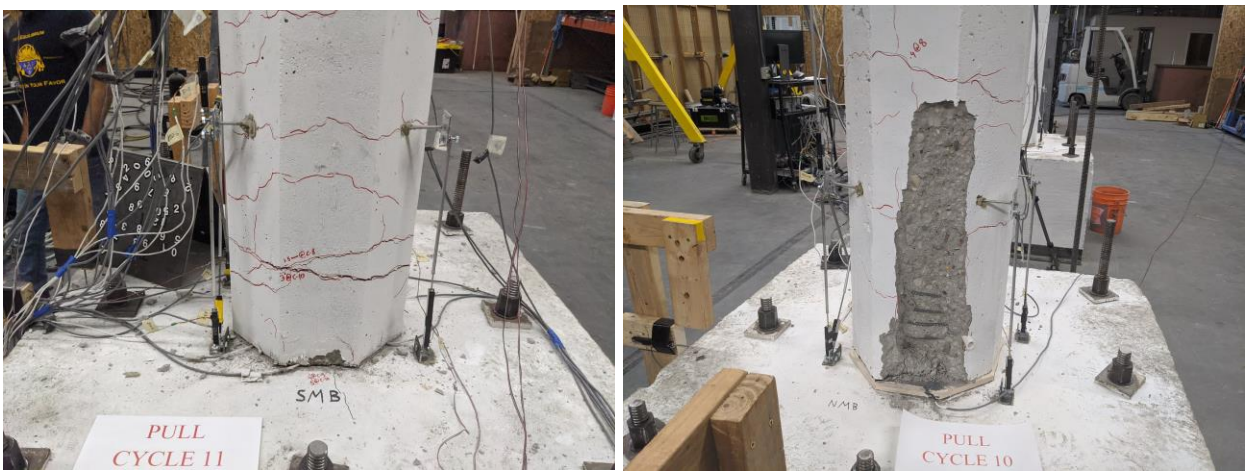

a) CIP Bent: 3.28% Drift **b) Precast Bent: 3.12% Drift**

Figure 5-3: CIP and Precast Bents Cycle 10/11

The CIP bent being terminated at cycle 15 correlated to a drift ratio of 4.94%, this closely correlates to the precast bent's drift ratio of 4.81%, at cycle 14. Figure 5.4a shows the fracture of the longitudinal reinforcing of the CIP bent, which resulted in the targeted 20% strength degradation resulting in the termination of the testing. Figure 5.4b provides the state of the precast bent at a drift ratio of 4.81%. As can be observed from the two images both specimens are exhibiting similar spalling damage. The slab spalling experienced by the precast bent resulted in greater spalling lengths from the interface than that of the CIP bent. The precast bent also exhibited far less depth penetration of damage, as the HSS pipe is enabling the inner concrete of the pier to remain confined and continue to resist lateral loading. Whereas the CIP bent is exhibiting a heightened amount of inner concrete failure, resulting in longitudinal reinforcing failure and reduced shear stability in the connection. The peak load experienced by the CIP and precast bent at the particular cycle were 53-kip and 68-kip, respectively. The greater resistance demonstrated by precast bent correlates to its ability to withstand an additional 10 cycles beyond this point.

a) CIP Bent: 4.94% Drift (Failure) **b) Precast Bent: 4.81% Drift**

Figure 5-4: CIP and Precast Bents Cycle 15/14

Another comparable observation point of the two specimens is the point at which each exhibited the maximum lateral capacity. For this each specimen produced its peak strength during the ninth cycle. The CIP bent demonstrated a maximum lateral capacity of 66-kip, at a drift ratio of 2.46%. The precast bent demonstrated a slightly higher lateral capacity and correlating drift ratio of 71.4-kip and 2.69%. Proving the connection to have a higher ultimate capacity and improved ductility, over that of the CIP bent. As the precast bent was able to withstand 24 complete cycles, whereas the CIP bent only exhibited capacity to withstand 15 complete cycles, the resilience of the proposed precast connection proves to far out perform that of traditional CIP connections.

5.3. HYSTERESIS TEST RESULTS

With the CIP bent having a maximum drift ratio of 4.94% (4.14 in. displacement), having performed 15 total cycles, and the precast bent continuing to a maximum of 9.15% (7.66 in. displacement), performing 24 total cycles, the resulting hysteresis are essential for comparing the

two systems. The resulting maximum forces of 66-kip and 71.4-kip applied to the CIP and precast bent, respectively, provide evidence that the two systems were of similar ultimate capacities and allows for the resiliency of the proposed connection to be observed. However, it is important to note that the precast bent column and cap were comprised of concrete that exhibited a compressive strength near to 5,000 psi., whereas the CIP bent piers and cap were comprised of concrete exhibiting a compressive strength less than 4,000 psi. This discrepancy in concrete strengths contributes to the differing ultimate capacities. Figures 5.5 and 5.6 provide the Force vs. Drift resulting hysteresis for the CIP and precast bents, respectively. The precast bent had an ultimate moment capacity of 498-kip-ft. which was 108% of the 468-kip-ft. exhibited by the CIP bent.

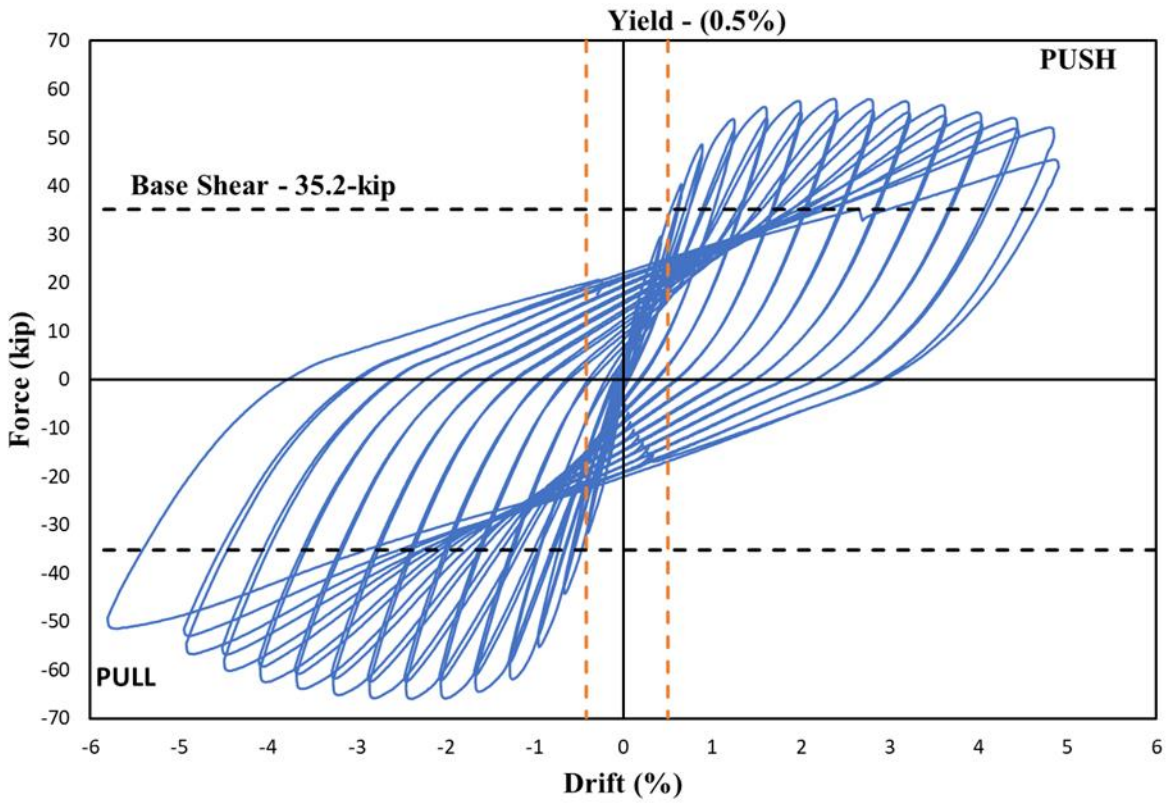

Figure 5-5: CIP Bent Force-Drift Hysteresis

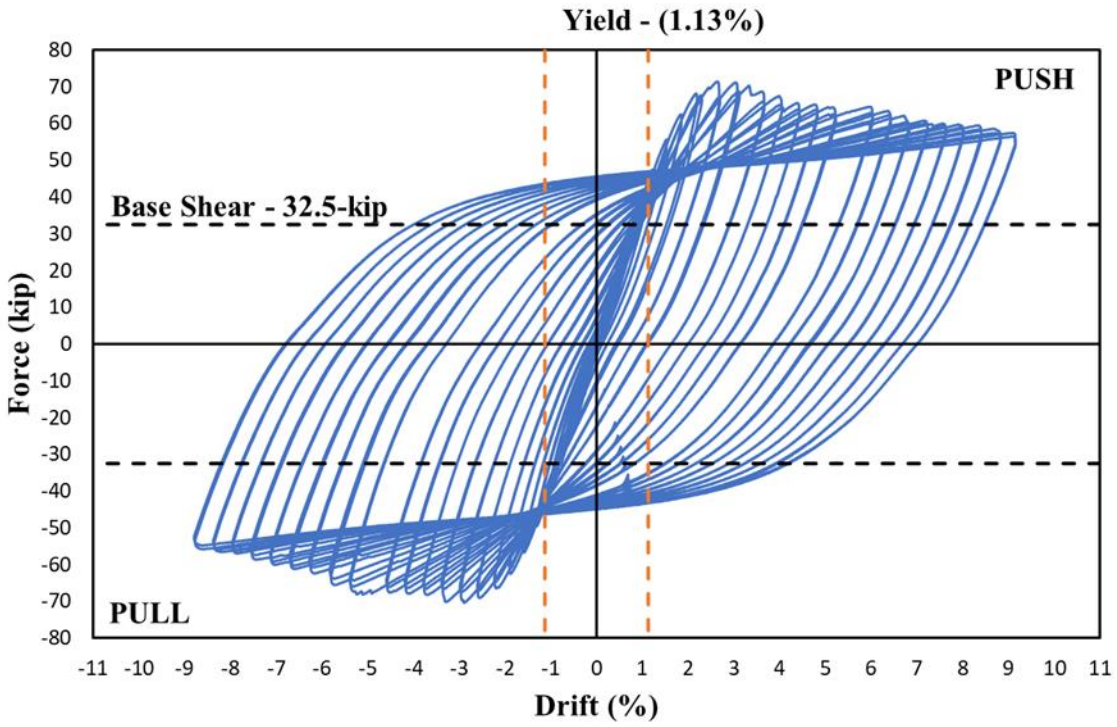

Figure 5-6: Precast Bent Force-Drift Hysteresis

From the hysteresis the yield of the precast bent can be seen at a drift ratio of 1.13%, more than double that of the 0.5% yield drift ratio of the CIP bent. From observation of the two hysteresis it can be seen that the precast force-drift hysteresis is a squarer shape, as it is consistently deep vertically, and maintains a more consistent width. Whereas the CIP bent is more oblong shaped, as it does not maintain stiffness as the precast bent does resulting in shallower loops as opposed to the deep loops of the precast bent. Another item of note is the degradation of strength exhibited by the two systems. Each specimen exhibited similar stiffness during its approach to ultimate lateral capacity. After reaching the ultimate capacity each demonstrated relative consistent strength degradation during continued cycles. The CIP bent degraded strength continually until fracture of longitudinal reinforcing resulted in significant strength loss. The precast bent showed similar consistent strength degradation, with accelerated

points as a result of amplified spalling not exhibited by the CIP bent. With the HSS pipe being further from the surface of the pier, it is assumed this aided the proposed connection to withstand additional cycles. With only periodic spalling of concrete the proposed connection in the precast bent is capable of withstanding far larger displacement and cycles due to the position of the HSS pipe deep within the pier. The longitudinal reinforcing in a CIP pier is much closer to the surface resulting in an inability to withstand large displacements and a high number of cycles under quasi-static loading.

5.4. BACKBONE CURVE

Figure 5.8 provides the two resultant backbone curves of the two systems. It can be observed that the precast bent exhibits a lower stiffness during the cycles of the test up to yielding. This is due to the presence of the elastomeric bearing allowing for small displacements to take place with minimal damage to the concrete. The difference in stiffness is seen from the differing of the slope in the backbone curves up to yielding. It can be determined the precast bent exhibits a stiffness of approximately 38.7-kip/in., where the CIP bent exhibits a stiffness of approximately 56.7-kip/in. Another significant difference is the performance after yielding of the two systems. The CIP bent demonstrates a very smooth progression up to ultimate capacity and then continues with a smooth degradation of strength until test completion. Whereas the precast bent similarly shows a smooth progression up to ultimate capacity. It does not have a smooth degradation of strength to test completion. It exhibits a stepped behavior with observable points of significant strength degradation taking place. These steps are identified as the slab spalling of the cover concrete. These constitute to significant reductions in strength that the CIP bent did not develop. The CIP bent slowly failed through yielding of the longitudinal reinforcing with increased cracking and reduced cracking compared to the precast bent.

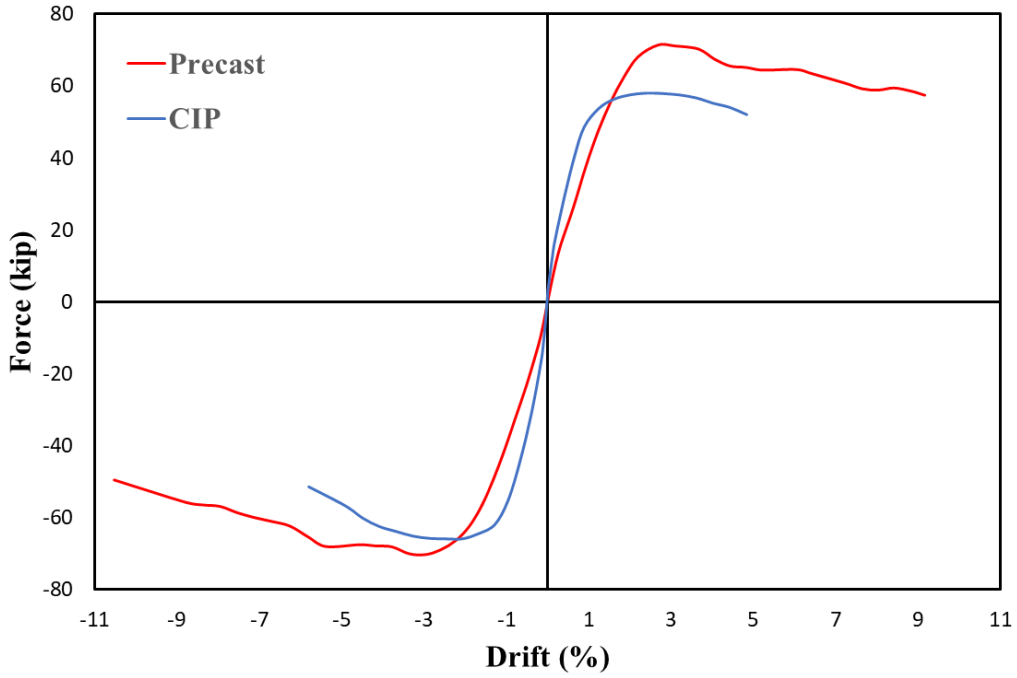

Figure 5-7: CIP and Precast Backbone Curve Comparison

5.5. DISSIPATED ENERGY

The comparison of the dissipated energy of the two systems provides a good basis of measure for the amount of resistance within the structure. As the CIP and precast bent withstood 15 and 24 total cycles, respectively, it is important to observe the cumulative energy dissipated at the following points, each loop, termination of the CIP bent test, and total dissipated by the precast bent. Table 5.2 provides a summary of the cumulative energy dissipated by the two systems throughout the duration of the test.

Table 5-2: CIP vs. Precast Bent Cumulative Energy Dissipation Per Cycle

Cycle	CIP	Precast
1	0.1	0.0
2	0.4	0.4
3	1.3	1.0
4	2.9	2.3
5	5.7	4.4
6	11.8	8.4
7	22.1	16.2
8	37.5	30.6
9	58.9	54.6
10	86.9	89.2
11	122.1	138.9
12	164.8	200.4
13	215.5	274.7
14	274.5	361.6
15	342.4	465.7
16	N/A	594.4
17	N/A	736.2
18	N/A	891.6
19	N/A	1060.8
20	N/A	1244.6
21	N/A	1442.1
22	N/A	1653.8
23	N/A	1879.8
24	N/A	2125.1

From examination of the cumulative energy dissipated as the test progressed, it can be seen that the CIP bent shows high dissipation at the start of the test. This is further reinforced by the higher stiffness exhibited by the CIP bent from examination of the backbone curves in the previous sections. At the tenth cycle the precast bent overtakes the CIP bent in cumulative dissipated energy. By the completion of the fifteenth cycle the precast bent has dissipated a total of 465.7-kJ compared to the 342.2-kJ dissipated by the CIP bent at failure. The precast bent then continues on for an additional nine cycles to finish the test with a total cumulative dissipated

energy of 2,125-kJ. Figure 5.8 provides the two systems cumulative dissipated energy plotted at each cycle.

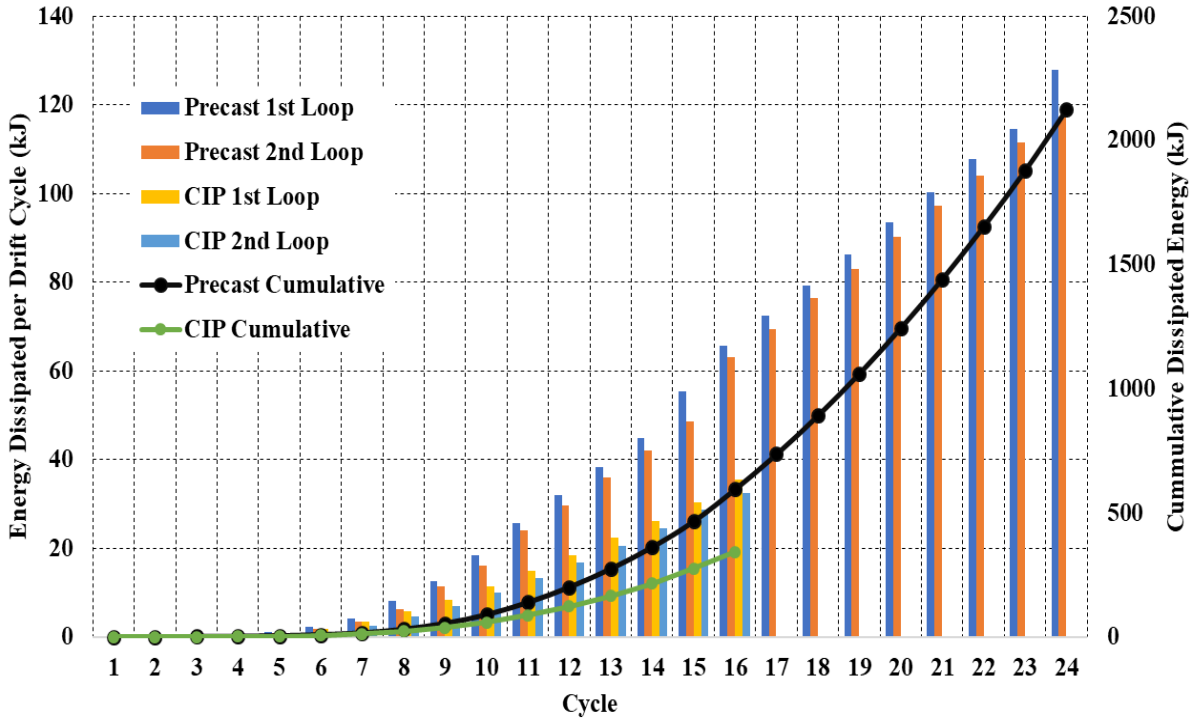

Figure 5-8: CIP and Precast Bent Cumulative Dissipated Energy

An area that proved similar for the two bent specimens was residual drift. As can be seen from Figure 5.9 provided below. The CIP bent exhibited slightly greater values of residual drift than that of the precast bent. Comparing the residual drifts at the failure of the CIP bent provides that the precast bent was displaying a residual drift of 90% when compared to the residual drift exhibited by the CIP specimen.

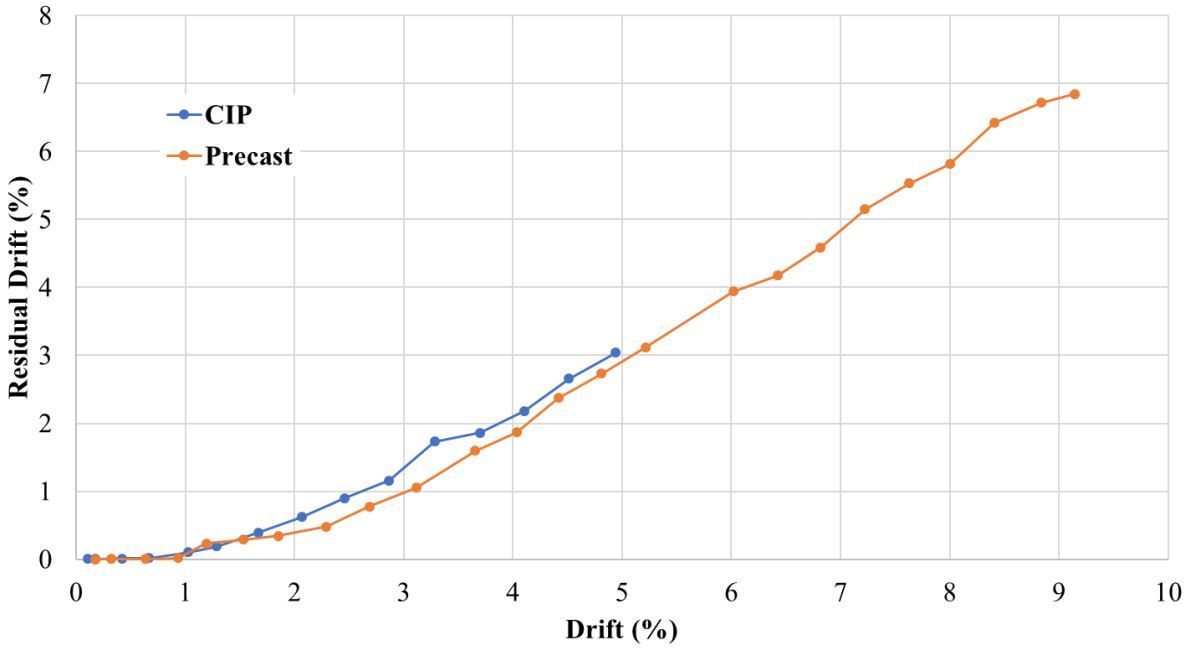

Figure 5-9: Residual Drift Comparison

Table 5.3 provides a summarized comparison of the overstrength factor and displacement ductility of the two specimens. Note the precast specimen exhibits a displacement ductility at ultimate base shear that is 55% and 80% at failure point in comparison to the CIP bent. This correlates to the precast bents reduced stiffness at low cycles.

Table 5-3: Overstrength Factor and Displacement Ductility Comparison

	CIP	Precast	Precast (% Based)
Overstrength Factor	1.76	2.18	124%
Displacement Ductility (Ultimate Base Shear)	3.69	2.03	55%
Displacement Ductility (Failure Point)	7.48	6.02	80%

5.6. CONCLUSION

The two systems performed as expected and designed, with each exhibiting similar capacity having the same overall dimensions and both being subjected to similar loading. The CIP bent developed significant cracking and failed due to longitudinal reinforcing fracture after a total of 15 cycles. The precast bent using the proposed connection exhibited reduced cracking, in comparison, with increased spalling and failed after 24 total cycles due to the HSS pipe deforming and ultimately tearing. The precast pier demonstrated a reduced stiffness, 38.7 kip/in., approaching ultimate capacity in comparison to the 56.7 kip/in. exhibited by the CIP bent. This reduced stiffness is due to the presence of the elastomeric bearing. The precast bent also achieved a higher ultimate capacity of 71.4-kip than that of the 66-kip achieved by the CIP bent. The two systems exhibited a great difference in the yield displacements. Resulting in initial yield displacement drift ratios of 0.5% and 1.13%, for the CIP and precast bent, respectively. However, in comparing global yield the two systems exhibited differing values, as the CIP bent had a global yield of displacement 0.596 in. and a correlating moment of 392-kip-ft. Whereas the precast bent exhibited a global yield at a displacement of 1.246 in. and correlating moment of 433-kip-ft. The two systems also exhibited differences in cumulative energy dissipation. As the reduced stiffness of the precast bent caused it to have lower energy dissipation at lower cycles, it slowly cumulated until the stability and added confinement of the HSS pipe allowed it to produce a more stable consistent response to the continued cycles. At the point of failure, the CIP bent demonstrated a cumulative dissipated energy of 342-kJ where the precast bent at similar cycles (15 total cycles) demonstrated a cumulative dissipated energy of 466-kJ. As the precast bent was capable of withstanding a total of 24 complete cycles the ultimate cumulative dissipated energy of the systems was 2,125-kJ. Additionally, the precast bent exhibited a slightly greater

overstrength factor, 2.18 for the precast bent verse 1.76 for the CIP bent. However, the precast bent exhibited reduced displacement ductility than that of the CIP bent. The precast bent having at minimum matched or exceeded the CIP bent in all categories, except low drift stiffness and displacement ductility due to the elastomeric bearing presence, the proposed connection used is said to have successfully emulated CIP construction under seismic loading. Table 6.1 provides a summarized comparison of the CIP bent and precast bent.

Table 5-4: Summarized Comparison Of CIP and Precast Bent

	CIP	Precast	Precast (% Based)
Max Force	66-kip	71.4-kip	108%
Max Displacement	4.14 in. (4.94%)	7.66 in. (9.15%)	185%
Moment Capacity	460-kip-ft.	498-kip-ft.	108%
Initial Stiffness	56.7-kip/in.	38.7-kip/in.	68%
Initial Yield	0.5% (0.42 in.)	1.13% (0.95 in.)	226%
Global Yield (Bilinear approximation)	0.7% (0.596 in.)	1.49% (1.246 in.)	209%
Correlating Moment Capacity at Global Yield	392-kip-ft.	433-kip-ft.	110%
Energy Dissipation	342 kJ	2,125 kJ (466 kJ)*	621% (136%)*
Overstrength Factor	1.76	2.18	124%
Displacement Ductility (Ultimate Base Shear)	3.69	2.03	55%
Displacement Ductility (Failure Point)	7.48	6.02	80%

*Precast Cumulative Dissipated Energy at Failure of CIP Bent

CHAPTER 6 CONCLUSIONS AND RECOMMENDATIONS

6.1. INTRODUCTION

As ABC has been rapidly developing in civil engineering over the past decades in the United States, research has continually pushed the limits of application within bridge construction. This can be contributed to the advantages it offers over that of traditional CIP construction. Among the advantages of ABC when building new, replacing, or rehabilitating bridges are reduced traffic disruption, improved on-site safety, increased quality, rapid erection, reduced work site footprint, and reduced onsite construction time. Despite these advantages, CIP construction is prevalently used in areas of seismic activity as the resulting structure is considered "monolithic". A number of solutions have been offered for this purpose, such as socket member, grouted duct, pipe-pin, and many others. Many of these have proved adequate in meeting the demands on the substructure in moderate to high seismic areas, however the processed have proved difficult to fabricate and assemble.

This research has investigated a simplified precast connection for use in precast substructure elements using a telescoping grouted steel pipe connection. The connection consists of a protruding HSS pipe from the pier, which is inserted into a larger HSS pipe cast in the footing and/or pier cap with a rubber elastomeric bearing at the interface. The pier pipe is fitted with centering fins to align it within the center of the foundation or cap pipe insert. After full erection of the piers and pier caps the voids between the HSS pipe are grouted in place. This process requires minimal construction bracing. The simplified proposed connection offers simple construction, increased construction tolerances, improved safety, and increased erection speed. The connection is comprised of non-proprietary elements allowing for improved detailing specifications.

The objectives of this research were as follows:

1. Construct and test a large scale two pier bridge bent using CIP construction under quasi-static cyclic loading.
2. Construct and test a large scale two pier bridge bent using ABC and precast technologies implementing the proposed pier connection to experimentally validate the connections performance.
3. Compare the seismic performance of the proposed pier connection to the CIP constructed bent.

6.2. EXPERIMENTAL CONCLUSIONS

With the CIP and precast bent having been design identical, in both dimensional and performance capacities, the two are easily compared. The two systems performed similar in nature, with the precast bent showing less overall damage than that of the CIP bent. The precast bent also achieved a higher moment capacity of 498-kip-ft., than that of the CIP bent, having achieved 468-kip-ft. The Precast bent withstood a total of 24 complete loading cycles, culminating in a final ultimate drift ratio of 9.15%. The CIP bent failed far short of the precast achievement, having withstood a total of 15 loading cycles, resulting in an ultimate drift ratio of 4.94%. The two specimens exhibited similar ultimate capacities at similar drift ratios during the experiment. The precast bent achieved a maximum force of 71.4-kip at a drift ratio of 2.69%. While the CIP bent achieved a maximum force of 66-kip at a drift ratio of 2.46%. Similarly, the precast bent dissipated a much higher amount of energy than that of the CIP bent, as it endured more loading cycles. The total dissipated energy of the precast and CIP bent was 2,125-kJ and 342-kJ. The precast bent had however dissipated more energy at the fifteenth cycle than that of the CIP bent, having dissipated a total of 466-kJ to that point.

From the experimental investigation and comparison of the specimens made in the research presented here several conclusions can be made:

- Compared to an equivalent cast-in-place pier, the precast pier with the proposed pipe connection achieved higher ultimate capacity (108% of CIP bent).
- The precast bent withstood small displacement without suffering hairline cracking due to the presence of the elastomeric bearing.
- The precast bent displayed better confinement through reduced cracking observed throughout the experimental program.
- The precast bent displayed far more resilience during the loading as it withstood an additional 9 loading cycles than that of the CIP bent.
- The resilience of the precast bent is demonstrated by the cumulative energy dissipation levels it was capable of achieving during testing.
- The precast bent displayed more energy dissipation at the point of failure for the CIP bent as once the precast bent had achieved ultimate capacity it displayed far less degradation than that of the CIP bent, constituting to its ability to withstand additional cycles.
- Buckling and tearing of the HSS pipe is observed during large drift ratios to be the failure mechanism of the proposed precast connection.
- The precast pier demonstrates a reduced stiffness as it approaches ultimate capacity than that of the CIP bent.
- The precast bent also exhibited a higher initial yield displacement of 1.13% drift ratio compared to the 0.5% drift exhibited by the CIP bent.
- The precast bent had a greater approximated global yield than that of the precast bent, 1.49% verse 1.07% drift ratio.

- The precast bent with the proposed precast connection proved capable of successfully emulating the CIP bent under similar quasi-static loading.

6.3. CONTINUED RESEARCH

To this point the proposed precast connection has proven to be suitable for emulating CIP construction and performing well under seismic loading. However, as with all innovations and new technologies further refinement the process, detailing, and design of the proposed precast connection is suggested to take place. Additional research is suggested in the following areas:

- Quantifying appropriate embedment lengths of both HSS sections.
- Quantifying the ideal unbonded length and refinement of the unbonded length positioning. This is suggested as the tearing failure of the HSS section takes place just inside the face of the footing or cap, which was not within the unbonded length used in this research.
- Proper identification of the elastomeric bearing thickness and a proper seal to ensure protection of the HSS pipe from corrosive materials.
- Further connection verification through either bi-directional quasi-static cyclic or shake table testing.
- Identification and research development of various repair and retrofitting of damaged connections.

REFERENCES

AASHTO. (2017). *AASHTO LRFD Bridge Design Specifications.* American Association of State Highway and Transportation Officials, 8th Edition.

ACI Committee 374. (2013). *Guide for testing reinforced concrete structural elements under slowly applied simulated seismic loads (ACI 374.2R-13).* American Concrete Institute, Farmington Hills, MI.

Brenes, F., Wood, S., and Kreger, M. (2006). *Anchorage Requirements for Grouted Vertical-Duct Connectors in Precast Bent Cap Systems.* Report No. 0-4176-S. Center for Transportation Research, the University of Texas at Austin, TX

Caltrans. (2013). *Seismic Design Criteria-Version 1.7. Caltrans.* California Department of Transportation, Sacramento, CA.

Ebrahimpour, A., Earles, B.E., Maskey, S., Tangarife, M., and Sorensen, A.D. (2016). *Seismic Performance of Columns with Grouted Couplers in Idaho Accelerated Bridge Construction Applications.* Idaho Transportation Department Research Program, Idaho State University, Pocatello, ID

Federal Highway Administration (2009). *Connection Details for Prefabricated Bridge Elements and Systems.* Report FHWA-PL-05-003. FHWA, Washington, D.C.

Haraladsson, O., Stanton, J. F., and Eberhard, M. O. (2011). *Laboratory Tests of Column-to-Footing Socket Connections.* Report No. FHWA-HIF-13-039. Federal Highway Administration, Office of Bridge Technology, Washington, D.C.

Lehman, D.E., and Roeder, W. (2012). *Rapid Construction of Bridge Piers with Improved Seismic Performance.* University of Washington, Seattle, WA

Mashal, M. (2015). *Post-Tensioned Earthquake Damage Resistant Technologies for Accelerated Bridge Construction.* University of Canterbury, Christchurch, N.Z.

Mashal, M., and Palermo, A. (2019a), "Low-damage seismic design for accelerated bridge construction.: *Journal for Bridge Engineering*

Mashal, M., and Palermo, A. (2019b). "Emulative seismic resistant technology for Accelerated Bridge Construction." *Soil Dynamics and Earthquake Engineering,* Elsevier Ltd, 124 (December 2018), 197-211

Mehrsoroush, A., and Saiidi, M.S. (2014). *Earthquake-Resistant Telescopic Pipe Pin Column Base Connections for Accelerated Bridge Construction.* 10th National Conference in Earthquake Engineering, Earthquake Engineering Research Institute, Anchorage, AK.

McCormac, J.C., and Brown, R.H. (2014) *Design of Reinforced Concrete.* Wiley, Hoboken, NJ

National Cooperative Highway Research Program (NCHRP). Synthesis of Highway Practice 119 (1985). *Prefabricated Bridge Elements and Systems.* Transportation Research Board (TRB), National Research Council, Washington, D.C.

NCHRP Synthesis 324 (2003). *Prefabricated Bridge Elements and Systems to Limit Traffic Disruption During Construction.* transportation Research Board, national Research Council, Washington, D.C.

Pampanin, S. et al. (2010). *PRESSS Technology Design Handbook.* NZCS, Auckland, N.Z.

Priestly, M.J.N., Calvi, G.M., and Kowalsky, M.J. (2007). *Displacement-Based Seismic Design of Structures. Earthquake Spectra,* IUSS Press.

Restrepo, J. I., Mander, J., and Holden, T. J. (2001). *New Generation of Structural Systems for Earthquake Resistance*. Proceedings of New Zealand Society for Earthquake Engineering (NZSEE) Conference, Wairakei, N.Z.

Tazarv, M., and Saiidi, M.S. (2015). *Design and Construction of Precast Bent Caps with Pocket Connections for High Seismic Regions.* Reno, NV.

U.S. Department of Transportation/Federal Highway Administration. (2019). "Accelerated Bridge Construction." https://www.fhwa.dot.gove/bridge/abc/

Wasserman, E.P., and Walker, J.H. (1996). *Integral Abutments for Steel Bridges.* American Iron and Steel Institute, Chicago, Ill.

APPENDIX A: CONSTRUCTION DRAWINGS

A.1. CIP BENT SPECIMEN

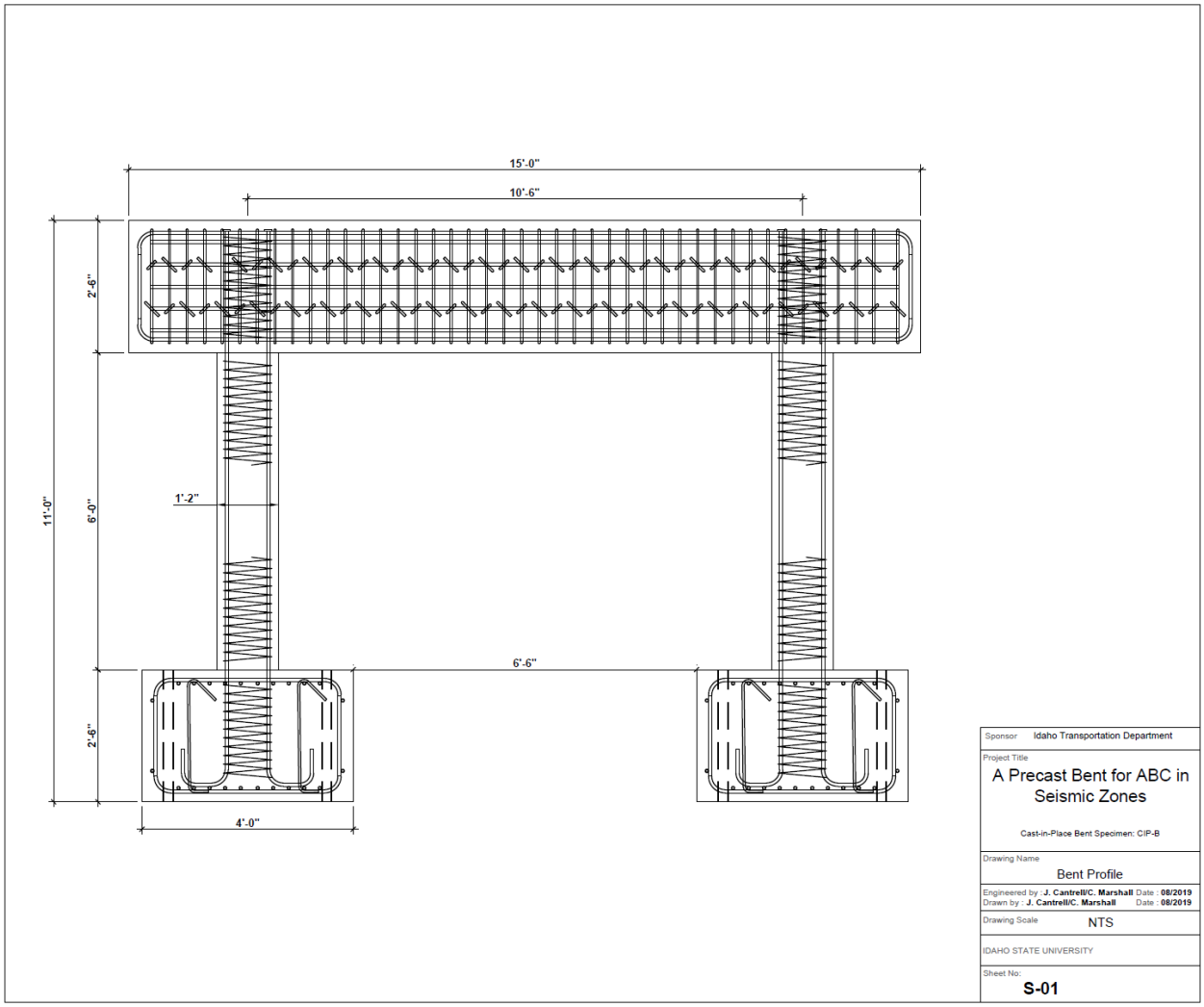

Figure A.0-1: CIP Bent Profile

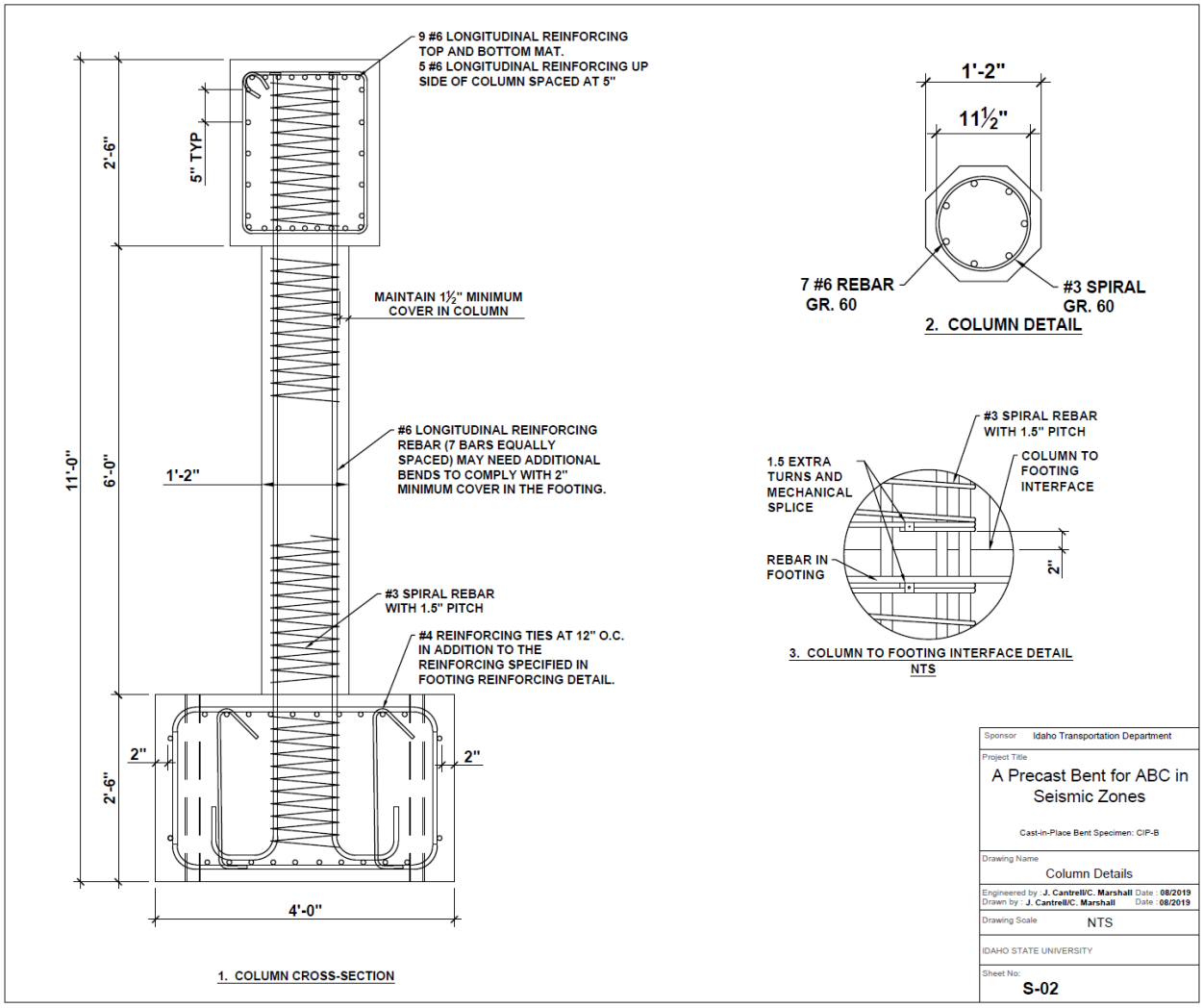

Figure A.0-2: CIP Column Detail

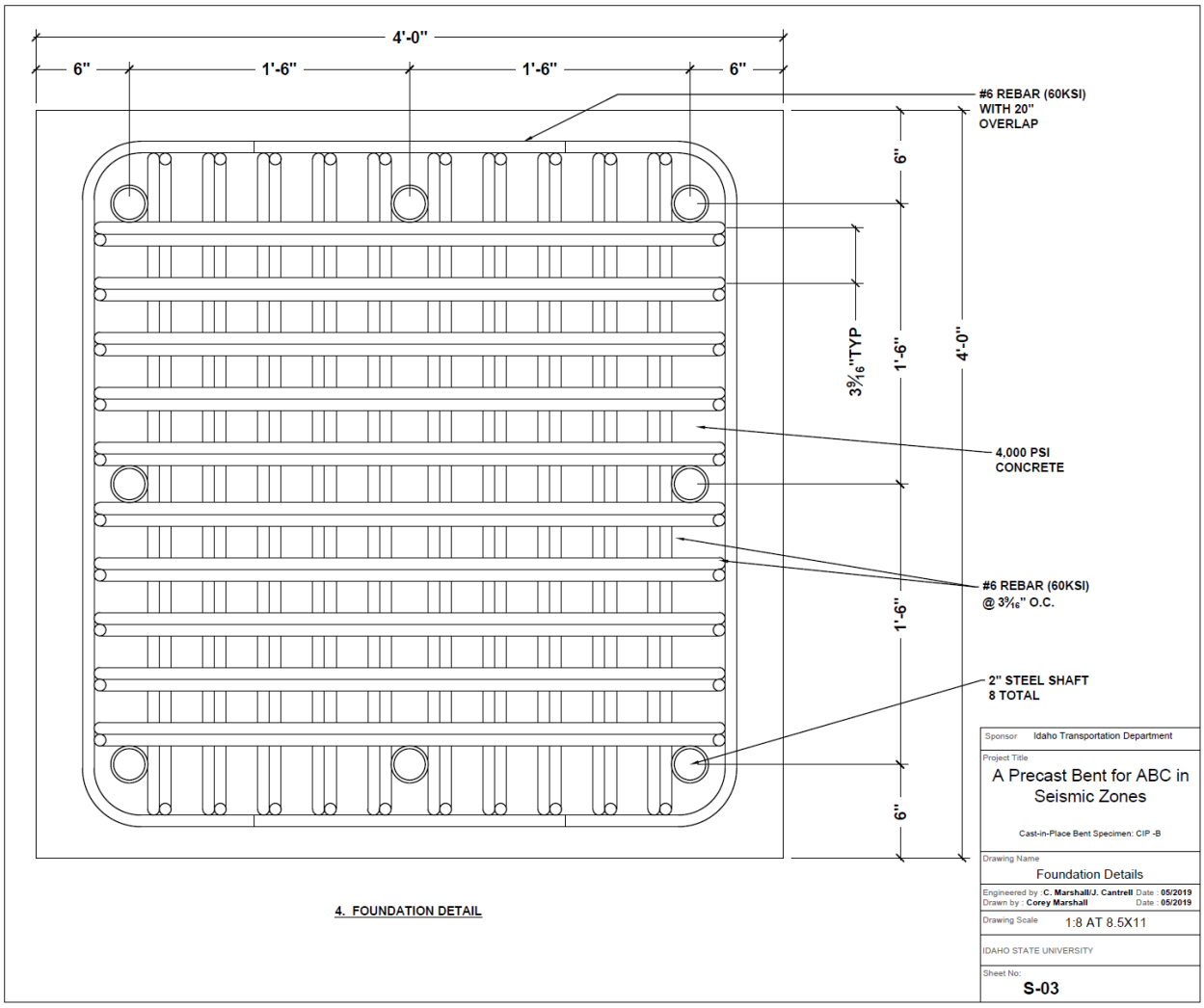

Figure A.0-3: CIP Footing Detail

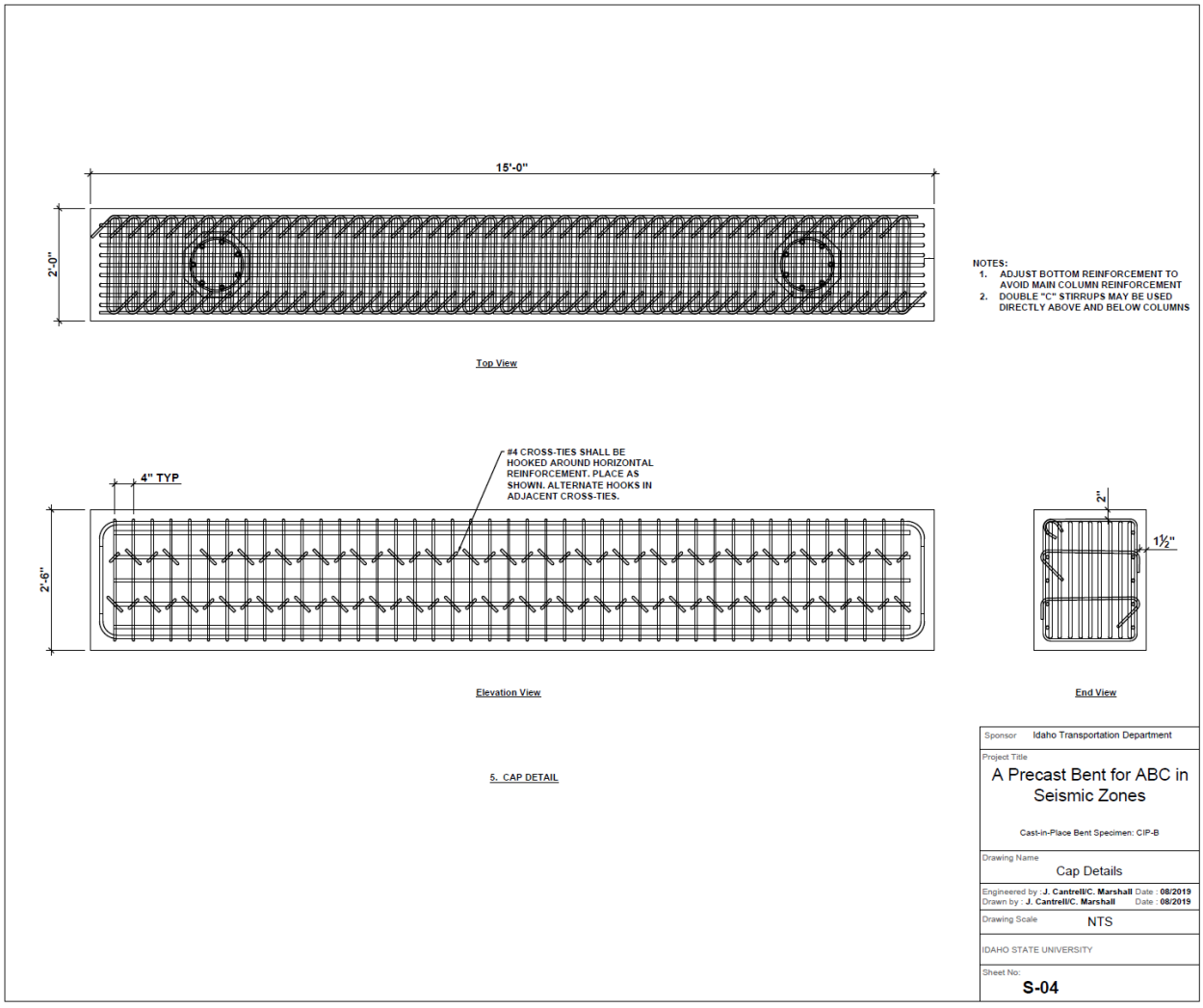

Figure A.0-4: CIP Cap Detail

A.2. PRECAST BENT SPECIMEN

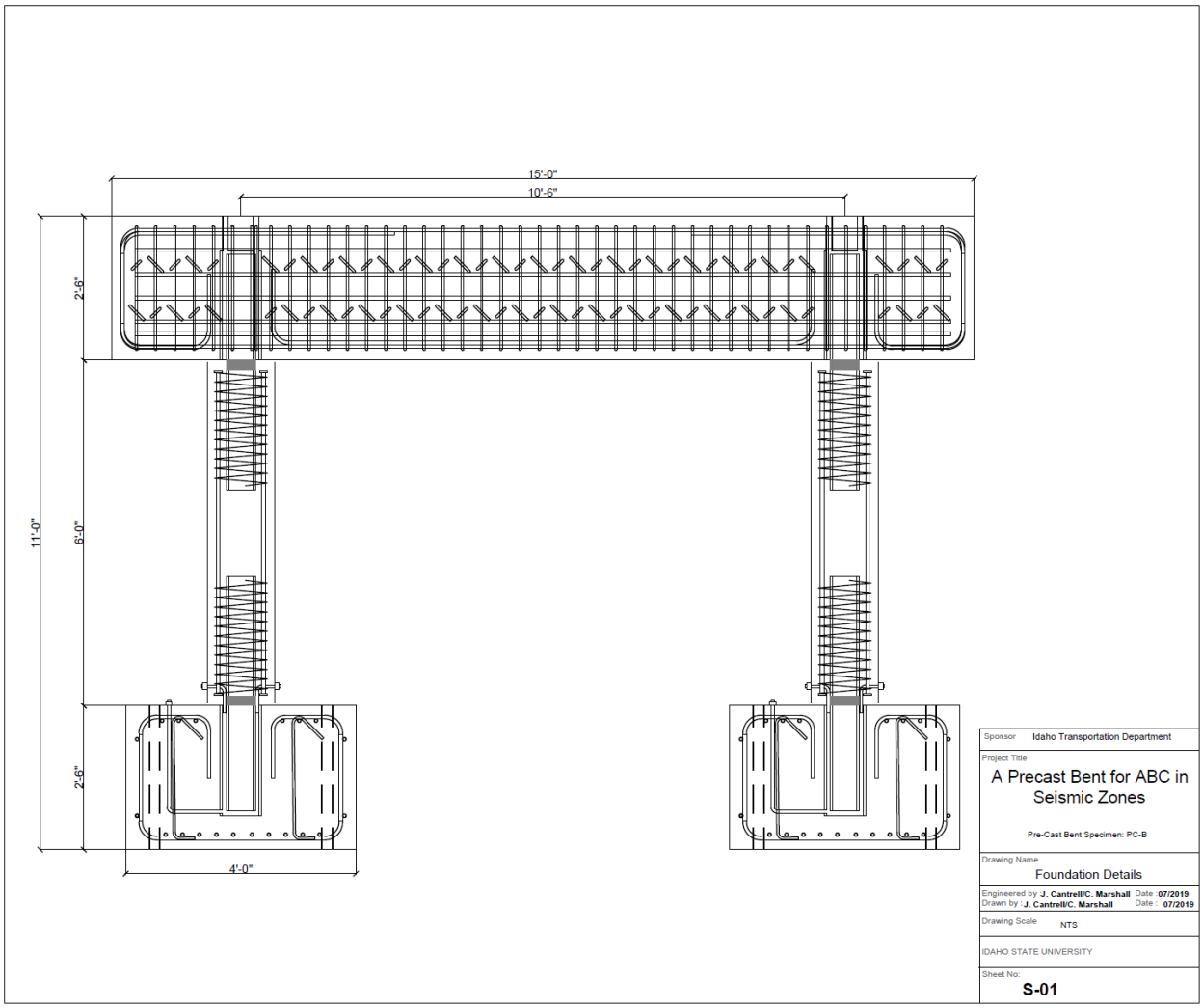

Figure A.0-5: Precast Bent Profile

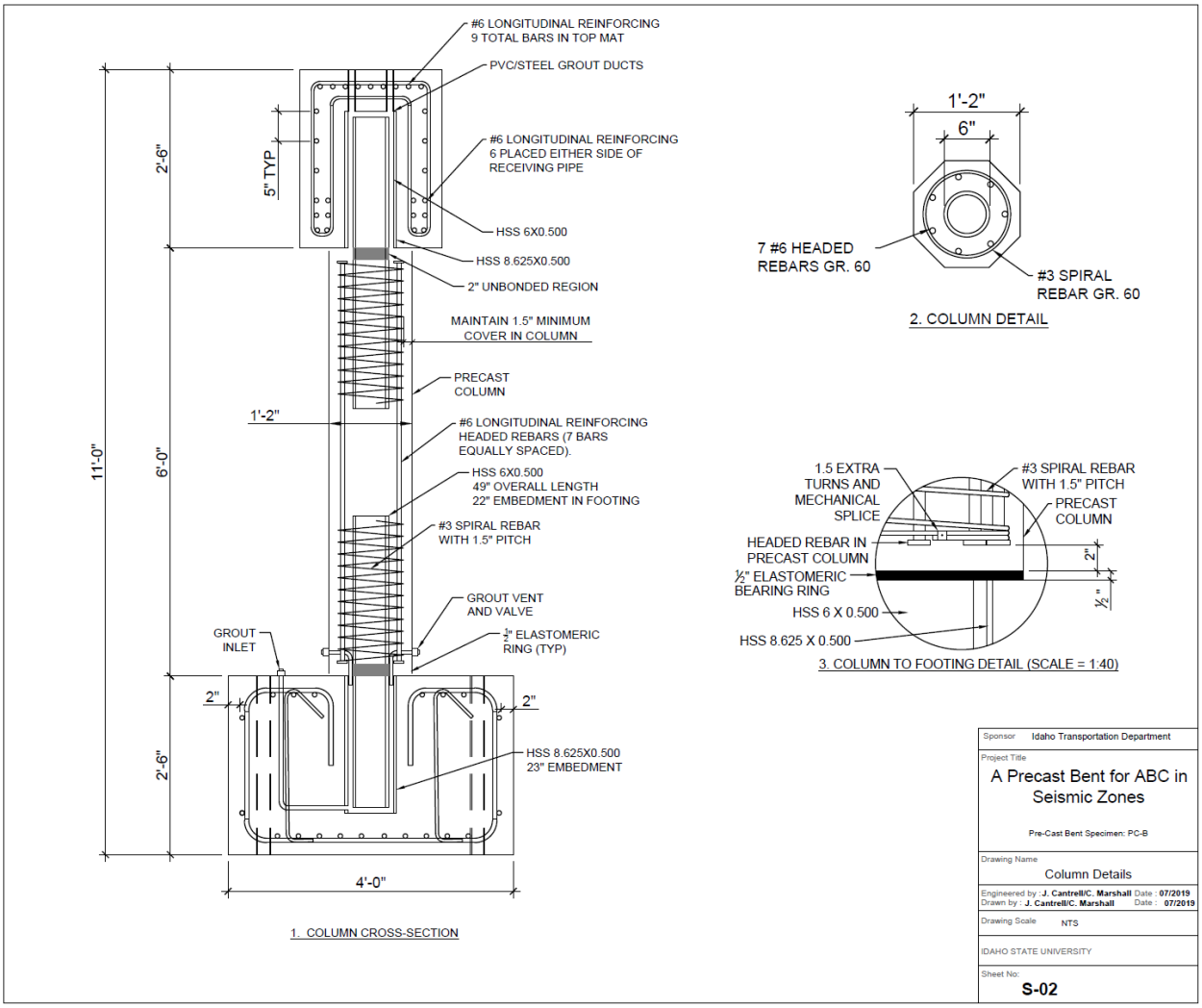

Figure A.0-6: Precast Column Detail

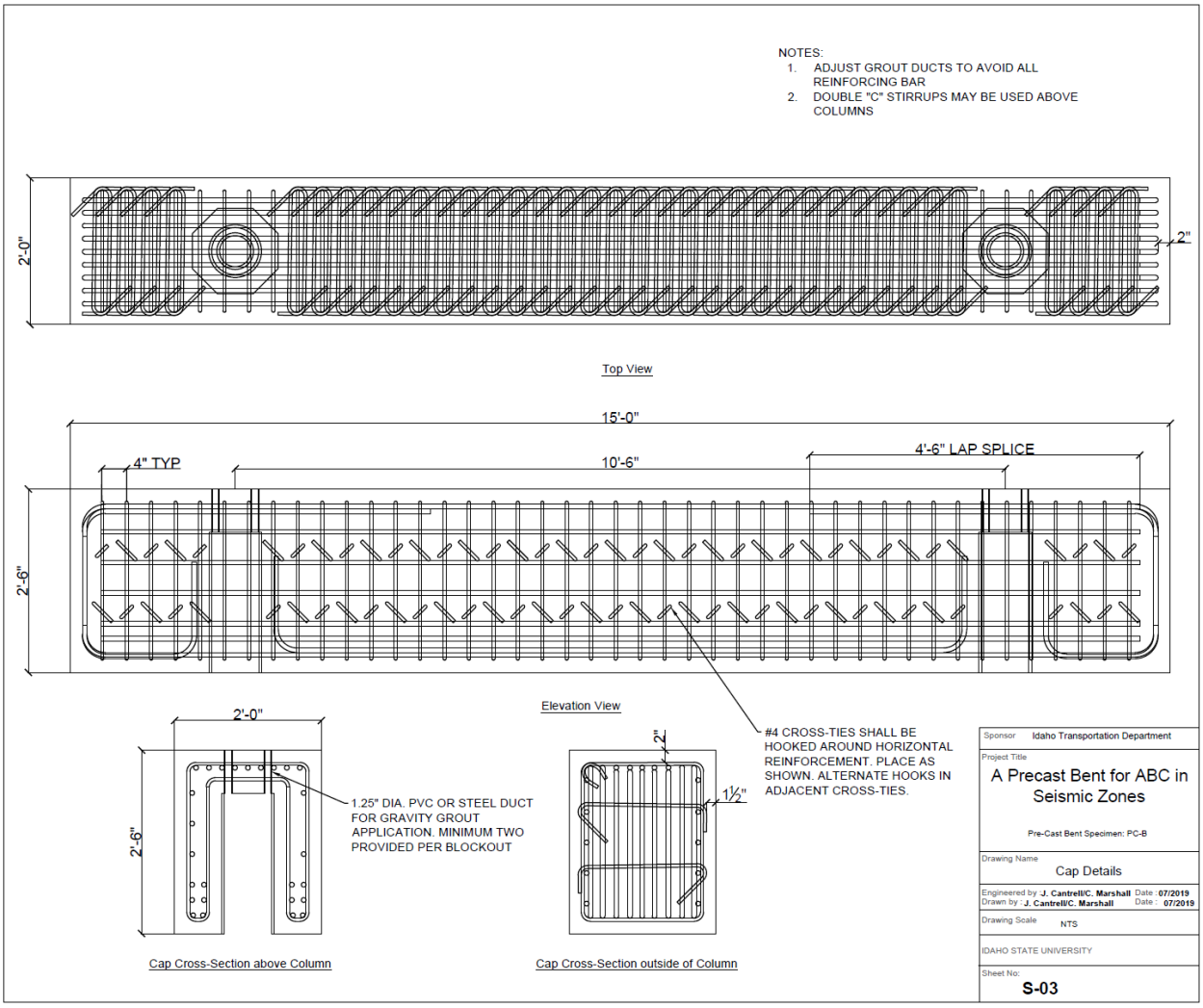

Figure A.0-7: Precast Cap Detail

APPENDIX B: DESIGN CALCULATIONS

B.1. CIP BENT COLUMNS

Circular Column Dimensions

Diameter =	14	in	Tensile strain =		0.002
Cover =	1.5	in	fy =	60	ksi
Stirrup =	3		f'c =	4	ksi
Long. Bar #=	6		Es =	29000	ksi
Total bars =	7		B1 =	0.85	(see pg 68)
Ds = 9.5	in				

Compression strain = -0.003

For equivalent rectangular Column (Figure 10.9)

B = Ag/(.8D) = 13.74

H = .8*D = 11.20

Hs = Ds*2/3 = 6.33

A's = 1.55

Cover = 2.43

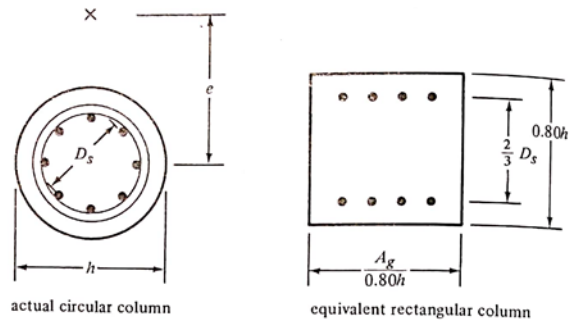

FIGURE 10.9 Replacing a circular column with an equivalent rectangular one.

Determine values of y and of the steel stains

y = 0.003 / (0.003 + 0.002) * 11.2= 6.72 in.

e's = ((6.72 - 2.43) / 6.72) * 0.003 = 0.00191 < 0.00207 Compression Steel Does Not Yield

es = ((11.2 - 6.72 - 2.43) / (11.2 - 6.72))*0.002 = 0.00091 < 0.00207 Tension Steel Does Not Yield

a = B1*c = 0.85 * 6.72 = 5.71 in.

Cc = B1*a*B*f'c = -266.93 k Fe = 0.75

C's = fy*A's-B1*A's*f'c =		-87.52	k				
Ts = es*E*A's =		40.97	k				
				Column height =		6.48	ft
Pn =	313.48	k		Vu =	14.65	kip	
Fe*Pn =	235.11						

Key values	Mn =	1139.33		in-k =	94.94	ft-k	
Input values	Fe*Mn =		854.50	in-k =	71.21	ft-k	

B.2. PRECAST BENT COLUMNS

Pipe Connection			fy =	42	ksi	AISC Table 2-4 pg 2-48
Pipe Diameter =	6	in.	fu =	58	ksi	AISC Table 2-4 pg 2-48
Pipe Thickness=	0.465	in.	f'c =	8	ksi	
Concrete Diameter =	5.07	in.	Es =	29000	ksi	

D/t =	12.90322581	< Good	103.57

As = 8.09 in2

Ac = 20.19 in2

Determine y value by changing the following values:

Applied axial load (P) =	50.0	kips		Ts =	355.02	kips	P + Ts =	405.0225634	kips
Ast =	8.453	in2	Cc =	143.38	kips	Cc + Cs =		405.0225634	kips

Acc = 18.866 in2 Cs = 261.64 kips 0 kips ** Set this value equal to zero using solver.

Asc = 6.230 in2

Determine y value by using the solver

Summing the moments about the c.g.c of the column:

y = 0.0 in. M = 32.81250014 kip-in.

** Set this value equal to zero using solver.

As = Asc + Ast = 8.09 in2

**Set this value equal to As using solver

WSDOT CH7

Po = 493.0 kips 7.10.2-5 compressive resistance of a member without consideration of flexure

C' = 0.537 < GOOD! 0.9 7.10.2-4

Eleff = 7.10.2-3

rm = 2.77 in. 7.10.2-9 radius to the center of the steel tube

Theta = 4.01 degrees 7.10.2-8 angle used to define c

c = 2.53 in. 7.10.2-7 one half the chord length of the tube in compression

Mn(y) = 678.68 in-kip = 56.6 ft-kip 7.10.2-6 nominal moment resistance as a function of the parameter y

APPENDIX C: GROUT PRODUCT DATA SHEET

BUILDING TRUST

PRODUCT DATA SHEET

SikaGrout®-328

High performance, precision, grout with extended working time

PRODUCT DESCRIPTION

SikaGrout®-328 is a non-shrink, non-metallic, cementitious precision grout powered by ViscoCrete technology. This grout provides extended working time and exceptional physical performance at fluid consistency. A structural, precision grout, SikaGrout®-328 can be placed from fluid to dry pack.

USES

- Where exceptional one day and ultimate compressive strengths are required.
- Applications requiring a pumpable grout.
- Non-shrink grouting of machinery and equipment, base plates sole plates, precast panels, beams, columns and curtain walls.
- Applications where a non-shrink grout is needed for maximum effective bearing area to transfer optimum load.
- For underwater application in conjunction with Sikament® 100 SC. Consult Technical Service for dosage information. Independent test data is available however on site testing is recommended to confirm performance under actual field conditions.
- For grouting rebar, bolts, dowels and pins, etc.

CHARACTERISTICS / ADVANTAGES

- Multiple fluidity with one material
- Reaches 10,000 psi in dry pack consistency
- Outstanding performance in fluid state
- Extended working time
- Excellent fluidity - sufficient time for placement
- Contains premium quality quartz aggregate
- Hardens free of segregation
- Non-metallic, will not stain or rust
- Shows positive expansion

APPROVALS / STANDARDS

- Meets ASTM-C 1107 (Grade B & C)
- SikaGrout®-328 is USDA certifiable

PRODUCT INFORMATION

Packaging	50 lb (22.7 kg) bag
Appearance / Color	Gray powder
Shelf Life	9 months from date of production if stored properly in original, unopened and undamaged sealed packaging
Storage Conditions	Store dry at 40–95 °F (4–35 °C) Protect from moisture. If damp, discard material

TECHNICAL INFORMATION

Compressive Strength

(ASTM C-109) 73 °F (23 °C) 50 % R.H.	Dry Pack	Plastic	Flowable	Fluid
1 day	5,000 psi (34.4 MPa)	4,500 psi (31 MPa)	4,000 psi (27.6 MPa)	3,500 psi (24.1 MPa)
3 day	8,000 psi (55.2 MPa)	6,500 psi (44.8 MPa)	6,000 psi (41.4 MPa)	5,500 psi (37.9 MPa)
14 day	9,200 psi (63.4 MPa)	7,000 psi (48.3 MPa)	6,700 psi (46.2 MPa)	6,500 psi (44.8 MPa)
28 day	10,000 psi (69 MPa)	8,200 psi (56.5 MPa)	8,000 psi (55.2 MPa)	7,500 psi (51.7 MPa)

Flexural Strength (ASTM C-293) 73 °F (23 °C) 50 % R.H.

	Fluid
3 day	1,100 psi (7.6 MPa)
7 day	1,200 psi (8.6 MPa)
28 day	1,300 psi (9 MPa)

Splitting Tensile Strength (ASTM C-496) 73 °F (23 °C) 50 % R.H.

	Fluid
3 day	350 psi (2.4 MPa)
7 day	400 psi (2.8 MPa)
28 day	650 psi (4.5 MPa)

Shear Strength (ASTM C-882 modified*)

	Fluid
3 day	950 psi (6.6 MPa)
7 day	1,750 psi (12.1 MPa)
28 day	2,000 psi (13.8 MPa)

*Mortar scrubbed into substrate at 73 °F (23 °C) and 50 % R.H.

Freeze-Thaw Stability 300 Cycles — 99 % (ASTM C-666)

APPLICATION INFORMATION

Mixing Ratio

Dry Pack	Plastic	Flowable	Fluid
5.5–6.0 pts (2.6–2.8 L)	6.5–7.0 pts (3.1–3.3 L)	7.0–7.5 pts (3.3–3.5 L)	8.0–8.5 pts (3.8–4 L)

Coverage

0.44 ft³ (0.01 m³) per bag at hfluid consistency
(Coverage figures do not include allowance for surface profile and porosity or material waste)

Layer Thickness

Min.	Max.
1/2" (12.7 mm)	6" (152.4 mm)

For application thicknesses of 6" or greater, consult Sika®'s Technical Service Department.

Flowability

Dry Pack	Plastic[1]	Flowable[1]	Fluid[2]
10–25 %	100–125 %	124–145 %	20–60 sec

[1]ASTM C-1437
[2]ASTM C-939

Product Temperature 65–75 °F (18–24 °C)

Ambient Air Temperature > 45 °F (7 °C)

Substrate Temperature > 45 °F (7 °C)

Set Time

	Dry Pack	Plastic	Flowable	Fluid
Initial	< 15 min	> 2 hr	> 3 hr	> 4 hr
Final	< 2 hr	< 6 hr	< 7 hr	< 8 hr

SURFACE PREPARATION

- Surface must be clean and sound. Remove all deteriorated concrete, dirt, oil, grease, and other bond-inhibiting materials from the area to be repaired.
- Anchor bolts to be grouted must be de-greased with suitable solvent.
- Concrete must be sound and roughened to promote mechanical adhesion.
- To ensure optimum repair results, the effectiveness of decontamination and preparation should be assessed by a pull-off test.
- Substrate should be Saturated Surface Dry (SSD) with clean water prior to application. No standing water should remain during application.

FORMING

- For pourable grout, construct forms to retain grout without leakage.
- Forms should be lined or coated with bond-breaker for easy removal.
- Forms should be sufficiently high to accommodate head of grout.
- Where grout-tight form is difficult to achieve, use SikaGrout®-328 in dry pack consistency.

MIXING

- Pour the water in the recommended proportion into a suitable mixing container.
- DO NOT OVER WATER!
- Ambient and material temperature should be as close as possible to 70 °F. If higher, use cold water; if colder, use warm water.
- While mixing slowly, add the powder to the water.
- Mix thoroughly for at least 5 minutes with low speed (400-600 rpm) using a Sika mixing paddle or a jiffy paddle to avoid entraining too much air and until homogenous with no lumps.

EXTENSION WITH AGGREGATES

- For deeper applications (plastic and flowable consistancy only), 25 lbs. of 3/8" (9.5 mm) coarse aggregate can be added.
- The aggregate must be non-reactive (reference ASTM C-1260, C-227 and C-289), clean, well graded, saturated surface dry, have low absorption and high density, and comply with ASTM C-33 size number 8 per Table 2.
- Variances in aggregate may result in different strengths.
- Add pea gravel after the water and SikaGrout®-328.

APPLICATION

- Within 60 minutes after mixing, place grout into forms in normal manner to avoid air entrapment.
- Vibrate, pump, or ram grout as necessary to achieve flow or compaction.
- SikaGrout®-328 must be confined leaving minimum exposed surface.
- After grout has achieved final set, remove forms, trim or shape exposed grout shoulders to designed profile.
- SikaGrout®-328 is an excellent grout for pumping, even at high flow. For pump recommendations, contact Technical Service.

CURING TREATMENT

- Wet cure for a minimum of 3 days or apply a curing compound which complies with ASTM C-309 on exposed surfaces.

LIMITATIONS

- Do not use as a patching or overlay mortar or in unconfined areas.
- As with all cement based materials, avoid contact with aluminum to prevent adverse chemical reaction and possible product failure. Insulate potential areas of contact by coating aluminum bars, rails, posts etc.with an appropriate epoxy such as Sikadur 32 Hi-Mod.

BASIS OF PRODUCT DATA

Results may differ based upon statistical variations depending upon mixing methods and equipment, temperature, application methods, test methods, actual site conditions and curing conditions.

OTHER RESTRICTIONS

See Legal Disclaimer.

ENVIRONMENTAL, HEALTH AND SAFETY

For further information and advice regarding transportation, handling, storage and disposal of chemical products, user should refer to the actual Safety Data Sheets containing physical, environmental, toxicological and other safety related data. User must read the current actual Safety Data Sheets before using any products. In case of an emergency, call CHEMTREC at 1-800-424-9300, International 703-527-3887.

DIRECTIVE 2004/42/CE - LIMITATION OF EMISSIONS OF VOC

0 g/l (EPA method 24)

LEGAL DISCLAIMER

- **KEEP CONTAINER TIGHTLY CLOSED**
- **KEEP OUT OF REACH OF CHILDREN**
- **NOT FOR INTERNAL CONSUMPTION**
- **FOR INDUSTRIAL USE ONLY**
- **FOR PROFESSIONAL USE ONLY**

Prior to each use of any product of Sika Corporation, its subsidiaries or affiliates ("SIKA"), the user must always read and follow the warnings and instructions on the product's most current product label, Product Data Sheet and Safety Data Sheet which are available at usa.sika.com or by calling SIKA's Technical Service Department at 1-800-933-7452. Nothing contained in any SIKA literature or materials relieves the user of the obligation to read and follow the warnings and instructions for each SIKA product as set forth in the current product label, Product Data Sheet and Safety Data Sheet prior to use of the SIKA product.

SIKA warrants this product for one year from date of installation to be free from manufacturing defects and to meet the technical properties on the current Product Data Sheet if used as directed within the product's shelf life. User determines suitability of product for intended use and assumes all risks. User's and/or buyer's sole remedy shall be limited to the purchase price or replacement of this product exclusive of any labor costs. **NO OTHER WARRANTIES EXPRESS OR IMPLIED SHALL APPLY INCLUDING ANY WARRANTY OF MERCHANTABILITY OR FITNESS FOR A PARTICULAR PURPOSE. SIKA SHALL NOT BE LIABLE UNDER ANY LEGAL THEORY FOR SPECIAL OR CONSEQUENTIAL DAMAGES. SIKA SHALL NOT BE RESPONSIBLE FOR THE USE OF THIS PRODUCT IN A MANNER TO INFRINGE ON ANY PATENT OR ANY OTHER INTELLECTUAL PROPERTY RIGHTS HELD BY OTHERS.**

Sale of SIKA products are subject to the Terms and Conditions of Sale which are available at https://usa.sika.com/en/group/SikaCorp/termsandconditions.html or by calling 1-800-933-7452.

Sika Corporation
201 Polito Avenue
Lyndhurst, NJ 07071
Phone: +1-800-933-7452
Fax: +1-201-933-6225
usa.sika.com

Sika Mexicana S.A. de C.V.
Carretera Libre Celaya Km. 8.5
Fracc. Industrial Balvanera
Corregidora, Queretaro
C.P. 76920
Phone: 52 442 2385800
Fax: 52 442 2250537